MAGNETIC ORDERING PHENOMENA

AT VERY LOW TEMPERATURES

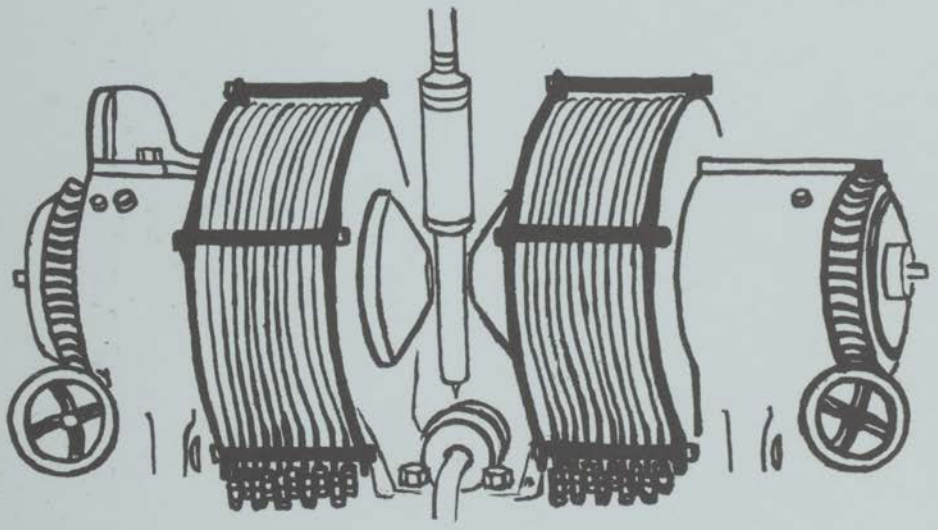

H. W. J. BLÖTE

MAGNETIC ORDERING PHENOMENA

AT VERY LOW TEMPERATURES

MAGNETIC ORDERING PHENOMENA

AT VERY LOW TEMPERATURES

PROEFSCHRIFT
TER VERKRIJGING VAN DE GRAAD VAN DOCTOR IN DE WISKUNDE EN NATUURWETENSCHAPPEN AAN DE RIJKSUNIVERSITEIT TE LEIDEN, OP GEZAG VAN DE RECTOR MAGNIFICUS DR. W.R.O. GOSLINGS, HOOGLERAAR IN DE FACULTEIT DER GENEESKUNDE, VOLGENS BESLUIT VAN HET COLLEGE VAN DEKANEN TE VERDEDIGEN OP DONDERDAG 22 JUNI 1972 TE KLOKKE 15.15 UUR

DOOR

HENDRIK WILLEM JAN BLÖTE

GEBOREN TE LEIDEN IN 1943

DRUK: cv elve/labor vincit

PROMOTOR: PROF. DR. W.J. HUISKAMP

Aan mijn ouders

Aan Anke

CONTENTS

GENERAL INTRODUCTION AND SURVEY

The study of magnetism in ionic compounds has provided a remarkably rich source of information for physicists and chemists alike. This is partly due to the great variety in bonding complexes and ligand coordination structures, in which particularly 3d-transition elements are engaged. It is also due to the increasing refinement in measuring techniques, particularly those involving resonance methods, which has lead to detailed knowledge about single ion properties in many crystals. The empirical knowledge of single ion properties is, at least qualitatively, quite well understood in relation to ligand field theory.

In comparison, the existing information about magnetic interactions in ionic compounds is less extensive and is poorly understood. The localized character of the ionic wave function leads to the short range of the magnetic exchange interaction potential, which decreases rapidly with interionic distance. Consequently, the exchange interaction strength is strongly dependent on details of the ligand coordination of the magnetic ion, and may vary over many decades in chemically related compounds. This is demonstrated, for instance, in the large variation in magnetic interaction strengths exhibited in compounds of 3d-transition elements, in which planes of 3d-ions can be separated by a class of organic molecules of variable length, hence producing variable interplanar separations. A similarly large variation in superexchange is noticeable when the number of intervening ligands between 3d-elements is increased. Furthermore, since magnetic superexchange is correlated with covalency effects in ligand bonding, the chemical coordination of transition metal ions influences the magnetic interaction. Whereas a fair amount of experimental and theoretical investigations have been dedicated to octahedrally coordinated transition ion compounds, relatively little is known about the equally interesting tetrahedrally coordinated compounds. Several examples of tetrahedral coordination will be discussed in this thesis.

Historically, exchange interactions among magnetic ions, derived from implementing the rules of quantum mechanics, have been invoked in order to explain the occurrence of magnetic phase transitions at rather high temperatures, such as in transition metal elements. The information presented in this thesis includes magnetic phase transitions in transition metal compounds, in which the magnetic ions are separated by at least two non-magnetic ligands. These transitions occur at temperatures which are lower by roughly three orders of magnitude. Hence, for a systematic study of exchange interaction through the determination of the magnetic phase transition characteristics, measurements over many decades of temperature are required. One advantage of studying magnetic interactions at low temperatures consists of the following simplification.

In many of the compounds mentioned above and further discussed in this thesis, *e.g.* the tetrahedrally coordinated Co compound, rather low energy single ion eigenstates complicate the magnetic behaviour of these compounds when studied at ordinary temperatures. On the other hand, when cooling to the temperature of liquid helium or below, the ground states may exhibit simple and extremely interesting properties.
Another advantage is that the lattice heat capacity, which occurs in all solids, and which forms a sizeable hindrance to accurate measurement of magnetic heat capacity, is very small at these temperatures. Further, if strong magnetic interactions are present, the crystal lattice can be appreciably deformed by magnetic ordering, which reacts on the magnetic interactions. This complication, however, is not important below 1 K due to weakness of the interactions and smallness of the deformations.
The temperature interval in which measurements can be made, depends on the experimental technique used. Temperatures of about 1 K could be reached when liquid helium became available. After that time, new methods have been sought to reach still lower temperatures. Although in recent years new methods, based on the remarkable properties of the ^{3}He and ^{4}He liquids and their mixtures, have been developed, the most fruitful method undoubtedly has been that of adiabatic demagnetization. This method is based on the Zeeman interaction between ionic magnetic moments and an external magnetic field. The Zeeman energy is, in a sufficiently high magnetic field, larger than the thermal energy at liquid helium temperatures. Reduction of the magnetic field under adiabatic conditions leads to a corresponding temperature decrease. Temperatures of about 0.01 K can be reached by demagnetization of chromium potassium alum, and about 0.001 K by demagnetization of cerium magnesium nitrate. Gradually this temperature range has become available for experiments of various kinds, notably specific heat experiments.
Interionic magnetic interactions bring about an anomaly in the heat capacity at temperatures of the order of the interaction constant divided by Boltzmann's constant. For magnetic ions of the iron group, the interactions correspond roughly to an ordering temperature smaller than 1 K if their separation is greater than 6 Å, whereas for the rare earth ions this distance is about 4 Å. Such separations are realized in a large class of magnetic compounds. In order to investigate these substances, the demagnetization method can be applied.
In most cases, demagnetization of the sample does not give sufficiently low temperatures, and indirect cooling via a demagnetized cooling salt must be applied. The lowest temperatures thus obtained depend on the heat capacity of the sample. In favourable cases, measurements can be obtained from about 0.04 to 4 K. Some of the experimental aspects of measurements at these temperatures will be discussed in chapter I.
Several different types of magnetic interactions exist between ionic magnetic moments, *e.g.* long range dipolar interactions and short range (super)exchange interactions. These interactions can have a positive (ferromagnetic) or a negative (antiferromagnetic) sign. The form of the interaction further depends on the ionic spin quantumnumber and on the number of spatial components per spin that participate in the interaction. This number, which is called the spin dimensionality, equals three if the interaction is isotropic (so called Heisenberg

interactions). If the crystalline field imposes a constraint on the spin degrees of freedom, *e.g.* in a crystal plane, the spin dimensionality is (at most) two (XY interactions), and if the spin is constrained to a crystal axis, the spin dimensionality is one (Ising interactions).
The magnetic ordering phenomena also depend on the lattice geometry, in particular on the number of interacting neighbours. It is also possible to assign a 'dimensionality' to the magnetic lattice. For instance, if the magnetic interactions occur predominantly between spins arranged in relatively isolated chains, the lattice dimensionality is one, whereas for spins interacting in well-separated planes, the lattice dimensionality is two. If such isolated subsystems do not exist, obviously the lattice dimensionality is three.
In view of the multiplicity of these factors, it is not astonishing that a great variety of magnetic ordering phenomena exists, even for the relatively simple systems to which the following experiments have been restricted. The purpose of this thesis is to contribute to a better understanding of this multitude of phenomena, and to obtain information about the interactions (their form and their strength). The choice of the magnetic compounds is based mainly on the following criteria:
1. sufficiently well-known single ion properties,
2. relatively simple geometry of the *magnetic* ion sublattice, and
3. sufficiently weak magnetic interactions.

In chapter II, several numerical methods will be discussed, which in many cases can be used for the analysis of the experimental data, such that the character of the interactions may become clear. The later chapters will treat experiments with such magnetic systems and their interpretation.
The simplest form of magnetic interaction between a pair of magnetic ions is that of the Ising type. In chapter III, experimental results on rubidium cobalt chloride will be discussed, which are in complete agreement with the theory for the three-dimensional simple cubic Ising model for exchange interactions between nearest neighbours. Experiments on the isomorphous manganese compound Cs_3MnCl_5 have shown that this is a good example of the three-dimensional Heisenberg model, in which all three spatial components of neighbouring spins participate equally in the interactions. This compound, together with other manganese double chlorides, will be treated in chapter V. All these systems behave very differently from the Ising system discussed in chapter III.
In addition to magnetic dipole-dipole and exchange interactions, other interaction mechanisms also exist. For instance, electrical quadrupole-quadrupole (EQQ) interactions, or interactions via the crystal lattice (virtual phonon exchange, VPE) cause another type of coupling among magnetic moments. The EQQ and VPE couplings, however, are very weak in general, and they can be better investigated in the rare earth (4f) compounds, since exchange interactions in these compounds are much smaller than in the compounds of the iron group (3d) metals. Such interactions have been observed in the rare earth ethylsulfates, and appear to be strongest in cerium ethylsulfate. This substance is investigated in chapter IV. Since interactions in cerium ethylsulfate are at least one order of magnitude smaller than those in the other substances investigated here, experimental methods were used, which were not

applied in the other chapters. These methods involved direct demagnetization of the sample, and were applied at such low temperatures that no temperature equilibrium could be established between sample and thermometer. It is found that the interaction between nearest neighbouring cerium ions has a very remarkable form. The angular dependence resembles that of magnetic dipole interactions, but is of opposite sign. The interactions are found to occur predominantly in linear chains.

As already noted, rare earth compounds are characterized by much weaker exchange interactions than in comparable iron group compounds, and thus by the possibility of observation of further interaction types. If no data concerning these interactions are known beforehand, one should restrict oneself to systems having a simple geometry. In this respect, the rare earth double oxides of the pyrochlore structure, which are discussed in chapter VI, are good examples. The interactions with the 6 nearest neighbours are determined by the same parameters, and any further interacting neighbours are at least at twice the n.n. distance. For this reason, interactions with further neighbours are relatively weak, and the magnetic behaviour of these substances is mainly determined by nearest neighbour interaction. The geometry of the pyrochlore compounds is simpler than that of the rare earth oxides, and comparable to that of the rare earth garnets. Since the crystal structure of the pyrochlore compounds strongly influences the magnetic and caloric behaviour, calculations are given which relate experimentally observable quantities to the interaction strength for a few simple interaction types. The behaviour is then found to be strongly dependent on the spin dimensionality and the sign of the interaction. The experiments show the existence of compounds which obey reasonably well the behaviour that is expected for the pyrochlore Ising ferro- and antiferromagnet.

Summarizing: Sixteen magnetic compounds, exhibiting marked differences in spin dimensionality and lattice structure, are studied in this thesis. The experimental results, particularly on the heat capacity, provide valuable information concerning the magnetic interactions in those compounds.

CHAPTER I

THE EXPERIMENTAL TECHNIQUE

1. *Introduction*

Measurements at temperatures appreciably below that of liquid He require a technique which is rather different from that used at higher temperatures. This technique has a specific character which is determined by the thermal behaviour (specific heat, heat conductivity) of materials at these low temperatures. These properties differ markedly from those found, for instance, at room temperature. The so-called Fermi temperatures (of 'free electron gases' in normal metals) and Debye temperatures (of crystal lattices) are generally very large compared to 1 K. As a consequence, the number of thermally excited electrons in a normal metal is proportional to the temperature, and in a lattice the number of excitations is proportional to the third power of the temperature. Therefore, the specific heat of conduction electrons in metals, and of lattice vibrations are also proportional to T and T^3 respectively. Since the number of thermal excitations below 1 K is so small that scattering among excitations is unimportant, the heat conductivities of these systems also have a behaviour proportional to T and T^3.

Below 1 K, the (molar) electron and lattice heat capacities are very small compared to the gas constant R, in contrast to the values found at room temperature, which are generally in the order of magnitude of R. At these low temperatures, thermal boundary (Kapitza) resistance occurs between materials which are in mechanical contact with each other. The thermal boundary resistance is proportional to T^3. Among these conductivities, that of a normal metal decreases least rapidly with decreasing temperature. Hence metals are suitable for heat contact purposes at very low temperatures. In fact, the thermal resistance of a metal becomes negligible at sufficiently low T ($\approx$ 0.1 K), if contact and lattice resistances are connected in series, even with maximum contact areas. Further, the lattice conductivity of crystalline materials is much better than that of amorphous materials such as perspex, nylon, graphite and cotton. The latter materials can be utilized as mechanical support of those parts of an apparatus which should be thermally isolated.

Magnetic compounds may exhibit rather different heat capacities, in addition to the above mentioned contributions at low temperatures. Magnetic interactions can cause a large contribution to the heat capacity, of the order of R. Such contributions are encountered in the samples to be investigated, and they are utilized in cooling salts. These cooling salts consist of a paramagnet (at 1 K) which is usually isothermally magnetized at about 1 K and

subsequently adiabatically demagnetized into a magnetically ordered state (due to conservation of entropy) at a temperature far below 1 K. Due to the high heat capacity of the cooling salt at these low temperatures, a considerable amount of heat can be absorbed before the cooling salt is again 'warm' (≈ 1 K). Hence such a cooling salt can be used for the purpose of cooling a calorimeter to low temperatures.

2. *The demagnetization setup used for calorimetry*

The operation of a demagnetization apparatus and a calorimeter such as used here has earlier been described by Miedema[1,2]), Van Kempen[3]) and Wielinga[4]), and will be discussed here only briefly. A liquid helium cryostat, in conjunction with an iron core electromagnet provides the combination of low temperatures (≈ 1 K) and a strong magnetic field (≈ 20 kOe) required for adiabatic demagnetization. Inside the He dewar of the cryostat there was a vertical glass tube of 35 mm diameter and 50 cm length (fig. 1), which was connected to a high vacuum pump. At the lower end of the tube, a glass joint was mounted, in order to

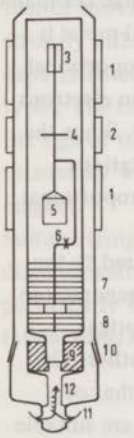

Fig. 1. A schematic picture of the apparatus in the liquid helium dewar. The vertical scale is three times more compressed than the horizontal scale in order to obtain a figure of reasonable dimensions. The meaning of the numbers is as follows: 1) susceptibility coil system, 2) heater coil, 3) susceptibility thermometer, 4) eddy current heater, 5) sample, 6) heat switch, 7) cooling salt for the calorimeter, 8) cooling salt for the thermal guard tube, 9) guard cooling salt, 10) glass joint, 11) electrical connections, 12) thin glass tube.

make the tube accessible. At the bottom of the male part of the joint stood a small glass tube with on its end the usual guard cooling salt. This guard salt should prevent most of the heat leak from the He bath via the small glass tube. On the guard salt a 24 mm diameter quartz tube was fixed concentrically in the 35 mm diameter tube. This quartz tube was cooled by

means of a second guard salt and coil foil glued onto the tubes outer surface, which served as a thermal screen to absorb most of the heat leak. Further, inside this guard tube were the main cooling salt (a), and the 'calorimeter', consisting of the sample (b), the heater (c), the thermometer (d) and the metal system (e). The cooling salt was thermally connected to the metal system via a heat switch. These components were fixed inside the guard tube by means of cotton threads.

3. *The cooling salt and the components of the calorimeter*

a. The cooling salt consisted of slices of chromium potassium alum single crystal which were clamped between brass plates, and screwed onto a central copper axis. Heat contact between the brass and the alum was improved by silicon grease. Heat contact between the brass plates and the copper axis was established by mechanical forces on the screw thread.
b. In most cases, the sample consisted of a finely powdered substance mixed with silicon grease. The mixture was brought into a small metal or perspex cylinder. A brush, consisting of many electrically insulated (in order to decrease eddy currents) copper wires was inserted for heat contact.
c. Heat input was provided either by a joule heater, or by an eddy current heater. The joule heater consisted of a manganin wire resistor of about 1 kΩ wound onto a 1 mm copper wire. The resistance of the heater was measured at low temperatures, and the heat input was directly found from the current which was led through the heater. Concerning the other method, eddy currents were generated in a copper ring by an alternating magnetic field, which was produced by a coil system around the 35 mm diameter glass tube. The heat input was proportional to the square of the current through the coil system. A calibration was obtained by a comparison of the heat input to that of the joule heater, and by measurements of a sample having a known heat capacity, namely terbium metal. For this heat capacity, we have taken experimental data of Anderson *et al.*[5]). Both calibrations gave identical results.
d. During the experiments, two types of thermometers have been used: magnetic and resistance thermometers. Of these, we shall first discuss the magnetic thermometers. These consisted of slices of paramagnetic material, glued between thin brass plates. A constant mechanical pressure was applied by thin nylon threads wound around the thermometer. In many cases, cerium magnesium nitrate (CMN) was used as thermometer material. A small amount of Cu was substituted for Mg in order to improve the spin-lattice heat contact[6,7]). Measurements of *e.g.* Mess *et al.*[8]) have shown that CMN follows a Curie-Weiss law down to very low temperatures. Parameters describing the Curie-Weiss law are found by calibration at liquid He temperatures. Thus susceptibility measurements of the thermometer provided a measure for the temperature. In other cases, cobalt cesium sulfate (CCS) was used as a thermometer. CMN has the advantage that its magnetic specific heat is less than 1% of that of CCS, and it obeys the Curie-Weiss law down to much lower temperatures. The advantage of CCS is that it has a higher sensitivity. This is important at relatively high temperatures,

where magnetic thermometers are the least sensitive. The susceptibility of the CCS thermometer was calibrated to the susceptibility of CMN, which showed that the CCS thermometer followed within experimental accuracy a Curie law at temperatures above 0.2 K. Even after thermally recycling many times to room temperature, it was found that the heat contact of thermometers of the above construction had not decreased substantially.
As a resistance thermometer, use was made of either carbon or germanium, the latter mainly at temperatures near 1 K, and the former at lower temperatures down to about 0.05 K. Carbon resistors have the advantage of having only a small sensitivity to a magnetic field (see Edelstein[9]) and Haasbroek[10])), which was particularly important for the experiments described in chapter IV. Further, the heat capacity of resistance thermometers is much lower than that of magnetic thermometers. A calibration of these resistance thermometers above 1 K was obtained by measurement of the He vapor pressure in the cryostat. Below 1 K, the resistance was calibrated to a CMN thermometer. For the purpose of interpolation and data handling by a computer, a polynomial in the logarithm of the resistance was fitted to the inverse temperature, so that the temperature could be computed from the resistance readings.
e. The metal system consisted of 1 or 1.5 mm diameter copper wires, which thermally connected the various parts of the calorimeter. The metal system was further connected via a heat switch to the cooling salt. This heat switch consisted of one or more ca. 0.3 mm diameter Sn or Pb wires. Since these metals are superconducting below He temperatures, electrons do not contribute to the heat conductivity, and heat transport is confined to the lattice. Thus the conductivity has T^3 temperature dependence and becomes very small at low temperatures. If a magnetic field of a few hundred Oe is applied, however, the metal returns to the normal state, and the electrons contribute to the heat transport again. This contribution is, at low temperatures, much larger than that of the lattice. Application of a magnetic field renders the heat switch conducting, in order to cool down the calorimeter by means of the cooling salt.

4. *The coil systems*

For the purpose of susceptibility measurements, coils are wound around the 35 mm glass tube (fig. 1). A primary coil supplies a 220 Hz alternating field at the sample or the magnetic thermometer. The magnetization due to this field is detected by a secondary coil. The susceptibility of the sample thus gives a contribution to the mutual inductance of this coil system. In order to reduce a.c. pick up, the secondary coil was split into two identical sections wound in opposite directions. The position of the sample is thus not in the centre of the coil system, but in one of the secondary sections. For the purpose of reducing the influence of other components of the apparatus, the primary and secondary coils were constructed such that the field due to a current through the coils decreased rapidly outside the coils. Particularly at the position of the cooling salt, which has a much larger volume than the sample, the sensitivity of the coil system should be very small. In practice the cooling salt was placed at

a distance of at least 8 cm off the center of a coil system, where the sensitivity was smaller by a factor of at least one million than at the position of maximum sensitivity.
Two such coil systems were mounted around the 35 mm tube, one for the susceptibility thermometer and one for the sample. Further, a coil was added for energizing the eddy current heater. Since the position of the copper ring was not precisely the same in each experiment, the heater coil was constructed in such a way that its field was constant within 2‰ over a distance of 9 mm. At somewhat larger distances, the field was made to decrease rapidly to about 1% at 25 mm from the coil centre. This arrangement was chosen as to reduce eddy current heating in other metal parts of the apparatus.

5. *Susceptibility measurements*

Signals from the secondary susceptibility coils were detected by means of a Hartshorn mutual inductance bridge. The principle of this method is that the mutual inductance of the susceptibility coil system is compensated by a variable mutual inductance. The out-of balance signal of the bridge was amplified and fed to a recorder. Out-of phase signals could be compensated by an auxiliary resistance network. A contribution to these 90 degree out-of phase signals arises if the sample exhibits hysteresis or relaxation effects (a non-zero χ''). The reading of this off-phase network is referred to as 'a.c. losses'.
The mutual inductance of the Hartshorn bridge is expressed in units called bridge turns, to be denoted by n. Hence, the relation between the molar susceptibility of the sample, χ, and n has the form

$$n - n_0 = a\chi \qquad (1)$$

where n_0 is the extrapolated bridge reading at infinite temperature, and a is a constant that is proportional to the sample volume and the sensitivity of the apparatus. The absolute accuracy of a is poor, in view of the lack of a precise determination of the position of the sample in the coil system. The determination of n_0 may present problems, since measurements of n above liquid He temperature are liable to inaccuracy due to thermal deformation of the susceptibility coil systems. In fact, the bridge reading was very sensitive to mechanical deformation. Therefore care has been taken to wind the coils as tightly as possible, avoiding open spaces.

6. *The determination of n_0*

In order to interpret susceptibility data, knowledge of n_0 is necessary. Since n_0 is not reproducible through thermal deformation, its value had to be found for each experiment. This is possible *e.g.* if one may assume that $\chi = 0$ for a certain bridge reading, which situation occurs *e.g.* in chapter III. Further, if the sample (or thermometer) follows the Curie law,

combination with eq. (1) gives

$$n - n_0 = h/T$$

where h is the product of a and the molar Curie constant. Then n_0 is simply found by a plot of n *vs* $1/T$ and extrapolation to $1/T = 0$.

If the sample obeys a Curie-Weiss relation, and the Curie-Weiss constant θ is unknown, the method is somewhat less simple. The relation between n and T is now written as

$$n - n_0 = h/(T - \theta). \tag{2}$$

Hence three constants, n_0, θ and h must be found from the experimental relation between n and T. For this purpose, one can calculate the quotient $\Delta n/\Delta T$ between successive data points. If eq. (2) is valid, this quotient is in first order approximation:

$$\frac{\Delta n}{\Delta T} \approx \frac{dn}{dT} \approx -\frac{(n - n_0)^2}{h} \quad \text{or} \quad |n - n_0| \approx \sqrt{|h|}\,\sqrt{|\,\Delta n/\Delta T\,|} \tag{3}$$

where n stands for the average of the two values which bound the interval. One then can estimate n_0 and h by plotting $\sqrt{|\Delta n/\Delta T|}$ *versus* n and extrapolating to the abscissa. When n_0 is known to a first approximation, one can include higher order terms:

$$|n - n_0| \approx \sqrt{|h|}\,\sqrt{|\Delta n/\Delta T|}\,\left[1 + \frac{(n - n_0)^2\,(\Delta T)^2}{8\,h^2}\right] \tag{4}$$

and now n_0 is derived more accurately from a plot of

$$\sqrt{|\Delta n/\Delta T|}\,\left[1 + \frac{(n - n_0)^2\,(\Delta T)^2}{8\,h^2}\right]$$

versus n. The linearity of this plot is a test of the validity of the Curie-Weiss relation. Knowing n_0 enables one to obtain the Curie-Weiss constant θ by plotting $1/(n - n_0)$ *versus* T, and the Curie constant is obtained as well.

7. *Heat capacity measurements*

After demagnetization of the cooling salts, the heat switch was closed in order to cool the sample. Subsequently, after opening the heat switch, the thermometer signal was continuously recorded. When the temperature behaviour had become reasonably linear in time, a discrete amount of heat input was applied. The thermometer signal was recorded again until it was linear over a sufficiently long period of time. A part of such a temperature recording, and the extrapolation to the middle of the heating period (solid line) are shown in fig. 2. Thus the effective temperature increase due to the known heat input was obtained. From these data the heat capacity of the calorimeter could be calculated.

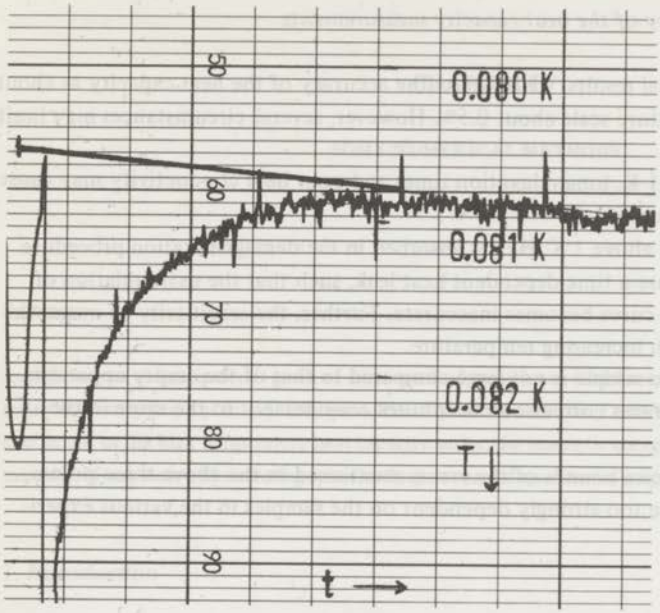

Fig. 2. A typical recording of a susceptibility thermometer after heating. The temperature scale is indicated in the figure. The full horizontal time scale corresponds to about 10 minutes. The full line is the extrapolation of the average calorimeter temperature to the middle of the heating period.

In general the sample mass was in the order of 1 g. The mass of the other parts of the calorimeter (the empty apparatus), such as grease, copper brush, metal system, heater and thermometer, was about 20 g. Thus the sample mass was only about 5% of the calorimeter. If the molar heat capacity of this sample was in the order of R, the empty apparatus contribution to the total heat capacity of the calorimeter was, generally speaking, a few percent. However, at temperatures where the sample heat capacity is small, the empty apparatus heat capacity becomes very important. Therefore, this heat capacity was measured in separate experiments. Metals and other solids are expected to give contributions proportional to T and T^3 to the heat capacity. From the thermometer, one may expect a magnetic contribution proportional to T^{-2}. However, the empty apparatus heat capacity, c_{empty}, could not be well fitted by a linear expression of three of these terms. This may be due to non-T^{-2} behaviour of the magnetic thermometer, such as observed in pure CMN[6]). A good fit was obtained by an expression

$$c_{\text{empty}} = a_1 T^{-2} + a_2 T^{-1} + a_3 + a_4 T + a_5 T^3$$

This expression provided an efficient method for the calculation of the empty apparatus correction during the processing of the experimental data.

8. *The experimental accuracy of the heat capacity measurements*

For most of our experimental results, we estimate the accuracy of the heat capacity as about 1%, and that of the temperature scale about 0.5%. However, several circumstances may limit the accuracy:

1. At temperatures below 0.1 K, long relaxation times and poor heat conductivity may cause long thermal equilibrium times.
2. At temperatures near and above 1 K, He gas absorbed in the demagnetization procedure may come free and then cause a time dependent heat leak, such that the extrapolation of the temperature *versus* time curve becomes inaccurate. Further, the sensititvity of magnetic thermometers decreases with increasing temperature.
3. If the heat capacity of the sample is not large compared to that of the empty apparatus, the error in the empty apparatus correction contributes considerably to the error in the result.

It is not possible to give precise bounds of the errors mentioned in the above three points, since these circumstances are too strongly dependent on the samples in the various experiments.

9. *The heat leak*

At low temperatures, a constant heat leak of about 0.15 erg/sec was measured. This may be due to residual gas and radiation not trapped by the guard tube, and perhaps vibrations from rotating pumps *etc*. Further, input of discrete heat portions varying from about 1 - 10000 erg were found to be due to strong 4 Hz vibrations of the soggy soil around the Kamerlingh Onnes Laboratory, generated by heavy traffic.

REFERENCES

1) Miedema, A.R., Thesis, University of Leiden, 1960.
2) Miedema, A.R., Wielinga, R.F. and Huiskamp, W.J., Physica **31** (1965) 1585.
3) Van Kempen, H., Thesis, University of Leiden, 1965.
4) Wielinga, R.F., Thesis, University of Leiden, 1968.
5) Anderson, A.C., Holmström, B. and Krusius, H., Phys. Rev. Letters **20** (1968) 154.
6) Lubbers, J., private communication.
7) Miedema, A.R., private communication.
8) Mess, K.W., Thesis, University of Leiden, 1969.
9) Edelstein, A.S. and Mess, K.W., Physica **31** (1965) 1707.
10) Haasbroek, J.N., Thesis, University of Leiden, 1971.

CHAPTER II

SOME NUMERICAL METHODS

Summary

In this chapter a description is given of some methods which are used for calculations of physical quantities for systems of interacting spins. These quantities are: the Curie-Weiss constant, the T^{-2} coefficient in the high temperature heat capacity series, the magnetic energy at $T = 0$, and the heat capacity of a system of interacting spins in the presence of an external magnetic field.

1. *Introduction*

Although precise theoretical predictions exist for the thermal and magnetic behaviour of several simple lattices containing magnetically interacting spins, for many magnetic systems such theories are not available. Fortunately it is possible to calculate several quantities for less simple systems. Procedures will be given for the calculation of the high-temperature asymptotic behaviour of the heat capacity (section 4) and of the Curie-Weiss constant (section 5). Such calculations have already been described by Van Vleck[1]) and Daniels[2]). Furthermore, classical methods will be given to derive the magnetic energy at zero temperature (sections 6 and 7). One method is that described by Luttinger and Tisza[3]). An essential part of all these methods consists of lattice summations, the convergence of which will be discussed. An approximative method, resembling the Bethe-Peierls-Weiss[4,5,6]) method to calculate the energy and heat capacity as function of temperature for a system of spins having interactions of the Ising type in the presence of a magnetic field, will be discussed in section 9. Finally, numerical results of the formalism of Yang and Yang[15]) for the ground state energy of anisotropic linear chains will be derived in section 10.

2. *The hamiltonian*

In describing the properties of the magnetic spins, in particular their interactions, we use mainly the notation of Daniels[2]), which we shall generalize to cases $s > \frac{1}{2}$. The g tensor of the i-th ion will be denoted by $g_{i\alpha\beta}$. The Greek suffixes have values 1, 2 or 3, and refer to the cartesian coordinate axes x, y or z respectively. The dummy suffix summation convent-

ion will be used for indices being of the Greek type. Hence we can write for the magnetic moment $\boldsymbol{\mu}_i$ of a spin i:

$$\mu_{i\alpha} = \mu_B g_{i\alpha\beta} s_{i\beta} ,$$

if the $s_{i\beta}$ are the spatial components of the spin labeled i. In gaussian units, the dipole-dipole interaction between spins i and j can now be written as

$$\mathcal{H}_{ij}^{dip} = \frac{\mu_B^2}{r_{ij}^3} \left(g_{i\alpha\beta} g_{j\gamma\beta} s_{i\alpha} s_{j\gamma} - \frac{3}{r_{ij}^2} g_{i\kappa\lambda} g_{j\mu\nu} r_{ij\lambda} r_{ij\nu} s_{i\kappa} s_{j\mu} \right). \tag{1a}$$

Here μ_B is the Bohr magneton, $r_{ij\alpha}$ the vector connecting the lattice positions i and j, and r_{ij} the length of this vector. If we define

$$T_{ij\alpha\beta} = \frac{\mu_B^2}{r_{ij}^3} \left(g_{i\alpha\gamma} g_{j\beta\gamma} - \frac{3}{r_{ij}^2} g_{i\alpha\lambda} g_{j\beta\nu} r_{ij\lambda} r_{ij\nu} \right) , \tag{1b}$$

we can write

$$\mathcal{H}_{ij}^{dip} = T_{ij\alpha\beta} s_{i\alpha} s_{j\beta} . \tag{1c}$$

Other types of bilinear spin-spin interactions can also be written in this form (see *e.g.* chapter VI, section 2):

$$\mathcal{H}_{ij}^{nondip} = J_{ij\alpha\beta} s_{i\alpha} s_{j\beta} . \tag{2}$$

Hence we shall write spin-spin interactions in the form

$$\mathcal{H}_{ij} = K_{ij\alpha\beta} s_{i\alpha} s_{j\beta} , \tag{3a}$$

$$K_{ij\alpha\beta} = T_{ij\alpha\beta} + J_{ij\alpha\beta} . \tag{3b}$$

The Zeeman interaction of a magnetic spin i is expressed by:

$$\mathcal{H}_i^Z = \mu_B H_\alpha g_{i\alpha\beta} s_{i\beta} = H_\alpha G_{i\alpha\beta} s_{i\beta} , \tag{4a}$$

where $G_{i\alpha\beta} = \mu_B g_{i\alpha\beta}$ (4b)

Hence the hamiltonian of a macroscopic system of N spins becomes

$$\mathcal{H} = \sum_{(ij)} K_{ij\alpha\beta} s_{i\alpha} s_{j\beta} + \sum_k H_\lambda G_{k\lambda\mu} s_{k\mu} . \tag{5}$$

Here (ij) means that during the summation, each pair of spins is counted once.

3. *The partition function*

For a calculation of observable physical quantities, we start from the partition function

$$Z = \sum_i \exp.(-E_i / kT),$$

where the summation is over the $(2s+1)^N$ energy levels. The computation of these levels can be circumvented by writing this expression as

$$Z = \mathrm{Sp}[\exp(-\mathcal{H}/kT)] = \sum_{j=0}^{\infty} \frac{1}{j!} \mathrm{Sp}[(-\mathcal{H}/kT)^j] , \tag{6}$$

which is independent of representation. If we substitute eq. (5) for $\mathcal{H}$ in this expression, it will be found that the second term is zero, since it contains s_{ia} only to the first power. Using this result, we find the first terms in the high temperature series expansion of the entropy S:

$$S/R = \frac{1}{N}\frac{\partial}{\partial T}(T \ln Z) = \ln(2s+1) - \frac{(2s+1)^{-N}\mathrm{Sp}(\mathcal{H}^2)}{2Nk^2T^2} + \frac{(2s+1)^{-N}\mathrm{Sp}(\mathcal{H}^3)}{3Nk^3T^3} + \ldots \tag{7}$$

The high temperature expansion of the susceptibility can also be found from Z. We shall define the susceptibility $\chi_{\alpha\beta}$ as the quotient of the magnetization component M_α in the α direction and the small magnetic field H_β in the β direction, which causes the magnetization. We can find $\chi_{\alpha\beta}$ from the equation

$$\chi_{\alpha\beta} = kT \frac{\partial}{\partial H_\alpha} \frac{\partial}{\partial H_\beta} (\ln Z).$$

Substituting eq. (6) gives the first terms of the series for $\chi_{\alpha\beta}$:

$$\chi_{\alpha\beta} = \frac{(2s+1)^{-N}\frac{\partial}{\partial H_\alpha}\frac{\partial}{\partial H_\beta}\mathrm{Sp}(\mathcal{H}^2)}{2kT} - \frac{(2s+1)^{-N}\frac{\partial}{\partial H_\alpha}\frac{\partial}{\partial H_\beta}\mathrm{Sp}(\mathcal{H}^3)}{6k^2T^2} + \ldots \tag{8}$$

4. *The asymptotic high temperature behaviour of the specific heat*

By relating the expansion of the entropy to that of the heat capacity c, one finds from eq. (7) for high temperatures

$$cT^2/R = \frac{(2s+1)^{-N}\mathrm{Sp}(\mathcal{H}^2)}{Nk^2}$$

If no magnetic field is present, we can use the hamiltonian defined by eqs. (1) tot (3). Using well-known trace theorems, we derive

$$\mathrm{Sp}(\mathcal{H}^2) = \mathrm{Sp}[(\sum_{(ij)} K_{ij\alpha\beta}s_{i\alpha}s_{i\beta})^2] = \tfrac{1}{9}s^2(s+1)^2(2s+1)^N \sum_{(ij)} (K_{ij\alpha\beta}K_{ij\alpha\beta}) .$$

If all spins are equivalent, we can take one arbitrary ion i and the expression reduces to

$$\mathrm{Sp}(\mathcal{H}^2) = \frac{N}{18}(2s+1)^N s^2(s+1)^2 \sum_{j=1}^{N} (K_{ij\alpha\beta}K_{ij\alpha\beta}) ,$$

and the T^{-2} coefficient becomes

$$c\,T^2/R = \frac{s^2(s+1)^2}{18k^2} \sum_{j=1}^{N} (K_{ij\alpha\beta}K_{ij\alpha\beta}) \tag{9}$$

If the K tensors are known, this expression can be calculated. If the magnetic ions are not equivalent, a summation over inequivalent ions i must be applied.

Nondipolar spin-spin interactions are in general confined to a few neighbours lying within a distance of about 10 Å. Dipolar interactions are proportional to r^{-3}, if r is the distance separating the interacting spins. Hence the terms in eq. (9) are proportional to r^{-6}. The number of magnetic spins in a shell between radii r and $r+\mathrm{d}r$ is proportional to $r^2\mathrm{d}r$, and the contribution to eq. (9) will be proportional to $r^{-4}\mathrm{d}r$. When we calculate the sum for all neighbours lying within a distance r, the sum will depend on r by a term proportional to r^{-3}. Apparently the sum converges rapidly, and thus is shape independent for a macroscopic crystal.

However, in order to calculate the right-hand side of eq. (9) with reasonable accuracy, the sum must include hundreds of magnetic neighbours j, and for each j, the $K_{ij\alpha\beta}$ elements must be calculated. Therefore the use of a digital computer is a powerful aid in these calculations, and a summation over thousands of neighbours can be carried out in a short time.

The convergence can further be improved by replacing the sum outside the sphere having radius r' by an integral. This procedure is discussed in appendix I.

Results of the calculations of T^{-2} coefficients are given in chapters III to VI.

5. *The susceptibility*

We can write expansion (8) as

$$\chi_{\alpha\beta} = \frac{C_{\alpha\beta}}{T} + \frac{C'_{\alpha\beta}}{T^2} \tag{10}$$

if we introduce

$$C_{\alpha\beta} = \frac{(2s+1)^{-N}}{2k} \frac{\partial}{\partial H_\alpha} \frac{\partial}{\partial H_\beta} \mathrm{Sp}(\mathcal{H}^2), \quad \text{and} \tag{11}$$

$$C'_{\alpha\beta} = -\frac{(2s+1)^{-N}}{6k^2} \frac{\partial}{\partial H_\alpha} \frac{\partial}{\partial H_\beta} \mathrm{Sp}(\mathcal{H}^3)\,. \tag{12}$$

Substituting eq. (5) into eq. (8), we need only consider terms in $\mathrm{Sp}(\mathcal{H}^2)$ that are dependent on H_α and H_β. Further, it is easy to see that the trace of the cross term between the spin-spin part and the Zeeman part vanishes. Thus the following trace must be calculated:

$$\mathrm{Sp}\Big(\sum_i \sum_j H_\kappa H_\mu G_{i\kappa\lambda} G_{j\mu\nu} s_{i\lambda} s_{j\nu}\Big) = \mathrm{Sp}\Big(\sum_i H_\kappa H_\mu G_{i\kappa\lambda} G_{i\mu\nu} s_{i\lambda} s_{i\nu}\Big) =$$

$$= -\tfrac{1}{3}(2s+1)^N s(s+1) \sum_i H_\kappa H_\mu G_{i\kappa\lambda} G_{i\mu\lambda} \,.$$

Hence, if all spins are equivalent, we derive

$$C_{\alpha\beta} = \frac{Ns(s+1)}{3k} G_{i\alpha\lambda} G_{i\beta\lambda} \,, \tag{13}$$

and otherwise we find $C_{\alpha\beta}$ by a summation over inequivalent ions i. This first term in the susceptibility series represents the Curie law, and $C_{\alpha\beta}$ is the Curie constant. For a further approximation we have to find $C'_{\alpha\beta}$. For small fields, we have to evaluate the field-independent part of $C'_{\alpha\beta}$, which follows from the terms in $\mathrm{Sp}(\mathcal{H}^3)$ which are quadratic in the field components. Thus we have to evaluate

$$3\mathrm{Sp}\Big(\sum_{(ij)} \sum_l \sum_m K_{ij\alpha\beta} G_{l\kappa\lambda} G_{m\mu\nu} H_\kappa H_\mu s_{i\alpha} s_{j\beta} s_{l\lambda} s_{m\nu}\Big) =$$

$$6\mathrm{Sp}\Big(\sum_{(ij)} K_{ij\alpha\beta} G_{i\kappa\lambda} G_{j\mu\nu} H_\kappa H_\mu s_{i\alpha} s_{j\beta} s_{i\lambda} s_{j\nu}\Big) = \tfrac{2}{3}(2s+1)^N s^2(s+1)^2 K_{ij\alpha\beta} G_{i\kappa\alpha} G_{j\mu\beta} H_\kappa H_\mu \,.$$

We obtain, if all spins are equivalent,

$$C'_{\alpha\beta} = -\frac{Ns^2(s+1)^2}{9k^2} \sum_{j\neq i}^{N} K_{ij\mu\nu} G_{i\alpha\mu} G_{j\beta\nu} \,, \tag{14}$$

and if inequivalent spins exist in the lattice, we obtain $C'_{\alpha\beta}$ by summation over the inequivalent spins labeled i. From expansion of the Curie-Weiss law

$$\chi = C/(T-\theta) = C/T + \theta C/T^2 + \ldots \tag{15}$$

one can see that the Curie-Weiss constant is given by the quotient of the coefficients of the second and first terms. We now define a unit vector h_α along the direction in which the infinitesimal measuring field is applied, and a unit vector m_β along the direction of magnetization measurement. The Curie-Weiss constant is then, according to eq. (15), given by

$$\theta = (C'_{\alpha\beta} h_\alpha m_\beta)/(C_{\mu\nu} h_\mu m_\nu).$$

The calculation of $C_{\mu\nu}$ is simple, but that of $C'_{\alpha\beta}$ in general requires summation over many interacting neighbours, and can better be programmed for a computer. As in section 4, it is useful to divide the calculation in two parts: a summation inside a sufficiently large sphere and an integration over a hypothetical continuum outside that sphere, where only long range dipolar forces are important. From eq. (1b), one expects a contribution proportional to $\mathrm{d}r/r$ from a spherical shell between radii r and $r+\mathrm{d}r$, and one might expect that the integral diverges for $r \to \infty$. However, the proportionality constant is zero as a consequence of angular cancellation. For a spherical sample, the integral thus vanishes, but otherwise the integral has to be evaluated. If we choose the radius of the spherical surface sufficiently large,

we may write the sum in eq. (14) as:

$$\sum_{j=1}^{m} \Big(\sum_{h,k,l} \frac{\delta_{\lambda\kappa}}{r_{ij'}^3} - \frac{3 r_\lambda r_\kappa}{r_{ij'}^5} \Big) G_{i\alpha\mu} G_{i\lambda\mu} G_{j\kappa\nu} G_{j\beta\nu} \ ,$$

where j' is the lattice site found by a translation of site j by

$$r_{ij'} = r_{ij} + ha + kb + lc$$

where h, k and l are integers and a, b and c are the axes of the crystallographic unit cell which contains m spins. If we consider the volume of summation as a continuum, the term between brackets can be replaced by an integral. From well-known electromagnetic theory, it is known that for a class of surfaces bounding the integration volume (spherical, ellipsoidal, infinitely long or infinitesimally flat) this integral is not dependent on the position inside the inner surface. The integral equals $-D_{\lambda\kappa}/V$, where V is the volume of the unit cell, and $D_{\lambda\kappa}$ the difference of the demagnetizing tensors of the inner spherical surface and the outer surface. Hence the contribution to $C'_{\alpha\beta}$ from spins outside the sphere amounts to

$$\frac{Ns^2(s+1)^2}{9k^2V} \sum_{j=1}^{m} D_{\lambda\kappa} G_{i\alpha\mu} G_{i\lambda\mu} G_{j\beta\nu} G_{j\kappa\mu} \ .$$

If the direction of the magnetization vector $M_\alpha = C_{\alpha\beta} H_\beta$ is along one of the principal axes of the demagnetizing tensor, we may replace that tensor by a scalar D. The contribution to $C'_{\alpha\beta}$ from spins outside the sphere can then be written

$$\frac{NDs^2(s+1)^2}{9k^2V} \sum_{j=1}^{m} G_{i\alpha\mu} G_{i\lambda\mu} G_{j\lambda\nu} G_{j\beta\nu} = \frac{D}{NV} C_{i\alpha\lambda} C_{\lambda\beta} \ ,$$

where $C_{i\alpha\lambda}$ is the Curie constant calculated for ion i only (eq. 13).
For the inner spherical surface, the contribution to the demagnetizing factor D amounts to $4\pi/3$, for a needle-shaped outer surface the contribution is zero (M_ν parallel to the major axis) and for a flat crystal (M_ν perpendicular to the plane of the crystal) it amounts to -2π. For a discussion about the convergence of the summation inside the sphere as a function of the radius, see section 8.

6. *The magnetic energy*

It is often useful to calculate the energy contribution due to dipolar interaction of an ordered spin system. For instance, this information is desired for deriving the dipolar anisotropy energy of a Heisenberg spin system (*e.g.* chapter V), and for Ising systems, one may be interested in the fraction of dipolar energy (*e.g.* chapter III). These energy calculations will be made in the classical approximation, which implies that the spins are considered as vectors s of length s having a definite orientation. This approximation is good if the anisotropy of the magnetic spins is strong, if the number of interacting neighbours of each

spin is high, and if the spin quantum number is high. In this approximation, the ionic magnetic moments are also considered as classical vectors given by

$\boldsymbol{\mu} = \mu_B g \cdot \boldsymbol{s}$.

The magnetic structures on the basis of which the energy was calculated, were all periodic, which means that a magnetic unit cell having axes a', b', c' exists, such that the magnetic lattice is invariant under translations $ha' + kb' + lc'$, where h, k and l are integers. In many cases, the axes of the magnetic cell coincide with those of the crystallographic cell. They should, however, not be confused with the crystallographic axes, since they are very different in other cases. The primes are added to avoid such confusion.

If the magnetic cell contains m spins, the magnetic structure is given by a set of m magnetic moment vectors $\boldsymbol{\mu}_i$. The dipolar energy per gram ion of an ordered crystal is now given by

$$E/R = \frac{1}{2mk} \sum_{i=1}^{m} \sum_{j \neq i}^{N} \left\{ \frac{\boldsymbol{\mu}_i \cdot \boldsymbol{\mu}_j}{r_{ij}^3} - 3 \frac{(\boldsymbol{\mu}_i \cdot \boldsymbol{r}_{ij})(\boldsymbol{\mu}_j \cdot \boldsymbol{r}_{ij})}{r_{ij}^5} \right\} = - \frac{1}{2mk} \sum_{i=1}^{m} \boldsymbol{\mu}_i \cdot \boldsymbol{H}_i ,$$

where $\boldsymbol{H}_i$ is the molecular field at site i, given by

$$\boldsymbol{H}_i = - \sum_{j \neq i}^{N} \left\{ \frac{\boldsymbol{\mu}_j}{r_{ij}^3} - 3 \frac{(\boldsymbol{\mu}_i \cdot \boldsymbol{r}_{ij}) \boldsymbol{r}_{ij}}{r_{ij}^5} \right\} .$$

This field can be split into two contributions, one originating from neighbours inside a sufficiently large sphere, having radius r' (the convergence properties are equal to those in section 5) and a contribution from a hypothetical continuum outside the sphere:

$$\boldsymbol{H}_i = - \sum_{j \neq i;\ r_{ij} < r'}^{N} \left\{ \frac{\boldsymbol{\mu}_j}{r_{ij}^3} - 3 \frac{(\boldsymbol{\mu}_i \cdot \boldsymbol{r}_{ij}) \boldsymbol{r}_{ij}}{r_{ij}^5} \right\} - \frac{D}{V} \sum_{n=1}^{m} \mu_n \qquad (16)$$

The first term gives the summation inside the sphere. The second term is zero for antiferromagnetic structures. The factor D is the difference of the demagnetizing factors of the inner spherical surface $(4\pi/3)$ and of the outer surface. Since the energy of a macroscopic ferromagnetic crystal is minimal if it is split into long domains having zero demagnetizing factors, we may substitute $D = 4\pi/3$ in eq. (16). For a treatment of the convergence of the sum inside a sphere, see section 8.

We emphasize that nondipolar interactions were not included in this energy calculation. In simple cases, nondipolar contributions can easily be added, while in more complicated cases the ground state is not known in general, so that other methods must be applied (next section). Results of this type of dipolar energy calculations can be found in chapters III, IV and V.

7. *The magnetic structure*

In simple magnetic systems such as *e.g.* a simple cubic lattice having only nearest neighbour Ising interactions, it is easy to see which magnetic structure has the lowest energy, but for more complicated systems, this is in general not a trivial problem. In order to solve this problem, we first study the behaviour of an isolated spin s, having quantumnumber s in a magnetic field H at T=0. The Zeeman hamiltonian for this system is

$$\mathcal{H} = -\mu_B H_\alpha g_{\alpha\beta} s_\beta .$$

We now introduce $h_\beta = \mu_B H_\alpha g_{\alpha\beta}$, which may be considered as an effective field acting on s, and new coordinate axes x' y' z' with z' along $\boldsymbol{h}$. The hamiltonian then reduces to $-h_z' s_z'$. The lowest eigenstate is that one having $s_z' = +s$. Hence the expectation value of s is given by

$$\langle s_\alpha \rangle = s h_\alpha / \sqrt{h_\beta h_\beta} \qquad (17)$$

This result was derived in coordinate system x'y'z' but is, of course, valid in all cartesian coordinate systems. The classical approximation which we will use, implies that the electronic spin is considered as a classical vector which equals the expectation value given in eq. (17). Since we are dealing with an assembly of spins, we add a Latin index to s, s_α and h_α, in order to distinguish between the different lattice sites. The $h_{i\alpha}$ follow from the hamiltonian given in eq. (3a):

$$h_{i\alpha} = \sum_{j \neq i} K_{ij\alpha\beta} s_{j\beta} , \qquad (18a)$$

and eq. (17) is now written as:

$$s_{i\alpha} = s_i h_{i\alpha} / \sqrt{h_\beta h_\beta} . \qquad (18b)$$

From eqs. (18), the $s_{i\alpha}$ can be solved in principle. However, a set of 3 N coupled equations is not tractable, and a simplification is introduced. We assume that the structure is periodic, such as described in section 6, and we choose a magnetic unit cell. This restriction can be alleviated since the influence of this choice on the result of the calculations can be demonstrated by repeating the procedure, starting from different cells. The gist of the method is that, if the cell contains m magnetic ions, we can describe the problem by 3 m coupled equations, which can be solved if m is not too large ($m \lesssim 32$), with help of a large digital computer. The magnetic cells are labeled by indices h, k and l. We choose the origin of our coordinate system at the origin of the cell labeled 0,0,0. In this cell we label the spins from 1 to m. Eqs. (18) can now, after some rearrangements, be written as:

$$\sum_{j=1}^{m} K'_{ij\alpha\beta} s_{j\beta} = c_i s_{i\alpha} \qquad (i = 1 \ldots m) , \qquad (19a)$$

$$c_i = \sqrt{\sum_j \sum_k K'_{ij\alpha\beta} K'_{ik\alpha\gamma} s_{j\beta} s_{k\gamma}} / s_i , \qquad (19b)$$

where

$$K'_{ij\alpha\beta} = \sum_{h,k,l;\, i \neq j'} K_{ij'\alpha\beta} \qquad (19c)$$

In expression (19c), j′ is the number of the spin whose position is determined by index j and the indices h, k, l, such as described in section 6. When we split the summation in eq. (19c) into a sum inside a sphere and an integration outside, and assume domain splitting for ferromagnets, we obtain the demagnetizing correction to $K'_{ij\alpha\beta}$. The condition under the summation sign in eq. (19c) excludes the term $K_{ii\alpha\beta}$ which is not desired. The c_i in eqs. (19) are proportionality constants. About the convergence of the lattice summation in eq. (19c), the same remarks as in section 5 can be made. By substitution of eq. (19a) in (19b), we obtain

$$s_i^2 = s_{i\alpha} s_{i\alpha} \,. \qquad (20)$$

This trivial result can be seen as a condition, the so-called strong constraint, which must be satisfied by solutions of eq. (19a), so that eq. (19b) is also satisfied. The energy of a spin configuration satisfying eqs. (19) is (per spin)

$$E/R = \frac{1}{2mk} \sum_{i=1}^{m} \sum_{j=1}^{m} K'_{ij\alpha\beta} s_{i\alpha} s_{j\beta} = \frac{1}{2mk} \sum_{i=1}^{m} c_i s_i^2 \,. \qquad (21)$$

Two methods will be applied to solve eqs. (19).

Method 1. The first method searches for solutions in which all c_i are identical, hence $c_i = c$. Thus the effective fields at all ionic sites are constrained to be equally strong, so that this method is in general only applicable to magnetic systems consisting of equivalent spins (equivalent in this sense, that all interactions in which these spins participate, are equally strong; this situation is realized if a crystallographic symmetry operation exists which transforms these spin sites into each other). Because the spin quantum numbers must be equal, they will be denoted by s. If we introduce new suffixes, according to

$$\left.\begin{aligned} s_u &= s_{i\alpha} \\ K'_{uv} &= K'_{ij\alpha\beta} \end{aligned}\right\} \qquad u = 3\,i + \alpha - 3, \quad v = 3\,j + \beta - 3,$$

we can write eq. (19a) as

$$\sum_{v=1}^{3m} K'_{uv} s_v = c s_u \,, \qquad (u = 1 \ldots 3m) \,. \qquad (22)$$

This is an eigenvalue equation which has 3m solutions. The corresponding eigenvalues will be denoted by c^u in order to obtain a notation different from that of c_i in eqs. (19). By summation of eq. (20), one finds

$$\sum_{u=1}^{3m} s_u s_u = m s^2 \,, \qquad (23)$$

the so-called weak constraint, which can always be satisfied by multiplying the s_u by a properly chosen constant. By a 'solution' of eq. (22) we shall from now on mean one which is normalized according to eq. (23). This does not, however, imply that the strong constraint (eq. 20) is also satisfied, and this must be checked for each solution of eq. (22). Degeneracy (different solutions of eq. (22) having equal c^u) can give complications. Even if 3m solutions of eq. (22) which also satisfy eq. (20) exist, it is often possible to form (new) solutions not satisfying eq. (20) by taking linear combinations of degenerate solutions. In that case, degenerate solutions obtained from eq. (22) by standard computer procedures, will in general not satisfy eq. (20), but properly chosen linear combinations will. Niemeyer[7,8]) has shown, that, if the magnetic unit cell consists of 2x2x2 Bravais cells containing 1 or 2 equivalent spins, eq. (20) is always satisfied. In our experience with more complicated cells, it has, in those cases that we tried, always been possible to form solutions satisfying eq. (20) from a set of degenerate solutions. Nondegenerate solutions not satisfying eq. (20) do, of course, not exist for a cell consisting of equivalent spins. If a solution of eq. (22) corresponding to the lowest eigenvalue, satisfies the strong constraint, then it is also a lowest-energy solution of eqs.(19). This can be understood by substitution of that solution into expression (21), which then attains its minimum value. This method was introduced by Luttinger and Tisza[3]). Daniels and Felsteiner[9]) have used it to find the energy of ordered cerium magnesium nitrate. The application of this method to a 2x2x2 simple Bravais unit cell was extensively discussed by Niemeyer[7]).

This method gives all solutions of eq. (22) for systems of equivalent spins, but we have to consider the possibility that solutions of eqs. (19) exist which do not satisfy eq. (22), and hence cannot be found by this method. Whether this situation can occur in practice, may be found by method 2 for solving eqs. (19).

Method 2. Solutions of eqs. (19) can also be obtained by iteration. We then start from a chosen set of vectors $s_{i\alpha}^{(0)}$ (a 'first approximation') and we calculate

$$h_{i\alpha}^{(0)} = \sum_{j=1}^{m} K'_{ij\alpha\beta} s_{j\beta}^{(0)} \qquad (i = 1 \ldots m),$$

which vector is proportional to what may be considered as the molecular field acting on the spin at site i (if the spin vectors would be given by the $s_{j\beta}^{(0)}$). A decrease of the energy is then obtained by rotating the spins towards the fields. A second approximation is thus given by

$$s_{i\alpha}^{(1)} = k_i^{(1)} (a s_{i\alpha}^{(0)} + h_{i\alpha}^{(0)}) \qquad (i = 1 \ldots m),$$

where a is an arbitrary constant which controls the convergence of this method. The $k_i^{(1)}$ are constants which are determined by the requirement that the $s_{i\alpha}^{(1)}$ must be normalized at length s_i (the strong constraint). In a similar way, further approximations $s_{i\alpha}^{(n)}$ can be obtained. The convergence rate can be judged from the variation of the energy, which can be calculated after each step according to eq. (21). If the convergence rate is not satisfactory, the parameter a can be adjusted. This method does not always converge to that structure

having the lowest energy. Therefore the actual calculations were done for several different 'first approximations' $s_{i\alpha}^{(0)}$. Application of this method has shown that indeed solutions of eqs. (19) exist for systems of equivalent spins, which do not satisfy eq. (22), because the c_i are not all equal. In table I, an example of such a magnetic structure is given for a magnetic pyrochlore lattice having only dipolar interactions determined by $s = \frac{1}{2}$, $g_{/\!/} = 1$, $g_{\perp} = 1$ and a lattice parameter $a = 10$ Å. The energy of this solution is $E/R = -0.00877$ K, which may be compared to a value -0.00897 K for the lowest energy value found by the eigenvalue

i	s_{i1}	s_{i2}	s_{i3}	$c_i/4k$ (K)
1	0.2147	0.3193	0.3193	−0.00906
2	0	−0.1677	0.4710	−0.00847
3	0.2147	0.3193	0.3193	−0.00906
4	0	0.4710	−0.1677	−0.00847
5	0	−0.1677	0.4710	−0.00847
6	−0.2147	0.3193	0.3193	−0.00906
7	0	0.4710	−0.1677	−0.00847
8	−0.2147	0.3193	0.3193	−0.00906
9	0.2147	0.3193	0.3193	−0.00906
10	0	0.4710	−0.1677	−0.00847
11	0.2147	0.3193	0.3193	−0.00906
12	0	−0.1677	0.4710	−0.00847
13	0	0.4710	−0.1677	−0.00847
14	−0.2147	0.3193	0.3193	−0.00906
15	0	−0.1677	0.4710	−0.00847
16	−0.2147	0.3193	0.3193	−0.00906

Table I. A solution of eqs. (19) which does not satisfy eq. (22). This solution was calculated for a cristobalite lattice having $a = 10$ Å, isotropic g tensors and dipolar interactions only. For the lattice positions, see chapter VI, table I.

method. For the crystal structure, the lattice positions, and the orientation of the $g_{/\!/}$ directions (which depends on the lattice position), see chapter VI. Further, the values of $c_i/4k$ are shown in table I. These numbers give in this case ($s = \frac{1}{2}$) the energy of spin i in the molecular field at site i.

For clarity, the main advantages and limitations of the two methods will be summarized:

1. Both methods are constrained to periodical magnetic structures, and in practice the magnetic cell may not contain more than about 32 spins. This means that *e.g.* most helical magnetic structures cannot be found by these methods.
2. Method 1 is in general only applicable to systems containing equivalent spins. For systems of inequivalent spins, method 1 gives solutions which in general do not satisfy the strong constraint. Method 2 may be used for systems having inequivalent spins.
3. Method 1 gives at once all solutions of eq. (22) (hence also the one having the lowest energy, in which we are mostly interested). The result of method 2 depends on the first

approximation $s_{i\alpha}^{(0)}$, which may be arbitrarily chosen before starting the calculations, and does not in general give certainty that the solution is that one having the lowest possible energy.

4. For systems of equivalent spins, method 2 may give solutions of eqs. (19) which cannot be found by method 1. An example is given in table I. In all cases studied here, however, the lowest-energy solution of method 1 satisfied the strong constraint and hence method 1 yielded the minimum energy solution of eqs. (19).

5. In contrast to method 1, method 2 is applicable when an external magnetic field is present.

The uncertainties in the results of these methods related to the above mentioned point 1 can be decreased by varying the choice of the magnetic cell, particularly also choosing larger cells.

As an example, a computer program working according to method 2, written in PL1 programming language, is shown in appendix II.

Results of these methods are given in chapter VI.

8. *The convergence of lattice sums having r^{-3} dependence*

The lattice sums for the calculation of the energy, the Curie-Weiss constant and the dipolar contributions to the $K'_{ij\alpha\beta}$ tensors in section 7 consist of terms which are proportional to the inverse third power of the distance to the origin. Convergence is yet obtained because of angular cancellation in spherical shells, at least if the inner radius is so large that the shell may be considered as a continuum. In practice, however, the cancellation is not complete and the lattice sums show considerable fluctuations as a function of the radius r' of the sphere in which the summation is carried out. This is demonstrated in fig. 1 in which the calculated dipolar energy gain E/R of possibly antiferromagnetically ordered cerium magnesium nitrate is shown for several values of r' up to 150 Å (open circles). The magnetic structure used for

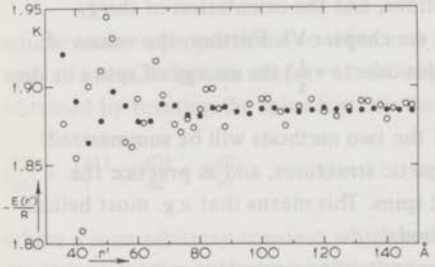

Fig. 1. The dipolar energy of (hypothetically) antiferromagnetically ordered CMN, calculated by summation of the contributions of all neighbours within a radius r'.

● data calculated using a weight function; ○ data calculated without use of a weight function.

The magnetic structure used for these calculations is given in table II.

i	positions			± b axis
1	0	0	1/4	+
2	0	0	3/4	−
3	1/6	1/3	7/12	−
4	1/6	1/3	1/12	+
5	1/3	2/3	11/12	+
6	1/3	2/3	5/12	−
7	1/2	0	1/4	−
8	1/2	0	3/4	+
9	2/3	1/3	7/12	+
10	2/3	1/3	1/12	−
11	5/6	2/3	11/12	−
12	5/6	2/3	5/12	+

Table II. The hypothetical antiferromagnetic structure of CMN for which the energy was calculated. The lattice positions are in units of the crystallographic a, b and c axes, for which we have used $a = 21.84$ Å, $b = 10.92$ Å, $c = 34.44$ Å. For the g value we have taken 1.82. The last column indicates whether the spin is aligned along the positive or negative b axis.

the calculations is shown in table II. Spin alignment was along the positive or negative b axis, and is indicated by + or − in the table. This structure was found by Daniels and Felsteiner[9]) as one having the lowest dipolar energy. However, if one includes a demagnetizing correction in the energy calculation and assumes splitting in needle-shaped domains, one obtains a comparable energy value for a ferromagnetic structure, as discussed by Mess *et al.*[10]).

The fluctuations in fig. 1 can be understood if we consider a plane containing parallel spins which lies at a distance r of the origin, which is much larger than the distances between neighbouring spins in that plane. If the radius r' of the sphere in which the summation takes place now becomes greater than r by Δr, we obtain a contribution to the lattice sum originating from a group of parallel spins at a distance between r' and r, hence occupying a surface of about $2\pi r\Delta r$ in the plane. Hence the lattice sum will approximately behave linearly as a function of r' until a new plane (or a set of planes) is encountered. These planes lie at regular intervals and hence it can be understood that a sort of periodic behaviour is visible in fig. 1. Above we found that the number of spins causing a 'fluctuation' is proportional to r', and for a sum of terms having r'^{-3} dependence, we thus expect fluctuations proportional to r'^{-2}. This is in approximate agreement with the data shown in fig. 1.

If high accuracy for the lattice sums is required, the summation must be carried out in a sphere having large r' which may take substantial time even for a fast computer. In such cases the method of Peverley and Meyer[11,12]) can be used which utilizes a weighting function for obtaining a smoothed value. This method is discussed in appendix III. As an illustration of this method, in fig. 1 weighted results using the exponential g function (III.3, appendix III) are shown by black circles for a number of r' values, in addition to the unweighted results

for the dipolar energy of CMN ordered according to the magnetic structure given in table II. As we expected, the convergence of the weighted sum is much better.

9. *A cluster method*

The caloric behaviour of simple magnetic systems is rather well known theoretically if a magnetic field is absent. In the presence of a magnetic field in general (not for linear Ising chains), one requires simplifications in the theoretical description. Such a simplification is introduced by *e.g.* the molecular field model. This simplification consists of replacing all spin-spin interactions by interaction of one spin with a mean (molecular) field which is proportional to the magnetization. Although the molecular field model has proven its usefulness in many applications, it is not astonishing that this simplification is too crude for some purposes, especially those where external field and magnetization are small or zero. In the latter case, the mean field is zero, and hence energy and specific heat are also found to be zero.

An improvement may be obtained if we do not replace all spin-spin interactions by a mean field, but if we retain the spin-spin interactions in a group (cluster) of spins having in its center one spin for which we shall calculate thermodynamical quantities. This method resembles the Bethe-Peierls-Weiss[4,5,6]) method. However, unlike BPW theory, the cluster used here may contain more spins than nearest neighbours of the central spin only, and interactions may occur among all these neighbours. Further, the calculations in this section are restricted to Ising systems. For other Ising cluster calculations, see *e.g.* Kikuchi[13]).

In these cluster theories, the mean field now replaces the interactions of spins inside the cluster with their neighbours outside. The value of this mean field is found in the molecular field approximation by relating it to the expectation value of the relative magnetization M_1 of the central spin. For a cluster we may require that the mean field has such a value that the expectation value of the relative magnetization per spin M_t of the whole cluster equals that of the central spin. This problem becomes relatively simple if the interactions are of the $s = \frac{1}{2}$ n.n. Ising type:

$$\mathcal{H} = -\frac{1}{2} \sum_{(i,j)} J\sigma_{iz}\sigma_{jz} - \sum_{k} H\sigma_{kz} \qquad (24)$$

where J is the exchange constant, $\sigma_{iz} = 2s_{iz}$, and H stands for one half of the product of the Bohr magneton, the z component of the external field, and the g value. The summation indication (i,j) means here that each pair of n.n. is counted once. For simplicity, $\mathcal{H}$, J and H are taken in units K. If all individual spins are in states corresponding to $\sigma_{iz} = \pm 1$, then the system is in an eigenstate of $\mathcal{H}$. This state is determined by the set of all σ_{iz}. If we now make the above mentioned approximation, we can calculate the energy levels of a cluster consisting of n spins. Therefore we now define several constants determined by the set of σ_{kz}. Interactions of spins inside the cluster give a contribution to the energy

$$I_t = -\frac{1}{2} J \sum_{(i,j)} \sigma_{iz}\sigma_{jz} . \tag{25}$$

Each pair of n.n. in the cluster is counted once.

The relative magnetization of the whole cluster is

$$M_t = \frac{1}{n} \sum_k \sigma_{kz} . \tag{26}$$

The interaction between the mean field and a spin k which has c_k neighbours outside the cluster can be written as $\frac{1}{2} Jmc_k\sigma_{kz}$, where m is the relative magnetization of the hypothetical continuum outside the cluster. The interaction between the mean field and the whole cluster can now be written as mJM_u, if we define

$$M_u = \frac{1}{2} \sum_k c_k\sigma_{kz} . \tag{27}$$

The relative magnetization M_1 of the central spin simply equals

$$M_1 = \sigma_{1z} \tag{28}$$

The interaction energy of the central spin with its neighbours amounts to

$$I_1 = -\frac{1}{4} J \sum_{(1,j)} \sigma_{1z}\sigma_{jz} . \tag{29}$$

Because we are interested in the energy per spin, this is only one half of the sum of the pair interaction energies in which spin 1 participates. The total energy of spin 1 amounts to

$$E_1 = I_1 - M_1 H , \tag{30}$$

and the energy E of the whole cluster is

$$E = I_t - nM_tH - mJM_u . \tag{31}$$

In this expression, m is to be determined by requiring that the expectation value $f_1(m,T)$ of the central spin is equal to a function $f_2(m,T)$ which is in the molecular field theory equal to m, and for which we shall choose here the expectation value of the magnetization of the whole cluster. Thus we calculate $m(T)$ from the equation

$$f_1(m,T) = f_2(m,T) . \tag{32}$$

The thermal average of the energy per spin is obtained in this model by calculating the expectation value of E_1, thereby using the E values for a calculation of the Boltzmann factor. In order to obtain a short notation for the sums required for the following calculations, in table III several sums of the general form

$$a = \sum_i A_i \exp(E_i/kT) \qquad (i = 1 \ldots 2^n) \tag{33}$$

a	o	p	q	r	s	t	u	v	w	x	y	z
A	$M_t M_u$	M_t	E	M_1	M_t	$E_1 E$	$M_t E$	$M_u E_1$	M_u	E_1	$M_1 E$	$M_1 M_u$

Table III. Definition of several sums required for evaluation of c/R in eq. (37). The symbol a stands for $o, p \ldots$ which are defined by substituting for symbol A in eq. (33) the quantities $M_t M_u, M_t \ldots$ given in the lower row of this table.

are defined. With help of these sums, we can write the expectation value of the energy of spin 1:

$$<E_1> = x/s \,. \tag{34}$$

By differentiation one can obtain the heat capacity:

$$\frac{\mathrm{d}<E_1>}{\mathrm{d}T} = \left(\frac{\partial <E_1>}{\partial T}\right)_m + \left(\frac{\partial <E_1>}{\partial m}\right)_T \frac{\mathrm{d}m}{\mathrm{d}T} \,. \tag{35}$$

$\frac{\mathrm{d}m}{\mathrm{d}T}$ can be found from eq. (24):

$$\frac{\mathrm{d}m}{\mathrm{d}T} = -\left(\frac{\partial f_1}{\partial T} - \frac{\partial f_2}{\partial T}\right) \Big/ \left(\frac{\partial f_1}{\partial m} - \frac{\partial f_2}{\partial m}\right) \,. \tag{36}$$

Using the sums defined in table III and eq. (33), one obtains:

$$c/R = \frac{1}{T^2}\,[ts - qx + (v/s - wx/s^2)(-ys + rq + us - pq)/(zs - rw - os + wp)] \,. \tag{37}$$

This method will now be applied to interpret the heat capacity of cobalt formate dihydrate at low temperatures. From a series of experiments, which were discussed in ref. 14 by Matsuura *et al.*, it has been concluded that the spin system in this compound can be split into A planes, which order antiferromagnetically at 5.1 K, and B planes, which remain paramagnetic below that temperature. This situation occurs because the interactions in which B spins are involved, are much smaller than those among A spins. Each of the systems contains one half of the total number of spins. At 0.5 K a broad Schottky type anomaly was observed in the heat capacity (fig. 2). This suggests that the B spins are aligned in the molecular field originating from two neighbouring A spins, corresponding to an exchange constant $J_{AB}/k = 0.6$ K. The heat capacity at 0.5 K is, however, nearly 5% larger than one half of a two-level Schottky anomaly. This discrepancy is beyond experimental inaccuracy. It may be explained if we consider the effect of a nonzero interaction J_{BB} among nearest neighbours in the B planes. The Co spins have very anisotropic properties, and thus Ising type interactions are expected. Since the A planes order antiferromagnetically, the molecular field at the B sites is expected to be staggered. Therefore the situation is analogous to a system having an exchange interaction of the opposite sign, in a uniform *i.e.* non-staggered field. From the crystal structure, one concludes that each B spin has four equivalent B neighbours. Hence we may consider the B plane as a square lattice. Using these data,

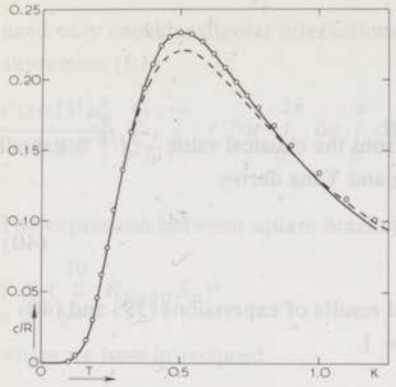

Fig. 2. Heat capacity of cobalt formate dihydrate per mole. The experimental data are given by small circles. The dashed line is a Schottky anomaly for $N/2$ Co spins, and the drawn line was obtained with use of the calculations described in this section.

– – – $J_{AB}/k = -0.6$ K, $J_{BB}/k = 0$ K

——— $J_{AB}/k = -0.53$ K, $J_{BB}/k = -0.04$ K.

the specific heat of the B spin systems was calculated as a function of temperature for several values of J_{BB}. A two-dimensional cluster of 9 spins arranged in a 3x3 square, was used. A good fit to the experimental data was obtained for $J_{AB}/k = -0.53$ K and an antiferromagnetic coupling between B spins $J_{BB}/k = -0.04$ K (fig. 2, solid line), except at relatively high temperatures where the A system may contribute. These results were very close to those found for a 5-spin cluster, consisting of a central spin plus its four nearest neighbours. Also results for an 11-spin cluster, which is defined by adding one pair of n.n. to a pair of n.n. in the 9-spin cluster, were practically identical. This suggests that in this case, where the exchange interaction is small compared to the external field, the approximation is good even for a small cluster.

10. *The ground state energy of anisotropic Heisenberg chains*

Yang and Yang[15]) have calculated the ground state energy of anisotropic linear Heisenberg chains, described by the following hamiltonian for a pair of neighbouring spins:

$$\mathcal{H}_{ij} = -J_{\perp}(s_{ix}s_{jx} + s_{iy}s_{jy}) - 2J_{\parallel}s_{iz}s_{jz} \tag{38}$$

They found that the ground state energy E is independent of the sign of $J_{\perp}$, and they derived expressions for E as a function of $J_{\parallel}$ and $J_{\perp}$. If $J_{\parallel}/|J_{\perp}| < -1$, then E is given by

$$E/R = \frac{|J_{\perp}|}{k}\left\{\tfrac{1}{4}\cosh\lambda - \frac{\sinh\lambda}{\lambda}\left[\tfrac{1}{2}\lambda + 2\lambda\sum_{n=1}^{\infty}\frac{1}{1+\exp(2\lambda n)}\right]\right\} \tag{39}$$

where λ is given by

$$\cosh \lambda = -J_{/\!/} / |J_{\perp}| \ , \qquad \lambda > 0.$$

The expression for E exhibits appreciable deviations from the classical value $\frac{1}{4} J_{/\!/}/k$ for small λ. In the case of $\lambda = 0$, that is the isotropic case, Yang and Yang derive

$$E/R = (\tfrac{1}{4} - \ln 2) \frac{|J_{\perp}|}{k} \tag{40}$$

which exceeds the classical value by 77.3%. Numerical results of expressions (39) and (40) are given in table IV for several values of $J_{/\!/}$, and $|J_{\perp}| = 1$.

$-J_{/\!/}/k$ (K)	$-E/R$ (K)	$-J_{/\!/}/k$ (K)	$-E/R$ (K)	$-J_{/\!/}/k$ (K)	$-E/R$ (K)
1	0.44315	1.25	0.48160	5	1.2995
1.001	0.44329	1.3	0.48968	6	1.5414
1.002	0.44344	1.4	0.50627	7	1.7855
1.005	0.44389	1.6	0.54117	8	2.0311
1.01	0.44463	1.8	0.57825	9	2.2777
1.02	0.44611	2.0	0.61722	10	2.5249
1.04	0.44909	2.2	0.65778	12	3.0208
1.06	0.45210	2.5	0.72101	15	3.7666
1.08	0.45512	3.0	0.83102	20	5.0125
1.1	0.45816	3.5	0.94497	30	7.5083
1.15	0.46584	4.0	1.0615	50	12.5050
1.2	0.47366	4.5	1.1799	100	25.0025

Table IV. Ground state energy of anisotropic Heisenberg chains for several values of $J_{/\!/}$, and $|J_{\perp}| = 1$.

Appendix I

For the calculation of the contribution to the T^{-2} coefficient in the heat capacity due to spins outside the sphere, we consider the crystal outside the sphere as a continuum which contains $m\mathrm{d}v/V$ magnetic ions in a volume element $\mathrm{d}v$, if the volume of the crystallographic cell is V and the cell contains m magnetic ions which may be inequivalent. From eq. (9) we find that the contribution to cT^2/R originating from integration over these volume elements amounts to

$$\int \frac{\mathrm{d}v}{V} \ \frac{s^2(s+1)^2}{18\,k^2} \ \sum_{j=1}^{m} K_{ij\alpha\beta} K_{ij\alpha_\nu} \tag{I.1}$$

The integration is outside a sphere having radius r', which is always chosen so large that we

need only consider dipolar interactions. If we introduce spherical coordinates, we obtain for expression (I.1)

$$\frac{s^2(s+1)^2\mu_B^4}{18\,k^2V}\sum_{j=1}^{m}\int_{r'}^{\infty} r^{-4}dr\int_0^{2\pi}d\varphi\int_0^{\pi}d\theta\,\sin\theta\,[\sum_{\alpha}\sum_{\beta}(g_{i\alpha\epsilon}g_{j\beta\epsilon}-3\,g_{i\alpha\mu}g_{j\beta\nu}\frac{r_\mu r_\nu}{r^2})^2] \qquad (I.2)$$

The expression between square brackets can be written as:

$$\sum_{\alpha}\sum_{\beta}(\sum_{p=1}^{10}R_{ij\alpha\beta p}\,S_p)^2 \qquad (I.3)$$

where we have introduced

$$\left.\begin{aligned} R_{ij\alpha\beta p} &= g_{i\alpha\epsilon}g_{j\beta\epsilon}\\ S_p &= 1\end{aligned}\right\}\quad \text{if } p = 1$$

and

$$\left.\begin{aligned} R_{ij\alpha\beta p} &= -\,3\,g_{i\alpha\mu}g_{j\beta\nu}\\ S_p &= \frac{r_\mu r_\nu}{r^2}\end{aligned}\right\}\quad \text{if } p = \mu + 3\nu - 2$$

Expression (I.3) can now also be written as

$$\sum_{\alpha}\sum_{\beta}\sum_{p=1}^{10}\sum_{q=1}^{10}R_{ij\alpha\beta p}R_{ij\alpha\beta q}S_pS_q = \sum_{t=1}^{100}U_{ijt}V_t$$

if we define

$$\left.\begin{aligned} U_{ijt} &= \sum_{\alpha}\sum_{\beta}R_{ij\alpha\beta p}R_{ij\alpha\beta q}\\ V_t &= S_pS_q\end{aligned}\right\}\quad \text{with } t = p + 10q - 10$$

The hundred V_t elements are goniometrical functions of φ and θ independent of the length of r, and the U_{ijt} elements are independent of φ and θ. Therefore expression (I.2) reduces to

$$\sum_{j=1}^{m}\frac{s^2(s+1)^2\mu_B^4}{54\,k^2Vr'^3}\sum_{t=1}^{100}U_{ijt}I_t \qquad (I.4)$$

where I_t is given by

$$I_t = \int_0^{2\pi}d\varphi\int_0^{\pi}d\theta\;V_t(\theta,\varphi)\sin\theta\;.$$

By symmetry arguments one can see that only 28 of these integrals are nonzero and that only four of these are independent. Using expression (I.4), only the U_{ijt} elements have to be calculated from the g tensors, to find the contribution of the continuum outside the sphere.

```
/*BEPALING MAGNETISCHE STRUCTUUR TGV DIPOOL E.A.INTERACTIES*/
SPINOR:PROC OPTIONS(MAIN);
       DCL(H,I,IF2,IF3,IF4,J,JS,JV,K,KF,L,M,N,NF,NH,NK,NL,NR,NI,NIO,
       NT,NO,NA,NB,MG)FIXED BIN(31);
       DCL(A,B,C,GR,S,E,SPIN,EF,SOM,COSA,SINA,COSB,SINB,COSC,SINC,RT,
       GR1,GR2,P,AFV,QF,DA,DB,DC,DF,CH,CK,CL,SF,VF,V,GE,GL,GF,EV,GEW,
       Q,EXE,EXL,RM3,RM5,TOL,AA,AB,AC,AV(3),BV(3),CV(3),R(3),RR(3,3))
       FLOAT(16);
       DCL(TEKST)CHAR(80);
       GET LIST(TEKST);IF TEKST='EINDE' THEN STOP;
OVER:  PUT PAGE LIST(TEKST);
       AFV=0.2;QF=0.3113;
       NH=1;NK=1;NL=1;MG=1;GE,GL=0;NR=0;GF=1;DF=4.1888;E=1E+50;
       TOL=0.0001;SF=1;VF=1;NF=1;IF2=10;IF3=30;IF4=60;KF=0;JS=1;JV=1;
       M=1;GR=1;A,B,C=1;COSA,COSB,COSC=0;SPIN=0.5;GET DATA;
       N=M;M=M*NH*NK*NL;
       A=A*NH;B=B*NK;C=C*NL;
       PUT SKIP DATA(NH,NK,NL);
       PUT SKIP DATA(A,B,C);
       PUT SKIP DATA(COSA,COSB,COSC);
       PUT SKIP EDIT('SPIN=')(A);
       IF FLOOR(SPIN+0.25)=FLOOR(SPIN+0.75)
       THEN PUT EDIT(FLOOR(SPIN+0.5))(F(2,0));
       ELSE PUT EDIT(FLOOR(SPIN*2+0.5),'/2')(F(2,0),A);
       PUT SKIP DATA(DF);
PROG:  BEGIN;DCL(X(M),Y(M),Z(M),SR(M,3),VR(N,3),VT(M,M,3,3),
       GRE(MG),GRL(MG),GTE(MG,3,3),GTL(MG,3,3),G(MG,3,3),
       ERE(MG),ERL(MG))FLOAT(16);
       DCL(NG(M))FIXED BIN(31);
VERV:  CALL VBER;
       CALL PDEF;
       CALL GBER;
       CALL SDEF;
       CALL SPRT;
       CALL GRBR;
       CALL TBER;
VOEG:  CALL MBER;
       CALL VPRT;
       CALL EBER;
       CALL CNTR;
       CALL KLAP;
       CALL SPRT;
       CALL MBER;
       CALL VPRT;
       CALL EBER;
       CALL CNTR;
LOOP:  CALL RBER;
       CALL SPRT;
       CALL MBER;
       CALL VPRT;
       CALL EBER;
       CALL CNTR;
```

```
      IF NF¬<0 THEN GOTO LOOP;
      PUT SKIP DATA(GR);
      PUT SKIP DATA(NI);
      GET LIST(TEKST);IF TEKST='EINDE' THEN STOP;
      IF TEKST='STAND' THEN DO;NR,KF=0;NF=1;GET DATA;E=1E+50;
      PUT PAGE LIST('HERHALING VAN DE BEREKENING MET NIEUWE STANDEN');
      CALL SDEF;CALL SPRT;GOTO VOEG;END;
      GOTO OVER;
VBER: PROC;/*DEF ASSENSTELSEL TOV ABC ASSEN*/
      SINA=SQRT(1-COSA*COSA);
      SINB=SQRT(1-COSB*COSB);
      SINC=SQRT(1-COSC*COSC);
      AV(1)=A;AV(2)=0;AV(3)=0;
      BV(1)=B*COSC;BV(2)=B*SINC;BV(3)=0;
      CV(1)=C*COSB;CV(2)=C*(COSA-COSB*COSC)/SINC;
      CV(3)=SQRT(C*C-CV(1)*CV(1)-CV(2)*CV(2));
      V=AV(1)*BV(2)*CV(3);END VBER;
GRBR: PROC;/*BEREKENING NH,NK EN NL*/
ABOL: R(1)=BV(2)*CV(3)-BV(3)*CV(2);
      R(2)=BV(3)*CV(1)-BV(1)*CV(3);
      R(3)=BV(1)*CV(2)-BV(2)*CV(1);
      SOM=0;S=0;DO I=1 TO 3;S=S+R(I)*AV(I);SOM=SOM+R(I)*R(I);
      END;S=ABS(S)/SQRT(SOM);NH=GR/S+1;
BBOL: R(1)=CV(2)*AV(3)-CV(3)*AV(2);
      R(2)=CV(3)*AV(1)-CV(1)*AV(3);
      R(3)=CV(1)*AV(2)-CV(2)*AV(1);
      SOM=0;S=0;DO I=1 TO 3;S=S+R(I)*BV(I);SOM=SOM+R(I)*R(I);
      END;S=ABS(S)/SQRT(SOM);NK=GR/S+1;
CBOL: R(1)=AV(2)*BV(3)-AV(3)*BV(2);
      R(2)=AV(3)*BV(1)-AV(1)*BV(3);
      R(3)=AV(1)*BV(2)-AV(2)*BV(1);
      SOM=0;S=0;DO I=1 TO 3;S=S+R(I)*CV(I);SOM=SOM+R(I)*R(I);
      END;S=ABS(S)/SQRT(SOM);NL=GR/S+1;
      END GRBR;
PDEF: PROC;/*DEFINITIE IONPLAATSEN*/
      NI=0;DO I=1 TO N;
      GET LIST(XI(I),YI(I),ZI(I),NG(I));END;
      DO H=1 TO NH;CH=H-1;DO K=1 TO NK;CK=K-1;DO L=1 TO NL;CL=L-1;
      DO I=1 TO N;NI=NI+1;
      IF NI>N THEN DO;
      NG(NI)=NG(I);
      XI(NI)=XI(I)+CH/NH;
      YI(NI)=YI(I)+CK/NK;
      ZI(NI)=ZI(I)+CL/NL;
      END;ELSE DO;
      XI(NI)=XI(I)/NH;
      YI(NI)=YI(I)/NK;
      ZI(NI)=ZI(I)/NL;
      END;END;END;END;END;
      PUT SKIP(2)EDIT('POSITIES IONEN')(X(9),A);
      PUT SKIP;DO I=1 TO N;
      PUT SKIP EDIT(I,XI(I),YI(I),ZI(I),NG(I))(F(3),3 F(10,6),F(4));
      END;END PDEF;
GBER: PROC;/*GEEF COEFFICIENTEN VOORK RICHT*/
      DCL ROT(3,3)FLOAT(16);
      DO I=1 TO MG;IF(GE=0)&(GL=0)THEN GET LIST(GRE(I),GRL(I));
      ELSE DO;GRE(I)=GE;GRL(I)=GL;END;
      GET LIST(AA,AB,AC);
      PUT SKIP(2)EDIT('TENSOR NR',I,'COEFF.VOORK.RICHT.:',AA,AB,AC)
      (A,F(4),A(4),A,F(12,4),F(12,4),F(12,4));
      PUT SKIP(2)EDIT('G EVENWIJDIG TENSOR','G LOODRECHT TENSOR')
      (X(4),A,X(10),A);
      IF(AA=0)&(AB=0)THEN DO;ROT=0;DO J=1 TO 3;ROT(J,J)=1;END;END;
      ELSE DO;S=SQRT(AA*AA+AB*AB+AC*AC);
      AA=AA/S;AB=AB/S;AC=AC/S;S=SQRT(AA*AA+AB*AB);
      ROT(1,1)= AB/S;ROT(1,2)=AA*AC/S;ROT(1,3)=AA;
      ROT(2,1)=-AA/S;ROT(2,2)=AB*AC/S;ROT(2,3)=AB;
      ROT(3,1)=0    ;ROT(3,2)=-S     ;ROT(3,3)=AC;
      END;DO J=1 TO 3;PUT SKIP(2);DO K=1 TO 3;
      GTE(I,J,K)=ROT(J,3)*ROT(K,3);
      PUT EDIT(GTE(I,J,K))(X(2),F(7,4));END;DO K=1 TO 3;
      GTL(I,J,K)=ROT(J,1)*ROT(K,1)+ROT(J,2)*ROT(K,2);
      PUT EDIT(GTL(I,J,K))(X(2),F(7,4));
      END;END;END;
      PUT SKIP(2)DATA(GE,GL,GF);PUT SKIP;
      DO I=1 TO MG;PUT SKIP DATA(GRE(I),GRL(I));END;
      DO I=1 TO MG;DO J=1 TO 3;DO K=1 TO 3;
      G(I,J,K)=GF*GRE(I)*GTE(I,J,K)+GF*GRL(I)*GTL(I,J,K);
      END;END;END;END GBER;
SDEF: PROC;/*GEEF N SPINS HUN RICHTING*/
      DO I=1 TO M;DO J=1 TO 3;GET LIST(SR(I,J));
      END;END;CALL NORM;END SDEF;
KLAP: PROC;/*ZET SPINS MET VELD MEE*/
      DO H=1 TO M;DO L=1 TO M;P=0;DO K=1 TO 3;
      P=P+SR(L,K)*VR(L,K);END;
      IF P<-(ABS(EF)+ABS(QF/(A**3)))*1.0E-4 THEN DO;
      DO K=1 TO 3;SR(L,K)=-SR(L,K);END;
      CALL MBER;L=M;END;END;END;END KLAP;
NORM: PROC;/*NORMERING SPINVECTOR*/
      DO I=1 TO M;S=0;DO J=1 TO 3;
      P=SR(I,J);IF ABS(P)<1E-20 THEN DO;P=0;SR(I,J)=0;END;
      S=S+P*P;END;S=SQRT(S);IF S=0 THEN DO;
      SR(I,3)=1;S=1;END;DO J=1 TO 3;
      SR(I,J)=SR(I,J)*SPIN/S;END;END;END NORM;
TBER: PROC;/*BEREKENING INTERACTIETENSOREN*/
```

```
      NI=0;DO NIO=1 TO M;NO=NG(NIO);DO I=1 TO NIO;NT=NG(I);
      DO J=1 TO 3;DO N=1 TO 3;
      P=0;DO NA=1 TO 3;P=P+G(NO,J,NA)*G(NT,N,NA);END;
      VT(NIO,I,J,N)=QF*DF*P/V;END;END;RR=0;
      DA=XI(NIO)-XI(I);DB=YI(NIO)-YI(I);DC=ZI(NIO)-ZI(I);
      DO H=-NH TO NH;CH=H;AA=CH+DA;
      DO K=-NK TO NK;CK=K;AB=CK+DB;
      DO L=-NL TO NL;CL=L;AC=CL+DC;
      SOM=0;DO J=1 TO 3;S=AA*AV(J)+AB*BV(J)+AC*CV(J);
      R(J)=S;SOM=SOM+S*S;END;RT=SQRT(SOM);
      IF (RT>TOL)&(RT<GR) THEN DO;NI=NI+1;
      IF AFV=0 THEN GEW=1;ELSE GEW=1-EXP((RT-CR)*AFV);
      RM3=(RT**(-3))*GEW*CF;RM5=-RM3*3.0/(RT*RT);
      DO NA=1 TO 3;RR(NA,NA)=RR(NA,NA)+RM3;
      DO NB=1 TO 3;RR(NA,NB)=RR(NA,NB)+RM5*R(NA)*R(NB);
      END;END;END;END;END;END;
      DO J=1 TO 3;DO N=1 TO 3;P=0;
      DO NA=1 TO 3;DO NB=1 TO 3;P=P+G(NO,J,NA)*G(NT,N,NB)*RR(NA,NB);
      END;END;VT(NIO,I,J,N)=VT(NIO,I,J,N)-P;
      END;END;END;END;
      PUT SKIP(4)EDIT('DIFCOLWISSELWERKING')(A);
      PUT SKIP DATA(GR,NI,QF);
EXCH: GET LIST(GR1);IF GR1>0 THEN DO;GET LIST(GR2,EF,EXE,EXL);
      PUT SKIP(2)EDIT('EXCHANGEPARAMETERS')(X(11),A);
      PUT DATA(EF);PUT SKIP;Q=-EF;
      DO I=1 TO MG;IF (EXE=0)&(EXL=0) THEN GET LIST(ERE(I),ERL(I));
      ELSE DO;ERE(I)=EXE;ERL(I)=EXL;END;
      PUT SKIP DATA(ERE(I),ERL(I));END;
      PUT SKIP;NI=0;DO NIC=1 TO M;NO=NG(NIC);DO I=1 TO NIO;NT=NG(I);
      DA=XI(NIO)-XI(I);DB=YI(NIO)-YI(I);DC=ZI(NIO)-ZI(I);
      DO H=-1,0,1;CH=H;AA=CH+DA;
      DO K=-1,0,1;CK=K;AB=CK+DB;
      DO L=-1,0,1;CL=L;AC=CL+DC;
      SOM=0;DO J=1 TO 3;S=AA*AV(J)+AB*BV(J)+AC*CV(J);
      R(J)=S;SCM=SOM+S*S;END;RT=SQRT(SCM);
      IF (RT>GR1)&(RT<GR2) THEN DO;NI=NI+1;
      PUT SKIP EDIT('NR ICN 1 :',NIO,'NR ION 2 :',I,'HKL :',H,K,L,
      'AFSTAND :',RT)(2(A,F(4),X(3)),A,3 F(3),X(3),A,F(10,6));
      RR=0;DO J=1 TO 3;DO N=1 TO 3;DO NA=1 TO 3;
      RR(J,N)=GTE(NO,J,NA)*GTE(NT,N,NA)*ERE(NC)*ERE(NT)*Q+
      RR(J,N)+GTE(NO,J,NA)*GTL(NT,N,NA)*ERE(NO)*ERL(NT)*Q+
      GTL(NO,J,NA)*GTE(NT,N,NA)*ERL(NO)*ERE(NT)*Q+
      GTL(NO,J,NA)*GTL(NT,N,NA)*ERL(NO)*ERL(NT)*Q;
      END;END;END;
      DO J=1 TO 3;DO N=1 TO 3;VT(NIO,I,J,N)=VT(NIC,I,J,N)-RR(J,N);
      END;END;END;END;ENC;END;END;END;
      PUT SKIP(2)DATA(GR1,GR2,NI);GOTO EXCH;END;
      DO I=2 TO M;J=I-1;DO NIO=1 TO J;DO NA=1 TO 3;DO NB=1 TO 3;
      VT(NIC,I,NA,NB)=VT(I,NIO,NB,NA);
      END;END;END;END;ENC TBER;
MBER: PROC;/*BEREKENING VELD TER PLAATSE VAN CE ICNEN*/
      DO NIO=1 TO M;DO J=1 TO 3;VR(NIO,J)=0;
      DO I=1 TO M;DO N=1 TO 3;
      VR(NIO,J)=VR(NIO,J)+VT(NIO,I,J,N)*SR(I,N);
      END;END;END;END;ENC MBER;
NRMR: PROC;/*NORMEER R OP 1*/
      RT=0;DO K=1 TO 3;RT=RT+R(K)**2;END;RT=SQRT(RT);
      IF RT>0 THEN DO K=1 TO 3;R(K)=R(K)/RT;END;
      END NRMR;
RBER: PROC;/*RICHT SPINS IN VELD VAN HUN BUREN*/
      DO I=1 TO M;DO J=1 TO 3;R(J)=VR(I,J);END;
      CALL NRMR;DO J=1 TO 3;SR(I,J)=SR(I,J)*SF+R(J)*SPIN*VF;END;END;
      CALL NORM;END RBER;
SPRT: PROC;/*DRUK SPINVECTCREN AF*/
      IF JS=1 THEN DO;
      PUT SKIP(2)EDIT('STANDEN')(X(10),A);
      PUT SKIP;DO I=1 TO M;PUT SKIP;
      PUT EDIT(I,(SR(I,J)DO J=1 TO 3))(F(3),3 F(10,4));
      END;END;END SPRT;
VPRT: PROC;/*DRUK VELDVECTCREN AF*/
      IF JV=1 THEN DO;
      PUT SKIP(2)EDIT('VELCEN')(X(10),A);
      PUT SKIP;DO I=1 TO M;PUT SKIP;
      PUT EDIT(I,(VR(I,J)DO J=1 TO 3))(F(3),3 F(10,4));
      END;END;END VPRT;
CNTR: PROC;/*CONTROLE OP STADIUM ITERATIEPROCES*/
      NR=NR+1;
      IF E¬<EV THEN NF=NF-1;
      IF NR=IF2 THEN NF=2;
      IF NR=IF3 THEN NF=3;
      IF NR=IF4 THEN NF=4;
      IF KF=-1 THEN NF=-1;ELSE DO;
      IF NF=1 THEN DO;SF=2;VF=1;JS=1;JV=1;END;
      IF NF=2 THEN DO;SF=1;VF=1;JS=0;JV=0;KF=KF+1;
      IF KF=5 THEN DO;KF=C;JS=1;JV=0;END;END;
      IF NF=3 THEN DO;SF= C;VF=1;JS=0;JV=0;KF=KF+1;
      IF KF=5 THEN DO;KF=C;JS=1;JV=0;END;END;
      IF NF=4 THEN DO;JS=1;JV=1;KF=-1;END;
      END;END CNTR;
EBER: PROC;/*BEREKENING ENERGIE */
      EV=E;E=0;DO I=1 TO M;DO J=1 TO 3;E=E+SR(I,J)*VR(I,J);END;END;
      E=-E/FLOAT(M);
      PUT SKIP(2)EDIT('FASE',NF,'NR=',NR,'E/R=',E)
      (A,F(3),X(4),A,F(4),X(4),A,E(16,8));END EBER;
EIND: END PROG;END SPINOR;
```

Suppose that we wish to calculate a lattice sum

$$A(r') = \sum_{r_i < r'} f(r_i)$$

over all lattice sites r_i within a radius r' from the origin. If $A(r')$ has a limit $A(\infty)$ for $r' \to \infty$ and $A(r')$ fluctuates about this limit, and if these fluctuations decrease when r' increases, we can define a 'smoothed value' of the lattice sum:

$$\bar{A}(r') = \int_0^{r'} G(r'')\, A(r'')\, \mathrm{d}r'' \qquad \text{(III.1)}$$

which will be a better approximation of $A(\infty)$ than $A(r')$ if the weight function $G(r'')$ is chosen carefully.

This function must satisfy the following requirements:

1. $G(r'')$ must be very small if $r'' \ll r'$ since then $A(r'')$ is not a good approximation of $A(\infty)$.
2. $G(r'')$ must be an increasing function of r'' because $A(r'')$ becomes a better approximation of $A(\infty)$ if r'' increases.
3. $\lim_{\Delta r' \to 0} \int_{r'-\Delta r'}^{r'} G(r'')\, \mathrm{d}r''$ must be zero, otherwise $\bar{A}(r')$ will contain a finite unsmoothed contribution from $A(r')$ which exhibits the fluctuations which we wish to avoid.

Expression (III.1) defining $\bar{A}(r')$ can be rearranged according to

$$\bar{A}(r') = \int_0^{r'} G(r'') \sum_{r_i < r''} f(r_i)\, \mathrm{d}r'' = \sum_{r_i < r'} f(r_i) \int_{r_i}^{r'} G(r'')\, \mathrm{d}r'' = \sum_{r_i < r'} f(r_i)\, g(r_i, r')$$

where $g(r_i, r') = \int_{r_i}^{r'} G(r'')\, \mathrm{d}r''$.

The calculation of $\bar{A}(r')$ can now be executed without calculating $A(r'')$ for all values of r''. An additional practical condition for the new weight function g is that it must be one simply calculable. For the weight function we have chosen

$$G(r'') = \frac{1}{a} \exp[(r''-r')/a]$$

with $a \approx 0.1\, r'$, corresponding to

$$g(r_i,r') = 1 - \exp[(r_i-r')/a] \tag{III.2}$$

or

$$G(r'') = 0 \qquad \text{if } r'' \leqslant r' - a$$
$$G(r'') = 3(r''+a-r')^2/a^3 \qquad \text{if } r'' > r' - a$$

with $a \approx 0.3\, r'$, corresponding to

$$\left.\begin{aligned} g(r_i,r') &= 1 && \text{if } r_i \leqslant r' - a \\ g(r_i,r') &= 1 - (1-\frac{r_i-r'}{a})^3 && \text{if } r_i > r' - a \end{aligned}\right\} \tag{III.3}$$

REFERENCES

1) Van Vleck, J.H., J. Chem. Phys. **5** (1937) 320
2) Daniels, J.M., Proc. Phys. Soc. (Lond) **A64** (1953) 673
3) Luttinger, J.M. and Tisza, L., Phys. Rev. **70** (1946) 954
4) Bethe, H.A., Proc. Roy. Soc. (Lond) **A150** (1935) 552
5) Peierls, R.E., Proc. Cambridge Phil. Soc. **32** (1936) 477
6) Weiss, P.R., Phys. Rev. **74** (1948) 1493
7) Niemeyer, T., Physica **57** (1972) 281
8) Niemeyer, T., private communication
9) Daniels, J.M. and Felsteiner, J., Can. J. Phys. **42** (1964) 1469
10) Mess, K.W., Lubbers, J., Niesen, L. and Huiskamp, W.J., Physica **41** (1969) 260
11) Peverley, J.R. and Meyer, P.H.E., Phys. Stat. Sol. **23** (1967) 35?
12) Peverley, J.R., J. Comp. Phys. **7** (1971) 83
13) Kikuchi, R. and Brush, S.G., J. Chem. Phys **47** (1967) 195
14) Matsuura, M., Blöte, H.W.J. and Huiskamp, W.J., Physica **50** (1970) 444
15) Yang, C.N. and Yang, C.P., Phys. Rev. **150** (1966) 327

CHAPTER III

HEAT-CAPACITY MEASUREMENTS ON Rb_3CoCl_5 COMPARED WITH THE ISING MODEL FOR A SIMPLE CUBIC LATTICE

Summary

Heat-capacity measurements on Rb_3CoCl_5 have shown a magnetic phase transition at 1.14 K. The behaviour of the powder susceptibility showed that the transition is to an antiferromagnetic phase. The analogy with the isomorphous cesium compound and the experimental data make it plausible that the Ising model is appropriate for Rb_3CoCl_5. It is shown that the specific heat agrees very well with accurate numerical predictions for the simple cubic Ising model.

1. *Introduction*

Experiments on Cs_3CoCl_5 have shown[1,2,3]) that this substance is a fairly good example of a simple cubic Ising lattice. In this chapter, heat capacity data will be presented on the isomorphous compound Rb_3CoCl_5. One may expect that the smaller ionic radius of Rb^+, and the correspondingly smaller lattice constants and Co-Co distances, will influence the values of the exchange constants. A comparison with theory may show whether the simple cubic Ising model is still applicable on this substance.

Unlike the two-dimensional case, for the three-dimensional Ising lattices no exact theoretical expression in closed form for the heat capacity is available. However, very precise computations exist for the heat capacity. In the last years, mathematical analysis of series expansions below and above the critical point has yielded analytical expressions for the specific heat which must be considered as having a higher precision than our experimental results. Therefore, these analytical expressions are for our purposes sufficiently precise, even although they do not represent a rigorous result for the heat capacity.

2. *Structure and spin hamiltonian*

Powell and Wells[4]) and Engberg and Soling[5]) have shown that Rb_3CoCl_5 is crystallographically isomorphous to Cs_3CoCl_5, which has tetragonal symmetry ($I\,4/mcm$, D_{4h}^{18}). The structure is also discussed in ref. 1 (for Cs_3CoCl_5) by Wielinga *et al.*, and in chapter V (for Cs_3MnCl_5) which is also isomorphous. The crystal structure is given in fig. 1 of chapter V. These

discussions show that all magnetic ions are magnetically equivalent, and that they form a simple tetragonal magnetic Bravais lattice. Four nearest neighbours (n.n.) are situated at 6.22 Å in the *a-a* plane, and two next nearest neighbours (n.n.n.) lie at 7.12 Å along the *c* axis.

Around each Co^{2+} ion, four Cl^- ions form a slightly distorted tetrahedron, in contrast to most other Co salts where the Co^{2+} ion is surrounded octahedrally. On account of the tetrahedral surrounding of Co^{2+} ions, the sign of the cubic crystal field parameter in Rb_3CoCl_5 (and in isomorphous compounds) is opposite to that usually found. In a cubic field, the $L = 3$ orbital multiplet is split in two triplets and a singlet. In nearly octahedrally coordinated Co salts, a triplet is lowest, and spin-orbit coupling together with low-symmetry crystal field components (if present) cause a further splitting into states which are in general a complicated mixture of orbital and spin functions. Due to the sign of the crystal field parameters in Rb_3CoCl_5 and its isomorphous compounds, the orbital level scheme is inverted, and the singlet is lowest. Therefore the magnetic properties of these Co ions become much simpler. Orbital magnetism is quenched, at least in first approximation, and the magnetic properties are mainly determined by the spin $S = \frac{3}{2}$ of Co^{2+}. In second order, the presence of a tetragonal component of the crystal field together with spin-orbit coupling, causes a splitting into two Kramers doublets described by $S_z = \pm\frac{3}{2}$ and $\pm\frac{1}{2}$. In Cs_3CoCl_5 it has been found that the $\pm\frac{3}{2}$ doublet is lowest[3]). This doublet cannot be split in first order by the S_x and S_y operators, from which it follows that only the z component can interact with neighbouring spins and an external field, or, in other words, the interactions among ground state Co spins are of the Ising type.

E.P.R. data on Cs_3CoCl_5[3,6]) have shown that the Zeeman splitting of the lowest Kramers doublet of the Co ion can be described by an (effective spin $s = \frac{1}{2}$) hamiltonian:

$$\mathcal{H}^z = g_{/\!/}\mu_B H_z s_z$$

with $g_{/\!/} = 7.23$, and with the z direction along the crystallographic *c* axis.

At temperatures much lower than the splitting between the two doublets (which corresponds to 12.4 K in Cs_3CoCl_5[1,3]), possible exchange interactions occur entirely among Co^{2+} ions in the ground state, and hence the (super)exchange mechanism causes Ising type interactions:

$$\mathcal{H}_{ij} = -2J_{ij}s_{iz}s_{jz}\,.$$

Further, E.P.R. measurements on Co pairs in a Cs_3ZnCl_5 lattice[7]) have shown that, apart of the sign, the interactions among nearest neighbours were approximately as large as those among neighbours along the *c* axis. Accordingly, Cs_3CoCl_5 proved to be a fairly good example of a simple cubic (s.c.) Ising lattice, as shown by caloric[1]) and magnetic[2]) experiments. The antiferromagnetic transition temperature for Cs_3CoCl_5 was found at $T_N = 0.52$ K. In view of the tetrahedral Cl^- surrounding of the Co^{2+} ions, we expect in the isomorphous rubidium compound Rb_3CoCl_5 also spin-only magnetism at low temperatures, but the relative position of the $S_z = \pm\frac{1}{2}$ and $\pm\frac{3}{2}$ doublets is uncertain, since this depends on the sign of the tetragonal distortion of the nearly-cubic crystal field, the sign of which is not known.

However, Co^{2+} ions in Cs_3CoCl_5, Cs_3CoBr_5 and Cs_3ZnCl_5 all have the $\pm\frac{3}{2}$ doublet lowest[6]).

3. *The experiment*

The sample was prepared by heating together stoichiometric quantities of RbCl and anhydrous $CoCl_2$, to a temperature of about 800 K in HCl atmosphere. The blue-violet polycrystalline mass was ground until the particle dimensions were about 0.2 mm. X-ray powder photographs showed that the structure was identical to that described in refs. 4 and 5.
The heat capacity of a powdered sample thus obtained exhibited a sharp peak at 1.14 K, which we attribute to magnetic ordering. The heat capacity data c/R are given in table I and are plotted in fig. 1 on a logarithmic scale *versus* the reduced temperature T/T_N (T_N = 1.14 K, the critical temperature). For a comparison, also data of Wielinga on Cs_3CoCl_5 have been shown as black dots, using T_N = 0.52 K[1]).

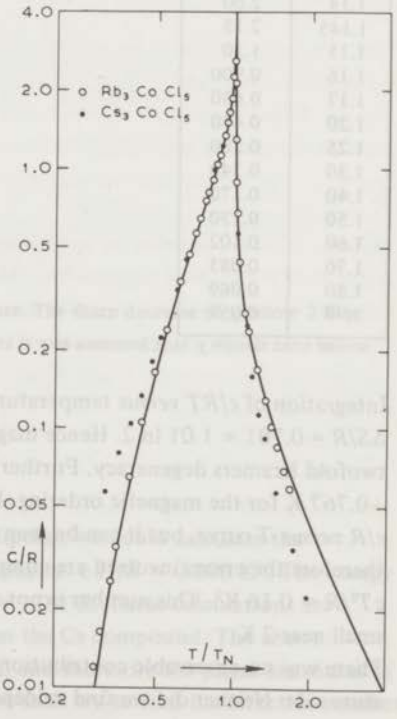

Fig. 1. Heat capacity of Rb_3CoCl_5 *versus* reduced temperature T/T_N. The circles represent the measured points, and the full curve is calculated for the simple cubic Ising model. For comparison, the heat capacity data on Cs_3CoCl_5 have been plotted as black dots.

Table I.

T(K)	c/R
0.30	0.0060
0.33	0.0120
0.35	0.0164
0.38	0.0258
0.40	0.0350
0.45	0.0650
0.50	0.107
0.56	0.165
0.62	0.240
0.70	0.370
0.76	0.470
0.80	0.570
0.84	0.650
0.88	0.750
0.90	0.810
0.94	0.910
0.98	1.05
1.00	1.13
1.04	1.35
1.06	1.50
1.08	1.67
1.10	1.85
1.12	2.25
1.14	2.60
1.145	2.15
1.15	1.30
1.16	0.900
1.17	0.680
1.20	0.440
1.25	0.280
1.30	0.240
1.40	0.170
1.50	0.130
1.60	0.102
1.70	0.085
1.80	0.069
1.90	0.059

Table I. Heat capacity c/R in dimensionless units *versus* temperature T.

Integration of c/RT *versus* temperature for the Rb compound yielded an entropy change $\Delta S/R = 0.701 \approx 1.01 \ln 2$. Hence magnetic ordering takes place between ions having only twofold Kramers degeneracy. Further, integration of c/R yielded a total energy $E/R = -0.767$ K for the magnetic ordering. Both integrations require some extrapolation of the c/R *versus* T curve, but it can be seen that the extrapolated portions are quite steep, and therefore the errors involved are comparatively small. At high temperatures ($\sim$ 2 K), we find $cT^2/R \approx 0.16$ K^2. This number is not so accurate, because the heat capacity becomes very small near 2 K.

There was no observable contribution from hyperfine structure coupling on the low temperature side. Neither did we find evidence for the presence of a Schottky specific heat arising

from the higher Kramers doublet. This shows that the splitting between the two doublets must be at least about 18 K.

The experiments also included 220 Hz a.c. powder susceptibility measurements at temperatures below 4.2 K. A low maximum in χ is reached near 2 K, below which χ decreased rapidly. The a.c. losses (chapter I) were constant above 2.5 K, which presumably indicates that χ'' is zero at those temperatures. Near 2 K, the a.c. losses reach appreciable values. Therefore the steep decrease of the susceptibility below 2 K is attributed to relaxation effects. Since the higher doublet is sufficiently distant, the susceptibility between 2.5 and 4.2 K may be expected to follow a Curie-Weiss law, but this temperature interval is too narrow to obtain an accurate fit of three unknown parameters (chapter I, section 6). Therefore, we have tried to obtain one parameter in another way. Below 1 K, the susceptibility was experimentally found to be constant, and we have assumed that it was zero. This assumption is correct if the magnetic spins have very anisotropic properties, hence if the $S_z = \pm\frac{3}{2}$ doublet is lowest. The assumption leads to a value of the constant n_0 (see chapter I) and now the Curie-Weiss law can be demonstrated by plotting the inverse susceptibility *versus* temperature (fig. 2). We then obtain a reasonably accurate Curie-Weiss constant $\theta = -1.5 \pm 0.2$ K.

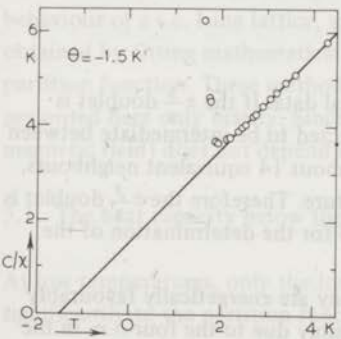

Fig. 2. Inverse a.c. susceptibility of Rb_3CoCl_5 *versus* temperature. The sharp decrease of χ below 2 K is attributed to relaxation effects. For the derivation of these data it was assumed that χ equals zero below 1 K (see text).

4. *Analysis of the experimental results*

If all spin-spin interactions in Rb_3CoCl_5 were purely dipolar, we could calculate the asymptotic high-temperature behaviour of the heat capacity: $cT^2/R = 0.005$ K^2. The energy of the magnetically ordered substance would be $E/R \approx -0.1$ K. These calculations are described in chapter II, and the g values are taken from the Cs compound. The above numbers are much smaller than the experimental data, and therefore the phase transition of Rb_3CoCl_5 is ascribed to exchange interactions. First we shall try to find the effective number

of interacting neighbours and the so called spin dimensionality from the experimental data. Therefore, we consider a system of spins, having an exchange interaction of arbitrary sign and absolute value J with z neighbours, and spin dimensionality d (which has the value 1 for Ising, 2 for XY, and 3 for Heisenberg type interactions). Dipolar interactions are neglected, and the hamiltonian for a pair of interacting spins becomes

$$\mathcal{H}_{ij} = \pm 2J \sum_{a=1}^{d} s_{ia} s_{ja} \qquad (1)$$

If a spin configuration exists in which each spin is surrounded only by neighbours which are energetically favourably oriented, then the energy at zero temperature is approximated by

$$E/R \approx -\tfrac{1}{4} zJ/k, \qquad (2)$$

and if such a configuration does not exist, $|E|$ is smaller. At high temperatures the heat capacity obeys

$$cT^2/R = \tfrac{1}{8} zdJ^2/k^2.$$

From these formulas one obtains

$$z/d \gtrsim E^2/2cT^2R \approx 7.$$

The latter value is found by substitution of the experimental data. If the $\pm\frac{3}{2}$ doublet is lowest then $d = 1$, and if the $\pm\frac{1}{2}$ doublet is lowest d is expected to be intermediate between 2 and 3. In the latter case, there would have to be at least about 14 equivalent neighbours, and this seems very improbable in view of the crystal structure. Therefore the $\pm\frac{3}{2}$ doublet is very probably lowest, and the assumption used in section 3 for the determination of the Curie-Weiss constant is justified.

Thus the effective number of neighbours is about 7, and they are energetically favourably oriented at $T = 0$. This suggests that the interactions are mainly due to the four n.n. in the a-a plane and the two n.n.n. along the c axis, and that these interactions are, at least in absolute value, approximately equal. Information about the signs of the exchange constants can be obtained from the Curie-Weiss constant θ. This constant can now be related to these exchange parameters:

$$\theta = 2J_{aa}/k + J_c/k$$

Substitution of the experimental value $\theta = -1.5 \pm 0.2$ K, and a comparison with eq. (2) leads to the conclusion that both J_{aa} and J_c are negative. This situation corresponds to $\theta = 2E/R$, which is satisfied within experimental error. This result indicates that in Rb_3CoCl_5 the magnetic ions are antiferromagnetically coupled to the 4 n.n. and the 2 n.n.n., which has also been found in the isomorphous compound Cs_3MnCl_5 (see chapter V). Hamman[8]) has also found that in Cs_3CoCl_5, these 6 neighbours are antiparallel at low temperatures, but this result is not in agreement with caloric and magnetic[1,2]) and pair resonance[7]) experiments.

We shall now consider the influence of dipolar interaction. As already pointed out in the beginning of this section, these interactions are too small to explain the magnetic transition observed at T_N = 1.14 K. Further, for Ising type dipolar and nondipolar interactions, the pair hamiltonian has the same form. Thus for the 4 n.n. and 2 n.n.n., dipolar interactions are accounted for by adding a dipolar contribution to the J_{ij} in eq. (1), and we shall consider now only the consequences of interactions of further neighbours. If these interactions are purely dipolar, they contribute only 0.0007 K^2 to the T^{-2} coefficient of the heat capacity, which is only 0.4% of the experimental number. Dipolar interactions of further neighbours give a contribution of about 0.001 K or 0.2% to the energy if we adopt the antiferromagnetic structure which follows from the preceding analysis. Therefore the *long-range* dipolar contribution to the magnetic energy is negligibly small.

5. *A comparison of the heat capacity to theory*

The analysis in section 4 suggests that Rb_3CoCl_5 is an example of a simple cubic (s.c.) Ising system, and a comparison of the experimental to the theoretically calculated heat capacity may be useful. Although no rigorous closed-form solution exists at present for the thermal behaviour of a s.c. Ising lattice, approximative methods exist. These approximations are obtained by fitting mathematical expressions to series obtained from expansion of the partition function. These methods were described in *e.g.* refs. 9, 10, 11 and they will be presented here only briefly. Since the thermal behaviour (in the absence of an external magnetic field) does not depend on the sign of J, we may choose a positive J.

5.1. The heat capacity below the transition point

At low temperatures, only the lowest energy levels of the magnetic system contribute significantly to the partition function, which is defined as

$$Z = \sum_i \exp(-E_i/kT).$$

The summation is over all states of the system. For a s.c. $s = \frac{1}{2}$ Ising system, the summation index i takes 2^N values. The E_i are the energy levels. From the s.c. hamiltonian it is easy to see that these levels are multiples of $2J$. Since the ground state energy is given by

$E_0 = -\frac{3}{2}NJ$, we can now write

$$Z = \exp(\tfrac{3}{2}NJ/kT) \sum_{i=0}^{\frac{3}{2}N} m_i [\exp(-2J/kT)]^i .$$

Here m_i is the multiplicity of the i-th level, which is the number of states in which 2i pair interactions are inverted with respect to the ground state. In practice, only about 15 terms

can be obtained, since the amount of work increases rapidly with i. From this series, the low temperature expansion of the heat capacity can be found:

$$c/R = (J/2kT)^2 \sum_{i=1}^{\frac{3}{2}N} a_i [\exp(-2J/kT)]^i. \qquad (3)$$

The coefficients a_i are found from the coefficients in the expansion of Z. Numerical values were obtained by Baker[12]). However, a number of about 15 terms is not sufficient to describe the heat capacity up to the immediate vicinity ($1 - T/T_c \lesssim 0.3$) of the critical point. Therefore the series are analytically continued by means of an expression from which one may expect to give a good description of the heat capacity also just below the critical temperature. In this case, the so called Padé approximant[10]) technique was used to analyze the heat capacity series. The [m,n] Padé approximant to a function $F(x)$ is written as

$$(1 + \sum_{i=1}^{n} b_i x^i)/(1 + \sum_{j=1}^{m} c_j x^j), \qquad (4)$$

and the coefficients b_i and c_j are obtained by equating the first n+m terms of the series expansion of $F(x)$ to those of the Padé approximant. Since $F(0)$ must be unity, power series have to be divided by their leading term before such an approximant can be calculated. Baker[13]) has calculated a [7,7] Padé approximant with help of which eq. (3) can be approximated by

$$c/R \approx 144(J/2kT)^2 \exp(-6J/kT)(\sum_{i=1}^{7} b_i x^i)/(\sum_{j=1}^{7} c_j x^j),$$

where x is a function of temperature, defined as

$$x = -\ln [1 - \exp(-2J/kT)/\exp(-2J/kT_c)].$$

The critical temperature T_c was given by $2J/kT_c = 0.886883$. The coefficients b_i and c_i are given in table II.

This approximant is, if T is sufficiently close to T_c, proportional to $\ln(1 - T/T_c)$, which contradicts later conclusions[14, 15, 16]) that the heat capacity diverges at T_c proportional to

i	b_i	c_i
1	5.4804176	5.4804176
2	12.642667	11.228545
3	16.200486	10.843288
4	12.805225	5.3955361
5	6.5316176	1.6749843
6	2.0627710	0.40180954
7	0.32542223	0.0022218833

Table II. Coefficients b_i (numerator) and c_i (denominator) of the [7,7] Padé approximant which was used for the calculation of the s.c. Ising heat capacity below T_c.

$(1 - T/T_c)^{-1/8}$. However, the difference becomes manifest only if $(1 - T/T_c) < 10^{-4}$, and hence it does not influence the comparison between theory and experiment intended here, since the experimental data exhibit a broadening of a few times 10^{-3}.

5.2. The heat capacity above the transition point

For high temperatures, the exponents of the partition function terms are small, and hence we can approximate Z by expansion of the exponential function for small argument. This type of expansion is given in chapter II, section 3, and leads for the s.c. Ising system to a heat capacity series in the form

$$c/R = \sum_{i=1}^{\infty} f_i T^{-2i}$$

Also in this case, only a limited number of terms can be obtained. A number of coefficients is given *e.g.* by Baker[12]). The high temperature series can be analyzed by the so called ratio method, which is applicable to series of which the ratio between successive terms becomes constant for high terms. In this case, a fit is obtained by equating the n available terms of the heat capacity series expansion (which for the s.c. Ising model contains only even terms) to that of the expression

$$A(1 - T_c^2/T^2)^{-\alpha} + \sum_{i=0}^{n} g_i T^{-2i}.$$

The parameters in the left-hand term are fitted such that the g_i coefficients converge to zero, or, strictly speaking, seem to converge in the range of i values for which f_i coefficients have been calculated.
Sykes[17]) has obtained such a fit, for which $A = 1.232$, $\alpha = \frac{1}{8}$, and $2J/kT_c = 0.88676$, which is very close to the value given in section 5.1. The g_i coefficients of the 'correction polynomial' are given in table III.

i	g_i
0	−1.2320
1	−0.0065
2	−0.0069
3	0.0030
4	0.0001

Table III. Coefficients g_i of the correction polynomial which was used for the calculation of the s.c. Ising heat capacity above T_c.

5.3. A comparison with the experimental data

The s.c. Ising heat capacity was calculated according to the methods given in sections 5.1 and 5.2. The results are given in table IV, and are also shown in fig. 1 *versus* T/T_c as the

T/T_c	c/R	T/T_c	c/R
0.1	1.97×10^{-9}	1.03	0.519
0.15	6.23×10^{-6}	1.04	0.460
0.2	2.96×10^{-4}	1.05	0.417
0.25	0.00272	1.06	0.382
0.3	0.01130	1.08	0.331
0.35	0.0303	1.1	0.293
0.4	0.0623	1.12	0.264
0.45	0.1085	1.14	0.240
0.5	0.1690	1.16	0.221
0.55	0.243	1.18	0.204
0.6	0.332	1.22	0.1776
0.65	0.435	1.26	0.1569
0.7	0.554	1.3	0.1403
0.75	0.692	1.35	0.1237
0.8	0.854	1.4	0.1103
0.84	1.007	1.5	0.0899
0.86	1.096	1.6	0.0753
0.88	1.194	1.7	0.0642
0.9	1.307	1.8	0.0556
0.92	1.438	2	0.0431
0.94	1.515	2.2	0.0346
0.95	1.699	2.4	0.0284
0.96	1.817	2.6	0.0238
0.97	1.962	3	0.01747
0.98	2.16	3.4	0.01340
0.99	2.48	3.8	0.01062
0.995	2.78	4.2	0.00863
0.998	3.17	4.6	0.00716
0.999	3.45	5	0.00603
1	∞	5.5	0.00497
1.001	1.437	6	0.00416
1.002	1.215	7	0.00304
1.005	0.951	8	0.00232
1.01	0.771	10	1.483×10^{-3}
1.02	0.607	15	6.57×10^{-4}
		20	3.69×10^{-4}

Table IV.

Calculated heat capacity of a s.c. Ising system.

drawn curve. The agreement between the simple cubic Ising heat capacity and the Rb_3CoCl_5 data is very nice, and is even better than in the case of Cs_3CoCl_5. This may be attributed to relatively smaller interactions with more distant neighbours than the 4 n.n. and 2 n.n.n. in the Rb compound. Dipolar interactions are relatively smaller in the Rb compound, because the exchange is about two times stronger, whereas dipolar interactions are only about 10% stronger (on basis of the differences in the lattice constants), if the g values in these two cobalt compounds are the same.

6. *Conclusions*

The thermal and magnetic behaviour of Rb_3CoCl_5 agree with the simple cubic Ising model. Thus the interactions of a Co spin with the 4 n.n. and the 2 n.n.n. are approximately equal and are given by an average interaction constant $J/k = -0.511$ K, as found from the magnetic energy corresponding to the heat capacity anomaly, and $J/k = -0.505$ K as found from the Néel temperature $T_N = 1.14$ K. These interaction constants include a contribution due to dipolar interaction. If we adopt the $g_{//}$ value of the Cs compound, the dipolar contribution to J/k amounts to -0.068 K for the 4 n.n. and to $+0.091$ K for the 2 n.n.n.

REFERENCES

1) Wielinga, R.F., Blöte, H.W.J., Roest, J.A. and Huiskamp, W.J., Physica **34** (1967) 223
2) Mess, K.W., Lagendijk, E., Curtis, D.A. and Huiskamp, W.J., Physica **34** (1967) 126
3) Beljers, H.G., Bongers, P.F., van Stapele, R.P. and Zijlstra, H., Phys. Letters **12** (1964) 81
4) Powell, H.M. and Wells, A.F., J. Chem. Soc. (1935) 359
5) Engberg, Å. and Soling, H., Acta Chem. Scand. **21** (1967) 168
6) Van Stapele, R.P., Beljers, H.G. Bongers, P.F. and Zijlstra, H., J. Chem. Phys. **44** (1966) 3719
7) Van Stapele, R.P., Henning, J.C.M., Hardeman, C.E.G. and Bongers, P.F., Phys. Rev. **150** (1966) 310
8) Hamman, J., Physica **43** (1969) 277
9) Domb, C., Adv. Phys. **9** (1960) 149,245
10) Baker, G.A., Advances in Theor. Phys. ed. Brueckner, K.A., Academic Press, New York 1965
11) Wielinga, R.F., Progr. Low Temp. Phys. ed. Gorter, C.J., vol. VI
12) Baker, G.A., Phys. Rev. **129** (1963) 99
13) Baker, G.A. private communication.
14) Gaunt, D.S. and Domb, C., J. Phys. C. **1** (1968) 1038
15) Baker, G.A. and Gaunt, D.S., Phys. Rev. **155** (1967) 545
16) Gaunt, D.S., Proc. Phys. Soc. **92** (1967) 150
17) Sykes, M.F., Hunter, D.L., McKenzie, D.S. and Heap, B.R., to be published in J. Phys. **A 5** (1972)

CHAPTER IV

THE BEHAVIOUR OF CERIUM ETHYLSULFATE BELOW 1 K

Summary

Results of heat capacity, magnetic susceptibility and demagnetization experiments on cerium ethylsulfate are reported. The demagnetization experiments did not indicate a sharp peak in the heat capacity. Instead, a low and broad anomaly was found, having its maximum at $T \approx 0.025$ K. The energy of the magnetic ordering of cerium ethylsulfate amounts to $E/R = -0.0245$ K, and the high temperature tail of the heat capacity corresponds to $cT^2/R = 6.7 \times 10^{-4}$ K^2. These values are smaller than those reported in other papers, but they are still too large to be explained by magnetic dipole-dipole interactions only. Cerium ethylsulfate does not behave like a simple Ising antiferromagnet, as one might have expected on basis of the high $g_{/\!/}/g_{\perp}$ ratio. The negative value of the Curie-Weiss constant $\theta_{/\!/} = -0.048$ K of the susceptibility in the direction of the c axis confirms the existence of antiferromagnetic interactions between the axial components of neighbouring spins, but the susceptibility measured perpendicular to the c axis indicates ferromagnetic interactions between equatorial components of the neighbouring spins. There are strong indications that the spins do not order completely parallel to the c axis at low temperatures, and that a spontaneous moment perpendicular to the c axis exists at very low entropies. The ferromagnetic character of cerium ethylsulfate in the plane of nearly-zero g value is believed to be due to the uncommon type of spin-spin interactions among Ce ions.

1. *Introduction*

In the past, many efforts have been made to investigate the low temperature magnetic and thermal properties of cerium ethylsulfate (CeES), resulting in about 30 publications on this subject.

It has been shown in several rare earth compounds (*e.g.* some of their ethylsulfates, cerium magnesium nitrate, erbium and dysprosium chloride hexahydrate), that the magnetic and thermal behaviour at low temperatures is mainly determined by magnetic dipole-dipole interactions[1,2,3]). In these compounds, the interionic distances are comparable to those in CeES. On the basis of magnetic dipole-dipole interactions only, for CeES one would expect asymptotic high temperature heat capacity behaviour according to $cT^2/R = 1.7 \times 10^{-4}$ K^2, and a magnetic ordering temperature of bout 0.02 K. However, adiabatic demagnetization experiments of Cooke *et al.*[4]), of Johnson and Meyer[5]), and an experiment

of Meyer and Smith[6]), gave appreciably larger cT^2/R values, namely about $12 \times 10^{-4} K^2$. A relatively high ordering temperature was also reported. The present investigation of CeES was originally intended to extend the direct specific heat measurements to lower temperatures. We measured (section 5) a heat capacity decreasing as $cT^2/R = 6.7 \times 10^{-4} K^2$, which is supported by further experimental results (section 3). The lack of agreement with the values reported in the literature has stimulated us to perform also susceptibility measurements and demagnetization experiments.

2. *Crystal structure, spin hamiltonian and interionic interactions*

The crystal structure was determined by Ketelaar[7]). The unit cell (fig. 1) has hexagonal symmetry and contains two Ce ions. Since the unit cell has inversion symmetry, the two Ce ions are magnetically equivalent. Each Ce^{3+} ion has two nearest neighbours (n.n.) lying at a distance of 7.11 Å along the c axis (z direction). Six next nearest neighbours (n.n.n.) are situated at distances of 8.86 Å, three of which at a distance $\frac{1}{2}c$ ($c = 7.11$ Å) above the equatorial plane and three at $\frac{1}{2}c$ below. Further neighbours are at a distance of at least 13.40 Å and will not be considered here, except for the calculation of dipolar sums.

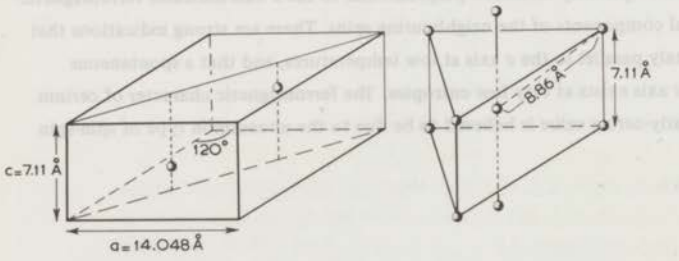

Fig. 1. Crystal structure of cerium ethylsulfate. Left-hand part: the positions of the two Ce ions in the hexagonal unit cell. These are: $\frac{1}{3}\ \frac{2}{3}\ \frac{1}{4}$ and $\frac{2}{3}\ \frac{1}{3}\ \frac{3}{4}$. Right-hand part: a Ce ion between its two nearest and six next nearest neighbours. As far as magnetic interactions are concerned, all Ce ions are equivalent.

Early susceptibility measurements of Fereday and Wiersma[8]) and optical rotation measurements (which can be related to the susceptibility) of Becquerel[9]) and Van den Handel[10]) indicated the existence of a Kramers doublet close to the ground doublet. The energy difference Δ of the two doublets and the g values were determined by Bogle *et al.*[11]) by susceptibility and E.P.R. measurements. The c axis was found to be the principal axis of the susceptibility and g tensors. Elliot and Stevens[12, 13]) could derive the wave functions by fitting the C_{3h} crystal field parameters to the experimental data. The lowest $J = \frac{5}{2}$ multiplet is split into three Kramers doublets, which can be approximately described by $J_z = \pm\frac{1}{2}, \pm\frac{3}{2}$,

$\pm\frac{5}{2}$. The energy difference between the lowest $J_z = \pm\frac{5}{2}$ doublet and the next higher $J_z = \pm\frac{1}{2}$ doublet, has further been derived from heat capacity measurements of Cooke *et al.*[4]), and of Meyer and Smith[6]), and from susceptibility measurements of Van den Broek and Van der Marel[14]), and Finn and Najafabadi[15]). A weighted average of the various results gives $\Delta/k = 6.75 \pm 0.1$ K. The position of the $J_z = \pm\frac{3}{2}$ doublet seems to be at least 20 times higher[13,16]) and its population may be neglected at liquid He temperatures and below. As a result, the ground state of the Ce^{3+} ion in CeES can be described by an effective spin $s = \frac{1}{2}$. Corresponding g values, according to Bogle *et al.*[11]), are $g_{\parallel} = 3.80 \pm 0.04$, $g_{\perp} = 0.2 \pm 0.1$. Van den Broek and Van der Marel[14]) found $g_{\parallel} = 3.75$ (± 2%). Recently, Finn and Najafabadi[15]) reported that $g_{\parallel} = 3.73$ was in good agreement with their susceptibility measurements between 1.1 and 4.2 K. The susceptibility, however, is influenced by interactions of the antiferromagnetic sign as evidenced by the Curie-Weiss constant $\theta_{\parallel} = -0.048$ K (section 4). This suggests that $g_{\parallel}$ is slightly larger than the results of Van den Broek *et al.*, and Finn *et al.* would indicate. E.P.R. experiments of Dweck and Seidel[17]) on concentrated CeES yielded $g_{\parallel} = 3.760 \pm 0.005$, and we shall adopt this value. E.P.R. measurements of Bogle *et al.*[11,13]) on Ce ions in the lanthanum ethylsulfate lattice showed $g_{\parallel} = 3.72 \pm 0.01$, $g_{\perp} = 0.2 \pm 0.05$. These latter values, however, may not be valid in concentrated CeES, because the g values depend on the crystal field parameters. This dependence is clearly demonstrated *e.g.* by the results of Anderson *et al.*[18]), who measured the g values of Ce^{3+} spins in europium, yttrium and lutetium ethylsulfate lattices. The variation of the crystal field parameters as a function of the rare-earth ionic radius is evident from an inversion of the two lowest doublets of Ce^{3+} ions in CeES when replacing most of the Ce by La[15]) and from measurements of Larson[19]) of Ce ions in other rare-earth ethylsulfate lattices. Regarding the spin hamiltonian, it should further be recalled that Ce has, due to the 100% abundance of even-even isotopes, no hyperfine interaction.

The first demagnetization experiments were done by De Haas and Wiersma[20]), who reached a lowest magnetic temperature of 0.08 K. Cooke, Whitley and Wolf[4]) performed demagnetizations starting from 7 kOe and 0.95 K. They reported a high temperature limit $cT^2/R = 11.2 \times 10^{-4}\ K^2$. This number was derived from the experimental S-T^* (entropy *versus* magnetic temperature C/χ, where C is the Curie constant) relation and by equating T^* to T at high temperatures (above 0.13 K). A low maximum in the magnetic susceptibility as a function of entropy was found, which suggested antiferromagnetic coupling between neighbouring Ce spins.

The experiments of Johnson and Meyer[5]) extended to lower entropies, since they used initial fields up to 25 kOe and an initial temperature of 0.9 K for their demagnetizations. They measured the zero field susceptibility as a function of the initial entropy. The existence of a maximum in the susceptibility was confirmed and interpreted as a Néel point. The temperature scale (*i.e.* the relation between temperature and *e.g.* susceptibility) was established in the following way:

1. at temperatures above the maximum in the susceptibility by measuring the relation between entropy and susceptibility (by demagnetization experiments) and the relation

between the susceptibility and the energy content (derived from the magnetic heat capacity) 2. at temperatures near the maximum and below by measuring the direct relation between entropy and energy content (the amount of energy required, to increase the magnetic entropy to R ln 2). The energy input was provided by gamma ray heating. A calibration of the heat input was made by application of the Curie-Weiss law at high entropies, and using the S-χ relation. The Curie-Weiss θ was reported to be about zero from the susceptibility at liquid He temperatures. From these data they derived the high temperature asymptotic behaviour of the anomaly below 1 K. Their result was close to that of Cooke *et al.*[4]). Further they measured isentropic magnetization curves and derived the magnetization as a function of entropy for several field strengths. From these functions, and the relation $dT = -(\partial M/\partial S)_H dH$, the temperature variation induced by adiabatic field variation was calculated. Minima in the T *vs* H curves were identified with the passage of a phase boundary between the paramagnetic and antiferromagnetic region, although this may not be strictly valid. An important result of the parallel (ℓ c axis) susceptibility (χ_ℓ) measurements of Johnson and Meyer is the low temperature limit, which is not zero as one would expect from *e.g.* molecular field and spin wave theory for a uniaxial antiferromagnet, but attains a constant value, corresponding to $T^* = 0.13$ K.

The experimental results on cT^2/R may be compared to the calculated value on the basis of dipolar interactions only. This calculation was first performed by Daniels[1]), who found $c_{\text{dip}} T^2/R = 1.93 \times 10^{-4}\ \text{K}^2$. However, using the same data, we obtain $1.74 \times 10^{-4}\ \text{K}^2$ (for other ethylsulfates there was close agreement). From the above comparison, it was concluded that in addition to dipolar interactions yet another kind of interaction exists in CeES which is appreciably stronger than the dipole coupling. Finkelstein and Mencher[21]) attempted to explain these interactions by considering the influence of electric quadrupole-quadrupole (Q-Q) coupling of the 4f charge clouds of neighbouring Ce ions. Although these charge clouds have nonzero quadrupole moment, this moment is the same for $J_z = +\frac{5}{2}$ and $J_z = -\frac{5}{2}$ states, and hence the Kramers degeneracy is not removed in first order. However, the Q-Q interaction induces admixture of higher $J_z = \pm\frac{1}{2}$ and $J_z = \pm\frac{3}{2}$ states into the ground state, and a second order perturbation calculation shows that the ground quadruplet of a pair of Ce^{3+} ions is split. These calculations have been reconsidered in papers of Bleaney[22]), Baker[23]), and Dweck and Seidel[17]). Baker[2]) considered interactions between the 4f charge clouds via the crystal lattice (virtual phonon exchange) and he concluded that this mechanism gave a better explanation of the interactions in CeES.

3. *Experimental part*

During most experiments a carbon resistor was used as a thermometer because the application of magnetic fields was required (see chapter I).

For magnetization of the CeES sample, a movable electromagnet producing a horizontal

field could be placed around the cryostat. The vertical position of the magnet and its direction in the horizontal plane could be varied. The mutual inductance coil system (chapter I) allowed susceptibility measurements only in the vertical direction.

The sample consisted of a CeES spherically shaped single crystal embedded in thin copper wires. Apiezon N grease was added for thermal contact between the sphere and the metal system. The copper wires were pressed firmly on the CeES surface by cotton wires. Two different spheres were used, one having 14.7 mm diameter and weighing 3.07 g, which we shall refer to as sphere I, and the other (sphere II) having 12.7 mm diameter and weighing 1.90 g. The larger sphere was mounted with its crystalline c axis in a direction intermediate between the vertical axis of the demagnetization apparatus and the horizontal plane. The reason for this was to have an appreciable g value both in the vertical direction for susceptibility measurements as well as in a horizontal direction for magnetizing the sample in the field produced by the horizontal iron magnet.

Since the direction of the c axis was not precisely known after the crystal had been mounted, magnetic measurements were employed to determine the angle between the crystalline c axis and the vertical axis of the susceptibility coil system. For this purpose, the sample was cooled in zero field to temperatures ranging between 0.13 and 0.21 K. In this temperature range, the zero-field heat capacity could be described by $c/R = b/T^2$ (section 5) and the susceptibility was found to follow a Curie-Weiss law (section 4). Hence, for small magnetic fields ($H \approx 100$ Oe), the entropy is expected to obey (see the appendix):

$$\ln 2 - S/R = \frac{g^2 \mu_B^2 H^2}{8k^2 (T-\theta)^2} + \frac{b}{2T^2} \qquad (1)$$

where g is the effective g value in the direction of the applied magnetic field H. Because of the large $g_{/\!/}/g_{\perp}$ ratio, the measured susceptibility is nearly proportional to the susceptibility along the $g_{/\!/}$ (c axis) direction, except if we would have measured close to the perpendicular direction. Therefore we may consider θ as a constant. The projection of the c axis was easily found from the temperature variation of the sample when a magnetic field of constant magnitude was slowly rotated in the horizontal plane. A pronounced minimum is reached when the magnetic field is aligned along the intersection line of the horizontal plane and the plane perpendicular to the c axis (the plane of minimum g). A pair of Helmholtz coils was placed around the cryostat in such a way that its field direction coincided with the projection of the c axis on the horizontal plane. A cylindrical coil was placed around the cryostat to provide a vertical field. Horizontal and vertical fields of about 100 Oe were applied, and the temperature variation of the carbon resistor was recorded. These experiments were carried out under adiabatic conditions so that we can apply eq. (1). From the temperature variations and the magnitudes of the magnetic fields, the ratio of the effective g values in the horizontal and vertical direction was evaluated. The $g_{\mathrm{vert}}/g_{\mathrm{hor}}$ ratio was 0.72, which corresponds to an angle of 36° between the c axis and the horizontal plane, and to $g_{\mathrm{vert}} = 2.19$ and $g_{\mathrm{hor}} = 3.06$ borrowing the results $g_{/\!/} = 3.76$[17]) and $g_{\perp} = 0.24$ from section 4. Absolute values of g_{vert} and g_{hor} can also be directly obtained from a comparison of eq. (1)

to the experimentally determined T *vs* H relation. These values are nearly 2% higher than the above set, but the difference lies within our experimental accuracy. The approximate agreement gives additional support for our b value for the high temperature limit of the low temperature specific heat anomaly (section 5).

The CeES sphere II was mounted with its c axis approximately horizontal. Measurement of the vertical susceptibility gave a low Curie constant (section 4) showing that the misalignment of the crystal axis was less than 3 degrees.

After completion of the experiments, inspection of the samples did not show decomposition and only minor cracks were found.

As a check, some of the heat capacity measurements were carried out in a different apparatus, using a sample consisting of slabs of single crystal, and a CMN susceptibility thermometer instead of a carbon resistor. The results of these measurements did not show appreciable systematic differences with the earlier ones and provided a measure for the accuracy (about 2%).

4. *The susceptibility*

4.1. Experiments on the Curie-Weiss relation

The procedure described in chapter I for analyzing susceptibility data was followed for magnetic susceptibility measurements at temperatures between 0.06 and 0.6 K for sphere I. It was found that the data obeyed a Curie-Weiss law and the inverse a.c. susceptibility is shown in fig. 2, utilizing the inverse Curie constant as a unit. Due to the large $g_{/\!/}/g_{\perp}$ ratio, the result is interpreted as $\chi_{/\!/}$. The Curie constant is in agreement with the corresponding effective g value derived in section 3 within experimental accuracy. The Curie-Weiss constant, as determined from fig. 2, namely $\theta_{\mathrm{I}} = -0.048$ K, has the antiferromagnetic sign. Susceptibility data are also shown in fig. 2 for sphere II. For this orientation, the Curie-Weiss constant $\theta_{\mathrm{II}} = +0.027$ K has the ferromagnetic sign and the Curie constant, which was about one hundredth of that of sphere I, corresponds to an effective g value $g = 0.26$. The loss of the experimental accuracy due to the much smaller Curie constant is at least partly compensated by the extension of the measurements to much lower magnetic temperatures. The c axis of sphere II was almost horizontal and hence the measurements apply to a direction near the plane of minimum g. However, we may not interpret these data as $\chi_{\perp}$ because a small deviation from the minimum g direction gives a large $\chi_{/\!/}$ contribution. Let us denote the angle between the axis of the susceptibility coil system and the plane of minimum g by α. Now, if $\alpha \ll 1$, we can describe the behaviour of the susceptibility χ by

$$\chi = \chi_{\perp} + \alpha^2 \chi_{/\!/}.$$

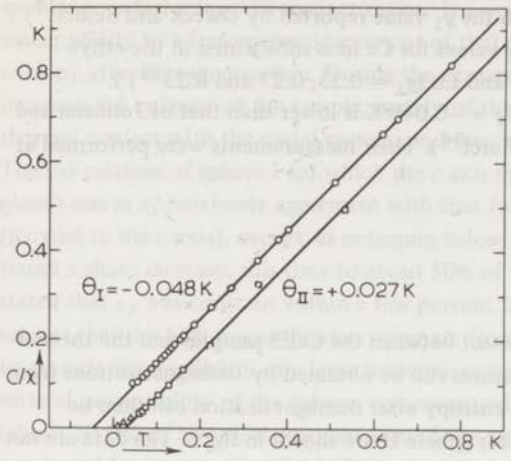

Fig. 2. Inverse susceptibility *versus* temperature data for cerium ethylsulfate.
○ sphere I, □ sphere II, △ sphere II, from χ-*S* data.
Because $g_{/\!/} \gg g_{\perp}$, the data for sphere I, which were obtained at an angle of 54° with the *c* axis, are interpreted as $\chi_{/\!/}$. For the same reason the data for sphere II, which were obtained at an angle of about 90° with the *c* axis, cannot directly be interpreted as $\chi_{\perp}$. The data for the two spheres show that the interactions between the z components of neighbouring spins are predominantly antiferromagnetic and that the interactions between the x and y components are predominantly ferromagnetic.

Substituting Curie-Weiss relations for $\chi_{\perp}$ and $\chi_{/\!/}$, one obtains for sufficiently large T:

$$\chi = \frac{C_{\perp} + a^2 C_{/\!/}}{T - (C_{\perp}\theta_{\perp} + a^2 C_{/\!/}\theta_{/\!/})/(C_{\perp} + a^2 C_{/\!/})} = \frac{C}{T - \theta} . \tag{3}$$

Apparently, the susceptibility obeys a new Curie-Weiss law, with Curie constant

$$C = C_{\perp} + a^2 C_{/\!/} \tag{4}$$

and a Curie-Weiss constant

$$\theta = \frac{C_{\perp}\theta_{\perp} + a^2 C_{/\!/}\theta_{/\!/}}{C_{\perp} + a^2 C_{/\!/}} \tag{5}$$

Because $C_{\perp} > 0$, we find from eq. (4) that $a < \sqrt{C/C_{/\!/}}$ or $a < 3$ degrees. The condition $a^2 \geqslant 0$ implies that $C_{\perp} \leqslant C$ or $g_{\perp} \leqslant 0.26$ (eq. 4) and $\theta_{\perp} \geqslant 0.027$ K (eq. 5).
The validity of the Curie-Weiss law (eq. 3) suggests that the value of $\theta_{\perp}$ is smaller than the lower bound of the temperature range of the measurements. The energy at $T = 0$ also imposes this upper bound for $\theta_{\perp}$, as will be seen in the discussion. Thus $\theta_{\perp} \leqslant 0.05$ K. From eqs. (4) and (5) we then calculate $g \geqslant 0.224$. The bounds for g must still be taken a little wider ($0.21 < g < 0.28$), in view of the inaccuracy of the determination of the Curie

constant. This result is in disagreement with the $g_\perp$ value reported by Dweck and Seidel[17]) ($g_\perp \leqslant 0.1$), but it fits well in the series of $g_\perp$ values for Ce ions substituted in the ethylsulfates of La ($g_\perp = 0.20$[13])) and of Eu, Y and Lu ($g_\perp = 0.23$, 0.27 and 0.23[18])).
It can further be remarked that our result $\theta_{/\!/} = -0.048$ K is lower than that of Johnson and Meyer[5]) and Van den Broek and Van der Marel[14]). Their measurements were performed at liquid He temperatures.

4.2. $\chi_\perp$ at low entropy

Below 0.06 K there was no proper heat contact between the CeES samples and the thermometer. Susceptibility data at lower temperatures can be obtained by demagnetizations from a known initial field and temperature. The entropy after demagnetization can then be calculated (see section 6). The data points for sphere II are shown in fig. 3. The data are not very accurate, because $\chi_\perp$ decreased rapidly in time, and further proved to be strongly

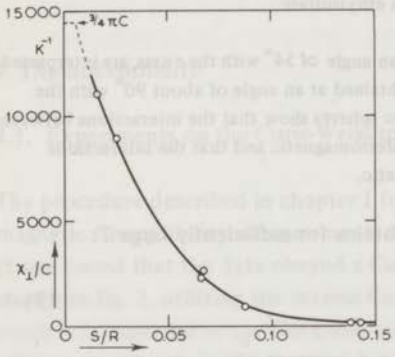

Fig. 3. The susceptibility of sphere II at low entropies. These data are interpreted as $\chi_\perp$ (see text). This picture suggests that at zero entropy $\chi_\perp$ will reach its saturation value of $3/4\pi$ for a sphere.

dependent on variations of the remanent field of a few Oe of the iron magnet. The susceptibility increases rapidly to high values when S becomes small. The χ-S relation can be transformed into a χ-T relation, using the S-T relation derived in section 6. Some of these data points are added to fig. 2. It is seen that the susceptibility increases less rapidly than according to the Curie-Weiss relation when T falls below 0.05 K. Nevertheless, the highest susceptibility value (observed at an entropy $S/R \approx 0.015$) corresponds to a magnetic temperature of 9×10^{-5} K. The ferromagnetic saturation value for sphere II corresponds to $T^* = 6.9 \times 10^{-5}$ K, and hence the highest observed susceptibility value amounts to $\frac{3}{4}$ of the saturation value. This suggests that in the limit of zero entropy, the ferromagnetic saturation value for the susceptibility of a sphere $\chi = 3/4\pi$ (χ per cm^3) will be reached, and that there may be a

spontaneous ferromagnetic magnetization. It seems reasonable to attribute the high susceptibility to a ferromagnetic moment of that part of the sample which had the lowest entropy after demagnetization. During the demagnetization, irreversible heat production increases the entropy of the sample, mainly of those parts of the sample which are in good thermal contact with the metal system, and thus entropy differences may arise.
The χ-S relation of sphere I (of which the c axis made an angle of 36° with the horizontal plane) was in approximate agreement with that found by Johnson and Meyer for $\chi_{/\!/}$ (parallel to the c axis), except at entropies below about $S/R = 0.05$, where again we found a sharp increase, this time to about 50% of the saturation value. Johnson and Meyer stated that $\chi_{/\!/}$ was constant within a few percent for $0.02 < S/R < 0.05$. All these data suggest that the high susceptibilities originate from $\chi_\perp$ (perpendicular to the c axis). In order to exclude the possibility of a large isotropic susceptibility contribution, the low-entropy vertical susceptibility of the spheres was measured as a function of a weak magnetic field (about 20 Oe) of a vertical solenoid around the sample. A maximum in the susceptibility was found for zero vertical field. These measurements were repeated in the presence of several horizontal magnetic fields H_{hor} along the projection of the c axis on the horizontal plane. The vertical field H_{ms} for which the maximum in the vertical susceptibility was reached, was measured as a function of H_{hor}. It was seen that H_{ms} was proportional to H_{hor}, and the ratio $H_{\mathrm{ms}}/H_{\mathrm{hor}}$ was about 0.7 for sphere I and about 0.05 for sphere II. Apparently, for weak fields, the vertical susceptibility is only dependent on the field component in the plane of minimum g. These data lead to an unambiguous interpretation of the large susceptibility as $\chi_\perp$. Unfortunately, no precise determination of the angle of the c axis of sphere II with the axis of the susceptibility coil system could be found from these measurements, because there is an uncertainty (about one or two degrees) in the direction of the latter axis with respect to the horizontal field. One might argue that even a small misalignment (*e.g.* 0.5°) of Johnson and Meyer's sample would have caused a visible increase of their susceptibility data at the lowest entropies. However, the absence of such an increase could possibly be due to a (small) irreversible entropy production in their demagnetization experiments. From fig. 3 it is seen that a rather small increase in S causes a drastic reduction of $\chi_\perp$.
From the susceptibility *versus* vertical field measurements we found that the large $\chi_\perp$ could be saturated in a magnetic field H of about 10 Oe. Integration of $\chi_\perp$ *versus* H gave an easy magnetization of about 140 gauss cm^3 per mole CeES. On basis of a $g_\perp$ value of 0.24, one calculates a maximum possible magnetization $\frac{1}{2} Ng\mu_B = 670$ gauss cm^3 per mole for complete spin alignment perpendicular to the c axis. Thus the presence of a Ce spin component in the a-a plane can explain this magnetization. The magnetization value calculated on basis of equilibrium proton polarization at the initial conditions before demagnetization of the sample ($H = 3874$ Oe, $T \approx 0.05$ K) is much smaller than the observed value. It should be noted that $\chi_\perp$ decreased rapidly (the 'lifetime' of $\chi_\perp$ was a few minutes) after demagnetization, due to the heat leak. $\chi_\perp$ was also found to be strongly dependent on the initial entropy, and it seems likely that experiments at still lower entropies would give higher magnetization values.

4.3. The frequency dependence of χ

We have also examined the frequency dependence of the susceptibility. In the liquid He temperature range, measurements at 1120, 260, 87, 20 Hz and ballistic measurements did not show any differences. Down to 0.1 K, the susceptibilities for 260 and 20 Hz were found to be equal. The large $\chi_\perp$ at low entropies was studied at 260 Hz and by ballistic measurements (using a d.c. field of 4 Oe), and comparable values were found. It should be remarked, however, that the ballistic (d.c.) measurements were not accurate due to the strong field dependence of $\chi_\perp$.

5. *The heat capacity measurements*

A joule heater, which was in thermal contact with the metal system in the apparatus, enabled us to produce a known amount of heat and hence to make heat capacity measurements by observing the temperature of the sample with a cerium magnesium nitrate or a carbon resistance thermometer. The heat capacity of the metal system and other parts of the 'empty calorimeter' were taken from separate experiments (chapter I) and subtracted. The corrected molar heat capacity is shown in fig. 4 on a logarithmic scale. Numerical data are presented in table I. From about 0.06 to 0.4 K the data points lie close to the straight line described by

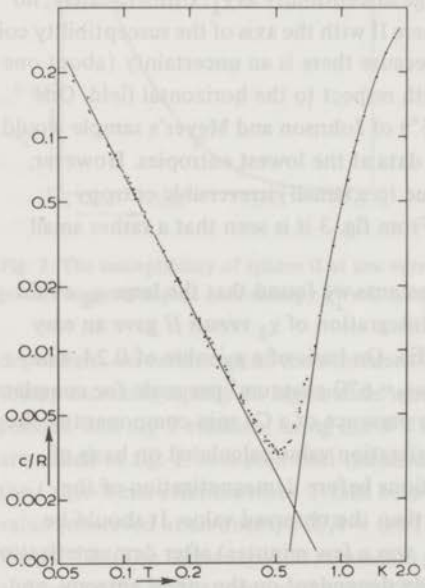

T (K)	c/R	T (K)	c/R
0.08	0.105	0.60	0.0041
0.09	0.083	0.65	0.0055
0.10	0.067	0.7	0.0078
0.12	0.047	0.75	0.0105
0.14	0.034	0.8	0.0145
0.16	0.0260	0.85	0.0208
0.18	0.0207	0.9	0.0290
0.20	0.0168	0.95	0.037
0.23	0.0126	1.0	0.048
0.26	0.0099	1.1	0.074
0.30	0.0076	1.2	0.103
0.34	0.0061	1.3	0.139
0.38	0.0051	1.4	0.175
0.42	0.0042	1.5	0.21
0.46	0.0037	1.6	0.25
0.50	0.0033	1.7	0.28
0.55	0.0034	1.8	0.31

Table I.
Heat capacity of CeES for $0.08\ \mathrm{K} < T < 1.8\ \mathrm{K}$.

Fig. 4. Heat capacity of cerium ethylsulfate. The straight line corresponds to $cT^2/R = 6.7 \times 10^{-4}\ \mathrm{K}^2$. The drawn curve is the calculated Schottky heat capacity for a splitting of $\Delta/k = 6.9$ K.

$cT^2/R = 6.7 \times 10^{-4}\,K^2$. As already noted in the introduction, this low temperature heat capacity is much smaller than the results (about $12 \times 10^{-4}\,K^2$) from earlier experiments[4,5,6]). However, these authors used a Curie-Weiss relation with θ about zero for their temperature determination, which introduces appreciable errors at temperatures below 1 K (see section 4). Further, they made demagnetizations from initial entropies of nearly R ln 2, in which case appreciable corrections are required by entropy contributions due to *e.g.* higher levels, which may cause systematic errors.

Returning to fig. 4, one sees that a minimum in the specific heat is reached at 0.52 K, and above that temperature an anomaly appears which has been observed in detail by Meyer and Smith[6]). The origin of this anomaly lies in the population of the $J_z = \pm\frac{1}{2}$ doublet. To our data we could fit the low-temperature side of a Schottky anomaly for two levels having a splitting of $\Delta/k = 6.9$ K. Agreement within experimental accuracy was obtained at temperatures between 0.8 and 1.7 K. The difference between our value for the splitting and that of Meyer and Smith[6]) ($\Delta/k = 6.7$ K) is not significant because our carbon resistance thermometer was not very sensitive at such high temperatures. Meyer and Smith[6]) have found that the heat capacity of this anomaly near its maximum (3 K) is higher than that expected on basis of a Schottky anomaly for two energy levels. Attempts to explain this by strong spin-phonon interactions have led to some theoretical publications[24,25,26]). Our experiments, although extending to temperatures of about 3 K, are not sufficiently accurate above 2 K to shed any further light on this problem.

6. *The Q-S measurements*

6.1. Experimental method

An experimental determination of the relation between the total heat content Q and the entropy S of the spin system of the sample can be obtained by a familiar method in adiabatic demagnetization experiments, known as the 'integral Q-S method'. The sample was slowly magnetized while the heat switch was closed, so that the magnetization heat was transported to the cooling salt. When the sample had reached the desired temperature T and magnetic field strength H (which determine S), the heat switch was opened in order to create adiabatic conditions. When temperature equilibrium was reached, the magnetic field was removed, and subsequently the joule heater was switched on, thereby developing a known amount of heat. When the temperature had reached a value at which good thermal contact between sample and thermometer existed, the heat input was stopped. From the initial conditions (T, H) and the total energy input, the Q-S relation was found.

6.2. Entropy corrections

The problem of calculating S from H and T was handled in the following way. In a first approximation, we can consider the sample as a simple two-level Zeeman system, of which the entropy S_z obeys the relation

$$S_z/R = \frac{\sum_i E_i \exp(-E_i/kT)}{kT \sum_i \exp(-E_i/kT)} + \ln \sum_i \exp(-E_i/kT) \qquad (6a)$$

with $E_i = \pm \frac{1}{2} g\mu_B H \quad (i=1, 2)$ (6b)

Several corrections must then be applied. The doublet at 6.75 K causes an increase of entropy, relative to eqs. (6). The entropy S_t of two doublets, separated by an energy distance Δ and having effective g values g_l (lower doublet) and g_h (higher doublet) is also given by the right part of eq. (6a), if we take

$E_i = -\frac{1}{2}\Delta \pm \frac{1}{2} g_l \mu_B H \quad (i=1, 2)$ and

$E_i = +\frac{1}{2}\Delta \pm \frac{1}{2} g_h \mu_B H \quad (i=3, 4).$

The correction ΔS_t is now defined by $\Delta S_t = S_t - S_z$. Further, the heat capacity of the lattice and the adjacent metal system (the empty calorimeter) was taken from separate experiments, and was as usual expressed in third and first powers of T respectively. The corresponding entropy contribution ΔS_e was calculated from these coefficients. The influence of the magnetization on the effective field acting on the Ce^{3+} spins was treated with the help of molecular field theory. The relative magnetization m for a two-level Zeeman spin system in an effective field H_m is given by

$$m = \frac{\sum_i s_i \exp(-g\mu_B H_m s_i/kT)}{\sum_i \frac{1}{2} \exp(-g\mu_B H_m s_i/kT)} \qquad (7)$$

with $s_i = \pm \frac{1}{2}$ (i=1, 2), and the molecular field approximation implies that

$$H_m = H + \frac{2k\theta_{//}}{g\mu_B} m \qquad (8)$$

where H is the external field. Eq. (8) was substituted in eq. (7) for H_m, yielding an equation from which the unknown m was obtained by an iteration method. H_m was found from eq. (8). Substitution of this value for H in the right-hand part of eq. (6a) gave the entropy S_m in the molecular field approximation. This correction amounts to $\Delta S_m = S_m - S_z$, and

the entropy S_i before demagnetization was simply calculated as

$$S_i = S_z + \Delta S_t + \Delta S_e + \Delta S_m.$$

Fluctuations in the mean field value, originating from neighbouring spins, have been neglected since the molecular field correction (< 500 Oe) was small compared to the external field, which was 3874 Oe in most cases.

An uncertainty in the entropy after demagnetization arises from the irreversible entropy gain during the demagnetization, caused by *e.g.* heating of the metal system by eddy currents. This entropy gain was approximately determined by auxiliary experiments, in which, after demagnetization, the field was returned to its initial value and the corresponding entropy increase ΔS_{irr} was calculated from the initial and final temperatures and the field. The entropy production was determined for several values of the initial entropy S_i. Fig. 5 shows the results for sphere II. The entropy gain ΔS_{irr} is seen to be strongly dependent on

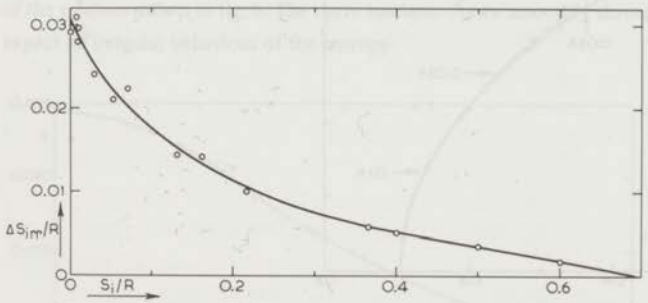

Fig. 5. The irreversible increase of entropy ΔS_{irr} after demagnetization and magnetization, as a function of the entropy S_i before demagnetization.

S_i. The increase of entropy after demagnetization is estimated as $\frac{1}{2}\Delta S_{irr}$. Hence after demagnetization, we use the following expression for the entropy:

$$S = S_z + \Delta S_t + \Delta S_e + \Delta S_m + \tfrac{1}{2}\Delta S_{irr}.$$

After the demagnetization, a known electrical current was led through the joule heater, and the heating was stopped when the sphere had reached a temperature T_f of about 0.2 K. Thus the heat input Q must be increased by a correction which was calculated by integrating the heat capacity above T_f. The heat Q must be considered as the energy required to heat the spin system to infinite temperature without populating the higher doublets. Therefore the heat capacity was taken to be $cT^2/R = 6.7 \times 10^{-4}\,K^2$ over the whole range of integration. Furthermore, a correction to Q was applied for the heat leak of about 0.1 erg/sec. For this purpose, the heat leak was measured after each Q-S data point measurement. (The heat leak into the Ce spin system just after demagnetization could be estimated by observing the decrease of $\chi_\perp$ in time and using the $\chi_\perp$-S (section 5) and Q-S relations. The leak was

comparable to the former value, which suggests that at low T the Ce spin system exchanges only very little heat with other systems (due to *e.g.* possible vibrations or rotations in the ethylsulfate lattice).)

6.3. Experimental results

Thus the Q-S data points were calculated from the experiments. The full curve in fig. 6 has been drawn through these data points, and the dashed line was calculated on basis of an extrapolation of the direct specific heat result $cT^2/R = 6.7 \times 10^{-4}\,\mathrm{K}^2$. At high entropies, the two curves coincide, which means that the Q-S and direct specific heat measurements are

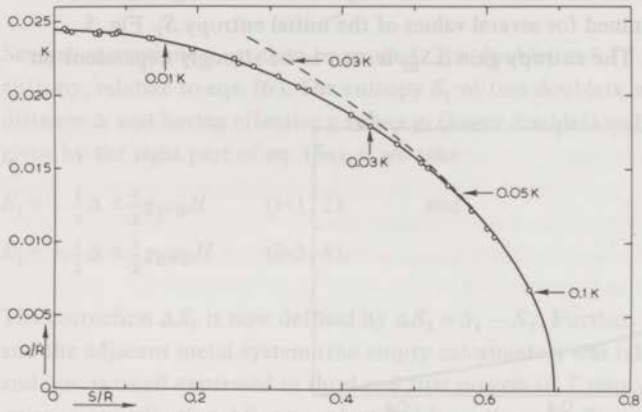

Fig. 6. The Q-S data. The heat Q required to increase the entropy of the ground-state Ce ions to R ln 2 is plotted *versus* the entropy (before heating). S. A large heat capacity peak, due to a collective magnetic phase transition, would correspond to a straight section in this curve. At $S = 0$, we find the energy of the magnetic ordering: $E/R = -0.0245$ K.

in good agreement. As for a comparison with the Q-S data of Johnson *et al.*[5]), a difference in the vertical (Q) scale by a factor of about 1.7 originates from the difference between the respective T^{-2} coefficients which has already been discussed in section 5. Further, a difference between the respective horizontal entropy scales, especially at low entropies, could be due to different procedures of entropy calculation. (This difference consists of the molecular field correction and the irreversible entropy gain which we have applied.)
From the Q-S relation one can obtain the temperature for each point of the curve by differentiating: $T = \mathrm{d}Q(S)/\mathrm{d}S$, yielding the T-S (fig. 7) and the T-Q (fig. 8) relations. From the T-Q relation, one derives the heat capacity by a second differentiation. These findings are plotted in fig. 9 as black dots which exhibit a broad and a low anomaly. Although the results at the high temperature side are in approximate agreement with direct heat capacity measurements, appreciable systematic errors may have been introduced by differentiating

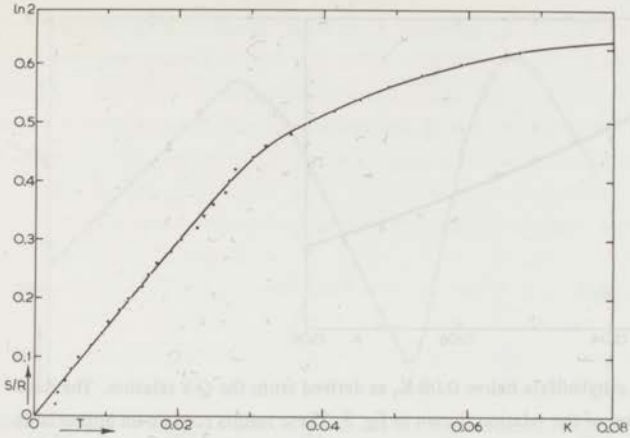

Fig. 7. The relation between entropy S and temperature T. The temperature was obtained by differentiation of the relation shown in fig. 6. The curve has been drawn smoothly through the points because we do not expect an irregular behaviour of the entropy.

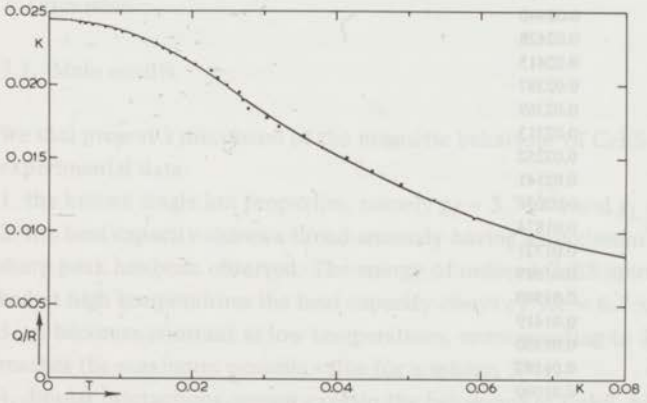

Fig. 8. The relation between the heat Q and the temperature. The rather small slope of this curve over the whole temperature range corresponds to the absence of a large heat capacity peak.

two times, hence one should consider fig. 9 as a somewhat qualitative picture. Especially the results below 0.015 K are tentative. The absence of a large anomalous peak is in qualitative agreement with the data of Johnson and Meyer[5]). We believe that on the basis of our data we can rule out the existence of a large peak due to a critical point at a temperature of about 0.04 K. If a sharp peak occurs, it is presumably a small one, or one to be found below 0.015 K, at the low temperature side of the anomaly, such as is observed for *e.g.* ytterbium titanate[27]) (see also chapter VI). From the small slope of the curve in fig. 6 at low entropies, it follows that the decrease of entropy extends to low temperatures and that

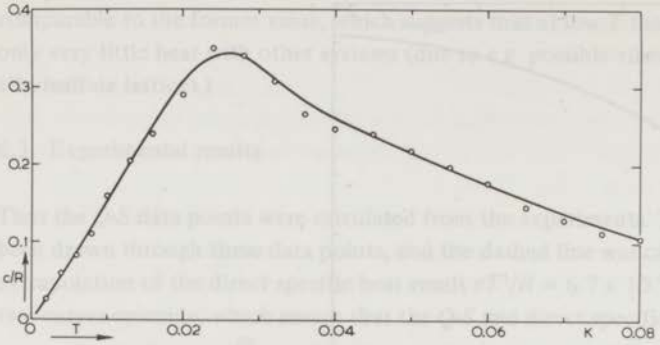

Fig. 9. The heat capacity of cerium ethylsulfate below 0.08 K, as derived from the Q-S relation. The data points are obtained by differentiation of the relation shown in fig. 8. These results contain an appreciable systematic error.

T (K)	c/R	S/R	Q/R (K)
0.0	0.0	0.0	0.02450
0.002	0.03	0.03	0.02440
0.004	0.06	0.06	0.02428
0.006	0.08	0.09	0.02415
0.008	0.11	0.12	0.02397
0.010	0.16	0.15	0.02369
0.013	0.20	0.20	0.02313
0.016	0.24	0.24	0.02252
0.020	0.29	0.30	0.02141
0.024	0.35	0.35	0.02031
0.028	0.34	0.41	0.01874
0.032	0.31	0.46	0.01721
0.036	0.26	0.49	0.01619
0.040	0.25	0.51	0.01540
0.045	0.24	0.54	0.01419
0.050	0.22	0.565	0.01300
0.055	0.20	0.585	0.01192
0.060	0.18	0.602	0.01090
0.070	0.13	0.627	0.00935
0.080	0.10	0.640	0.00842

Table II. Heat capacity, entropy and energy for $T < 0.08$ K. T and c were derived from the experimental Q-S relation by differentiation. Therefore the relation between Q and S is more accurate than all other relations in this table. Especially c may contain appreciable errors.

the heat capacity does not fall rapidly to zero below the maximum near to $T = 0.025$ K (cf. fig. 9). The heat capacity data from the Q-S measurements are plotted in fig. 10 on a logarithmic scale, together with direct heat capacity measurements: also data taken from Meyer and Smith[6]) are shown. These data cover four decades of temperature. A comparison between the two anomalies shows that the low temperature anomaly is even broader than the Schottky type curve at 3 K.

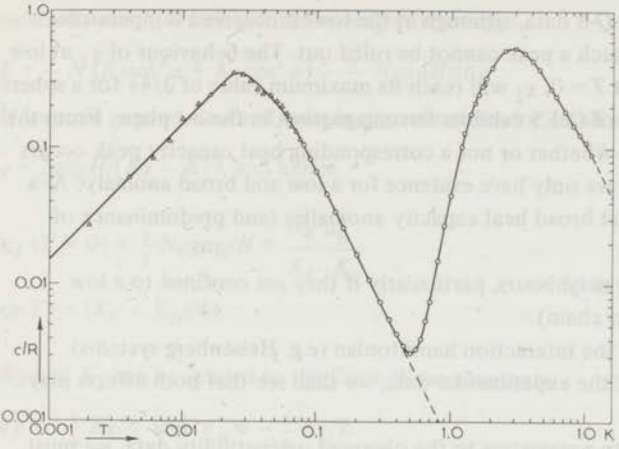

Fig. 10. The heat capacity of cerium ethylsulfate over four decades of temperature. □ data taken from Meyer and Smith[6]). ○ from direct heat capacity measurements. △ from the *Q-S* data.

7. *Discussion*

7.1. Main results

We shal present a discussion of the magnetic behaviour of CeES on basis of the following experimental data:

1. the known single ion properties, namely $g_{/\!/} = 3.76$[17]) and $g_{\perp} \approx 0.24$.
2. the heat capacity shows a broad anomaly having a maximum at $T \approx 0.025$ K, while no sharp peak has been observed. The energy of ordered CeES amounts to $E/R = -0.0245$ K, and at high temperatures the heat capacity obeys $cT^2/R = 6.7 \times 10^{-4}\,\mathrm{K}^2$.
3. $\chi_{/\!/}$ becomes constant at low temperatures, corresponding to $T^* = 0.13$ K[5]). $\chi_{\perp}$ nearly reaches the maximum possible value for a sphere, $3/4\pi$.
4. dipolar interactions cannot explain the behaviour of CeES, but they are not negligible.
5. the Curie-Weiss constants are $\theta_{/\!/} = -0.048 \pm 0.004$ K, $\theta_{\perp} \geqslant +0.027 \pm 0.005$ K.
6. the result of Dweck and Seidel[17]), to be discussed in section 7.3.

7.2. Possibility of a critical point

Johnson and Meyer[5]) inferred the existence of a critical point near 0.05 K from the maximum in $\chi_{/\!/}$ and from the minima in the *H-T* curves. However, calculations about non-long range ordering antiferromagnetic Ising linear chains, for example, also predicts a maximum in χ and minima in the adiabatic *H-T* curves (see *e.g.* ref. 30), and *e.g.* observations of Landau *et al.*[28]) show that the minima do not coincide with the critical point for the case of dysprosium aluminium garnet. Further, no evidence for a large heat capacity peak (at a

critical point) is found from the *Q-S* data, although at the lowest observed temperatures ($T < 0.015$ K) the existence of such a peak cannot be ruled out. The behaviour of $\chi_\perp$ at low entropies (fig. 3) suggests that at $T = 0$, $\chi_\perp$ will reach its maximum value of $3/4\pi$ for a sphere, and hence that the ground state of CeES exhibits ferromagnetism in the *a-a* plane. From the *Q-S* data we could not conclude whether or not a corresponding heat capacity peak occurs in that temperature range. Thús we only have evidence for a low and broad anomaly. As a general rule, it may be stated that broad heat capacity anomalies (and predominance of short range ordering) occur for:

a. a small number of interacting neighbours, particularly if they are confined to a low lattice dimensionality (*e.g.* linear chain).

b. a high spin dimensionality of the interaction hamiltonian (*e.g.* Heisenberg systems).

During the following analysis of the experimental data, we shall see that both effects play a role in CeES.

Before correlating the interaction parameters to the observed susceptibility data, we must consider the possibility of a deformation in the CeES lattice causing weak ferromagnetism. A rotation of the preferred $g_{/\!/}$ directions by an angle α of about 1° and a simple two-sublattice antiferromagnetic long range order might explain the easy magnetization, but the zero temperature limit of $\chi_{/\!/}$ would correspond to about $T^* = -\theta_{/\!/}/\sin^2\alpha$ or $\chi_{/\!/}$ less than one thousandth of the value reported by Johnson and Meyer. Therefore we shall propose a different magnetic structure and we shall investigate whether it is possible to interpret the susceptibility data without assuming a crystal lattice deformation.

7.3. Calculation of $\chi_{/\!/}$ for ferromagnetic alignment in the xy plane

Both molecular field and antiferromagnetic spin wave theory for an uniaxial antiferromagnet predict $\chi_{/\!/} = 0$ at the low entropy limit, but an explanation for the observed $\chi_{/\!/}$ value can be found if a magnetic moment in the *a-a* plane exists. A small magnetic field along the *c* axis will then slightly polarize the spins. In order to estimate this susceptibility, we shall now make a molecular field calculation, thereby not distinguishing between dipolar and other interactions in the hamiltonian for two interacting effective $s = \frac{1}{2}$ spins:

$$\mathcal{H}_{ij} = s_i \cdot K^{ij} \cdot s_j$$

We now define two parameters for a macroscopic system of equivalent spins:

$$K_{/\!/} = \frac{1}{N} \sum_{i \neq j} K^{ij}_{zz} \qquad K_\perp = \frac{1}{N} \sum_{i \neq j} K^{ij}_{xx}$$

We suppose axial symmetry around the z axis, ferromagnetic alignment in the xy plane, $K_{/\!/} > 0$ and $K_\perp < 0$. Note that the 'parallel' direction refers to the $g_{/\!/}$ direction and is perpendicular to the direction of spin alignment. If we apply a magnetic field H parallel to the z axis to such a system, the spins will rotate by an angle φ to the z axis. For a completely

ordered system, we can write the magnetic energy:

$$E = \tfrac{1}{8} N (K_{/\!/} \sin^2\varphi + K_\perp \cos^2\varphi) - \tfrac{1}{2} N g \mu_B H \sin\varphi$$

If we now expand $\sin\varphi$ and $\cos\varphi$ in a power series for small φ, and require $dE/d\varphi = 0$, we find $\varphi = 2g\mu_B H/(K_{/\!/} - K_\perp)$, and hence

$$\chi_{/\!/}\,(T \approx 0) = \tfrac{1}{2} N \varphi g \mu_B / H = \frac{N g^2 \mu_B^2}{K_{/\!/} - K_\perp}$$

or $T^* = (K_{/\!/} - K_\perp)/4k$

$K_{/\!/}$ and $K_\perp$ can be related to the Curie-Weiss constants:

$\theta_{/\!/} = -\tfrac{1}{4} K_{/\!/}/k$ and $\theta_\perp = -\tfrac{1}{4} K_\perp/k$.

Applying these relations to CeES, the $K_{/\!/}$ and $K_\perp$ values can now be derived from the susceptibility data in section 4, and we find $T^* \approx 0.1$ K, which has roughly the same magnitude as the experimental result 0.13 K[5]). Later in this discussion we shall see that $K_\perp$ is probably too small to account for the observed energy gain. The above calculation rather serves to demonstrate that an appreciable moment perpendicular to the c axis is related to a $\chi_{/\!/}$ value at low temperatures (T much smaller than the K/k values) of the same order of magnitude as the observed value. It is plausible that this also holds if there is only short range order in the *a-a* plane.

7.4. Magnitude of the interaction constants

For consideration of the spin-spin interaction, we shall now write the spin hamiltonian for a pair of ground state Ce ions as

$$\mathcal{H}_{ij} = \mu_B^2 \left\{ \frac{(g_i \cdot s_i)\cdot(g_j \cdot s_j)}{r_{ij}^3} - 3\,\frac{[(g_i \cdot s_i)\cdot r_{ij}][(g_j \cdot s_j)\cdot r_{ij}]}{r_{ij}^5} \right\} + s_i \cdot J^{ij} \cdot s_j$$

The first term describes the dipolar part, the second term the nondipolar part of the interaction. In view of the crystal structure of CeES (section 2), we suppose that the components $J^{ij}_{\alpha\beta}$ of the nondipolar interaction tensors are nonzero only for the 2 nearest neighbours (n n) and for the 6 next nearest neighbours (2n). These components can be related to the Curie-Weiss constants:

$$\theta_{/\!/} = -\tfrac{1}{2} J_{/\!/}^{nn}/k - \tfrac{3}{2} J_{/\!/}^{2n}/k + \theta_{/\!/ dip} = -\tfrac{1}{4} J_{/\!/}/k + \theta_{/\!/ dip} \qquad (9)$$

$$\theta_\perp = -\tfrac{1}{2} J_\perp^{nn}/k - \tfrac{3}{2} J_\perp^{2n}/k + \theta_{\perp dip} = -\tfrac{1}{4} J_\perp/k + \theta_{\perp dip} \qquad (10)$$

where we have neglected possible nonaxial terms in the J tensors and where we have introduced $J_{/\!/} = 2J_{/\!/}^{nn} + 6J_{/\!/}^{2n}$ and $J_{\perp} = 2J_{\perp}^{nn} + 6J_{\perp}^{2n}$. The calculation of the dipolar θ's has been described in chapter II and leads to

$$\theta_{/\!/\,dip} = +0.0153 \text{ K and } \theta_{\perp\,dip} = -0.000031 \text{ K}$$

if we take $g_{/\!/} = 3.76$ and $g_{\perp} = 0.24$ (section 4). From our susceptibility measurements we have found $\theta_{/\!/} = -0.048 \pm 0.004$ K, $\theta_{\perp} \geqslant +0.027 \pm 0.005$ K. Substituting these data in eqs. (9) and (10), we obtain $J_{/\!/}/k = 0.252 \pm 0.016$ K, $J_{\perp}/k \leqslant -0.108 \pm 0.020$ K. Dweck and Seidel[17]) have measured by an E.P.R. line shift method $(J_{/\!/} - J_{\perp})/2hc = 0.113 \pm 0.003$ cm^{-1} or $(J_{/\!/} - J_{\perp})/k = 0.324 \pm 0.009$ K. This experimental result and the results for $\theta_{/\!/}$ and $\theta_{\perp}$ are shown in fig. 11 as regions in the $J_{\perp} - J_{/\!/}$ diagram. A small triangle belongs to all three regions and the $J_{\perp}$ and $J_{/\!/}$ values must be in or close to this triangle. The values $\theta_{/\!/} = -0.045$ K, $\theta_{\perp} = +0.023$ K, corresponding to $J_{/\!/}/k = 0.24$ K, $J_{\perp}/k = -0.092$ K are a fit just within the bounds set by the accuracy of the experiments of Dweck and Seidel and of us.
Using these numbers, we can make a comparison with the experimental value of cT^2/R. We have computed the dipolar sum as described in chapter I, using $g_{/\!/} = 3.76$ and $g_{\perp} = 0.24$. For the case of axial symmetry of the nondipolar interaction we obtain

$$\begin{aligned} cT^2/R = \; & (1.67 \times 10^{-4} - 6.12 \times 10^{-3} J_{/\!/}^{nn}/k + 6.25 \times 10^{-2} J_{/\!/}^{nn\,2}/k^2 \\ & + 2.49 \times 10^{-5} J_{\perp}^{nn}/k + 1.25 \times 10^{-1} J_{\perp}^{nn\,2}/k^2 \\ & + 2.45 \times 10^{-3} J_{/\!/}^{2n}/k + 1.875 \times 10^{-1} J_{/\!/}^{2n\,2}/k^2 \\ & - 1.00 \times 10^{-3} J_{\perp}^{2n}/k + 3.75 \times 10^{-1} J_{\perp}^{2n\,2}/k^2)\ \text{K}^2 \end{aligned} \qquad (11)$$

We shall first investigate whether the experimental cT^2/R value can be explained by assuming nondipolar interactions among nearest neighbours only. To this end we calculate the values shown in column 1 of table III from eqs. (9) and (10) and substitute them in eq. (11). The result $cT^2/R = 5.97 \times 10^{-4}$ K^2 is too small, but sufficiently close to the experimental value (6.7×10^{-4} K^2) to indicate that the nondipolar interactions arise mainly from

		1	2	3	4	5	6	7	Exp. value
$J_{/\!/}^{nn}/k$	(K)	+0.120	+0.128	+0.120	+0.148	+0.108	+0.108	+0.144	
$J_{\perp}^{nn}/k$	(K)	−0.046	−0.046	−0.052	−0.018	−0.058	−0.058	−0.022	
$J_{/\!/}^{2n}/k$	(K)	0	0	0	0	0	+0.004	−0.008	
$J_{\perp}^{2n}/k$	(K)	0	0	0	0	0	+0.004	−0.008	
$\theta_{/\!/}$	(K)	−0.045	−0.049	−0.045	−0.059	−0.039	−0.045	−0.045	−0.048 ± 0.004
$\theta_{\perp}$	(K)	+0.023	+0.023	+0.026	+0.009	+0.029	+0.023	+0.023	⩾0.027 ± 0.005
$(J_{/\!/} - J_{\perp})/k$	(K)	+0.332	+0.348	+0.344	+0.332	+0.332	+0.332	+0.332	+0.324 ± 0.009[a]
cT^2/R	(10^{-4} K^2)	5.97	6.7	6.7	6.7	6.7	6.7	6.7	6.7 ± 0.2

[a] Value taken from ref. 17.

Table III. Seven sets of four nondipolar interaction parameters J are given. Dipolar interactions have to be added to the J values quoted here. The dipolar equivalent of $J_{/\!/}^{nn}/k$ amounts to −0.049 K. Further dipolar parameters are much smaller. From the parameters, four observable physical quantities were calculated. Agreement with the experimental values is obtained for columns 6 and 7.

the nearest neighbours. We can, of course, find close agreement with the experimental cT^2/R value if we substitute *e.g.* $J_{/\!/}^{nn}/k = -0.052$ K (column 3), which values are also in agreement with our susceptibility results. These numbers, however, lead to $(J_{/\!/} - J_\perp)/k$ values which are a few percent beyond the experimental accuracy of Dweck and Seidel. In columns 4 and 5, values are shown which fit well to the cT^2/R value and the Dweck and Seidel number, but the values of column 4 are in disagreement with both experimental θ values and the numbers in column 5 are not satisfactory in view of the $\theta_{/\!/}$ value. In fig. 11, the parameters of columns 2-5 correspond to four points lying on curve a, which illustrates relation (11) for zero next nearest neighbour interaction. No point of this curve a obeys the three experimental results. If we want a good fit with all experimental data, we have to

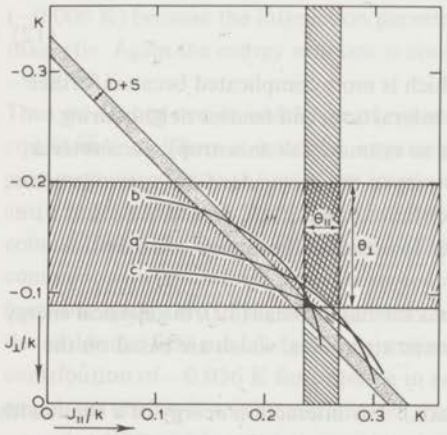

Fig. 11. The $J_\perp$–$J_{/\!/}$ diagram. The two lines marked D + S give the experimental result of Dweck and Seidel[17]): $(J_{/\!/} - J_\perp)/k = 0.324$ K. The experimental $\theta_{/\!/}$ and $\theta_\perp$ values (see text) also put bounds to the $J_{/\!/}$ and $J_\perp$ values resp. A small triangular region in this diagram obeys the three experimental results. Curves representing eq. (11) are shown for three isotropic n.n.n. interaction values:
curve a: $J^{2n}/k = 0$ K
curve b: $J^{2n}/k = -0.008$ K
curve c: $J^{2n}/k = +0.004$ K.

assume nondipolar next nearest neighbour (n.n.n.) interactions. Information about n.n.n. interactions has recently been obtained by Anderson *et al.*[18]) for Ce pairs in some non-magnetic rare earth ethylsulfates. They found several elements of the traceless (hence non-isotropic) part of this interaction which were different from the dipolar values by only a few times 10^{-4} K. Therefore we studied the effect of an isotropic n.n.n. interaction contribution J^{2n}. Good agreement with the experimental numbers is obtained for two sets of parameters shown in columns 6 and 7 of table III. For the corresponding J^{2n}/k values, eq. (11) is illustrated in fig. 11 as curve b ($J^{2n}/k = -0.008$ K) and curve c ($J^{2n}/k = +0.004$ K).

The experimental accuracies indicated in fig. 11 give an impression of the errors in the two sets of parameters, and we have to keep in mind that these parameters are liable to appreciable changes if one or more experimental numbers are outside their estimated bounds.

7.5. Linear chain calculations

We shall now investigate whether a choice between the two sets can be made by relating the experimental energy E at $T = 0$ with the J components. In both cases the interactions are predominantly of the linear chain type. Therefore we shall apply the formalism of Yang and Yang[29]) for anisotropic Heisenberg linear chains. These authors derived the energy E at $T = 0$ for such chains having only nearest neighbour interaction:

$$\mathcal{H}_{ij} = J[(s_{ix}s_{jx} + s_{iy}s_{jy}) + \Delta(s_{iz}s_{jz})] \qquad (12)$$

However, in this case we are studying a system which is more complicated because further neighbours within a chain have nonzero (dipolar) interaction, and nearest neighbouring chains are coupled by n.n.n. interactions. In order to estimate the anisotropy parameter Δ, we calculated the energy for some magnetic structures in the molecular field approximation, considering the spins as classical vectors having a definite orientation, namely $s \parallel c$ and $s \perp c$ axis. Further, this approximation makes it possible to estimate the energy contribution from interchain (n.n.n.) interactions.

Taking the interaction parameters of column 6, and the hamiltonian (12), the classical energy values were calculated for the following two magnetic structures, which are based on the signs of the J components:

1. antiferromagnetic chains along the c axis ($s \parallel c$ axis). The interaction energy of a chain with its three nearest neighbouring chains is zero and hence the result $E/R = -0.0152$ K is nearly completely due to intrachain interaction.

2. ferromagnetic chains (s in the a-a plane) along the c axis, which have their three nearest neighbouring chains antiparallel. This structure leads to $E/R = -0.0175$ K. A contribution -0.0145 K originates from intrachain interactions.

The anisotropy parameter Δ from eq. (12) may be estimated by taking the opposite of the quotient of the intrachain energies of structures 1 and 2 respectively, namely $\Delta = -1.05$. Using numerical results derived in chapter II, section 10, we find an energy -0.0261 K for intrachain interactions (this corresponds to an energy reduction of 72% relative to the classical result for structure 1. For an isotropic Heisenberg linear chain, having $\Delta = +1$, the energy reduction amounts to 77%). A further energy contribution arises from interchain (n.n.n.) interactions. Its value is expected to be intermediate between about zero (structure 1) and -0.003 K (structure 2). Hence, for the parameters shown in column 6 we estimate the energy at $T = 0$ to be $E/R \approx -0.0276$ K. In view of the approximations used in these calculations and the inaccuracy in the parameters used, we can only conclude that the set of parameters shown in column 6 of table III is compatible with the experimental energy gain $E/R = -0.0245$ K.

Similarly to the above procedure for column 6, we shall now compute the energy using the interaction parameters of column 7. A classical energy $E/R = -0.0242$ K was found for the structure labeled 1 above. This value is nearly completely due to intrachain interaction. Interchain interactions of column 7 have the ferromagnetic sign and therefore we define, instead of structure 2, a ferromagnetic structure 3 (all spins parallel in the *a-a* plane). The molecular field approximation gives an energy $E/R = -0.0115$ K from which -0.005 K is due to intrachain interaction. Hence we obtain an anisotropy parameter $\Delta = -4.4$ for the opposite of the quotient of the intrachain energies of structures 1 and 3. For column 7, we then find an intrachain energy -0.0254 K according to the data derived in chapter II. This corresponds to an energy reduction of 5% relative to structure 1. The interchain contribution is expected to be closer to that of structure 1 (about zero) than to that of structure 3 (-0.006 K) because the interaction parameters in column 7 are predominantly antiferromagnetic. Again the energy estimate is compatible with the experimental value $E/R = -0.0245$ K.

Thus we cannot decide which one of column 6 and 7 is to be preferred from these energy considerations. There is, however, experimental evidence favouring one of the two sets. The easy magnetization in the *a-a* plane (section 4) at low entropies is difficult to understand if antiferromagnetic interchain interactions (column 6) are present. Hence the parameters in column 7 give the best interpretation of the experimental data now available, and some comment may be useful. Since it is argued above that spin wave contributions to the magnetic energy are small, one may analyze the energy in various contributions,according to the molecular field model. In this approximation, nondipolar n.n. interactions give an energy contribution of -0.036 K for ordering in antiferromagnetic chains (*s*$\parallel$*c* axis). Nearest neighbour chains, if completely ordered, have zero interchain interaction energy, and next nearest neighbour chains are assumed to have zero nondipolar interaction (section 2) and their dipolar interaction energy is small. The total dipolar energy, which arises mainly from the two n.n., has the positive sign; for such a structure we calculated $E_{dip}/R = +0.0118$ K. The sum of the dipolar and nondipolar energies is liable to an estimated 5% correction for intrachain quantummechanical (spinwave) effects. Energy contributions from ferromagnetic interchain interactions are believed to be small.

Although quantummechanical effects only give a small energy contribution, they may give an explanation for the susceptibility behaviour (large $\chi_\perp$ values, nonzero $\chi_\parallel$ at low entropies), where the classical approach fails. To our knowledge, no calculations about this subject have been published for the type of interactions considered here.

For ordered antiferromagnetic chains, the interchain interactions are expected to be small (see above), and one would expect long range order to occur at low entropies only. This is in accordance with the absence of experimental evidence for a heat capacity peak (see section 6). Further, the heat capacity data are in qualitative agreement with results of Bonner and Fisher[30]) for anisotropic Heisenberg chains.

Conclusion.

The magnetic and thermal behaviour of CeES is dominated by anisotropic n.n. interaction, which gives short range ordering in linear chains. The type of ordering is antiferromagnetic as far as we consider the components along the hexagonal c axis of neighbouring spins. However, when we examine the behaviour of the spin components in the a-a plane, we find ferromagnetic properties.

Appendix

The entropy $S(H,T)$ of a system in a magnetic field H and at temperature T can be derived with help of the thermodynamical relation

$$\mathrm{d}S = \frac{c_H}{T}\,\mathrm{d}T + \left(\frac{\partial M}{\partial T}\right)_H \mathrm{d}H$$

c_H is the heat capacity in a constant magnetic field, and M is the magnetization.
If the zero-field heat capacity obeys

$$c_0 = \frac{b}{T^2}$$

we find by integration

$$S(0,\infty) - S(0,T) = \frac{b}{2T^2} \ .$$

If the susceptibility follows a Curie-Weiss law, we have for small fields ($g\mu_B H \ll kT$):

$$\left(\frac{\partial M}{\partial T}\right)_H = -\frac{CH}{(T-\theta)^2} \qquad \text{and hence we find}$$

$$S(0,\infty) - S(H,T) = \frac{b}{2T^2} + \frac{CH^2}{2(T-\theta)^2} \ .$$

REFERENCES

1) Daniels, J.M., Proc. Phys. Soc. **A 66** (1953) 673
2) Baker, J.M., J. Phys. **C 4** (1971) 1631
3) Lagendijk, E., Blöte, H.W.J. and Huiskamp, W.J., to be published in Physica 1972.
4) Cooke, A.H., Whitley, S. and Wolf, W.P., Proc. Phys. Soc. **B 68** (1955) 415.
5) Johnson, C.E. and Meyer, H., Proc. Roy. Soc. (Lond) **253** (1959) 199
6) Meyer, H. and Smith, P.L., J. Phys. Chem. Solids **9** (1959) 285
7) Ketelaar, J.A.A., Physica **4** (1937) 619
8) Fereday, R.A. and Wiersma, E.C., Physica **2** (1935) 575
9) Becquerel, J., de Haas, W.J. and van den Handel, J., Physica **5** (1938) 857
10) Van den Handel, J., thesis, University of Leiden, 1940
11) Bogle, G.S., Cooke, A.H. and Whitley, S., Proc. Phys. Soc. **A 64** (1951) 931
12) Elliot, R.J. and Stevens, K.W.H., Proc. Phys. Soc. **A 64** (1951) 933
13) Elliot, R.J. and Stevens, K.W.H., Proc. Roy. Soc. (Lond) **A 215** (1952) 437
14) Van den Broek, J. and Van der Marel, L.C., Physica **29** (1963) 948
15) Finn, C.B.P. and Najafabadi, B.M., J. Phys. **C 3** (1970) 330
16) Birgeneau, R.J., Phys. Rev. Lett. **19** (1967) 160.
17) Dweck, J. and Seidel, G., Phys. Rev. **146** (1966) 359
18) Anderson, R.J., Baker, J.M. and Birgeneau, R.J., J. Phys. **C 4** (1971) 1618.
19) Larson, G.H., Phys. Rev. **150** (1966) 264
20) De Haas, W.J. and Wiersma, E.C., Physica **2** (1935) 335
21) Finkelstein, R. and Mencher, A., J. Chem. Phys. **21** (1953) 472
22) Bleaney, B., Proc. Phys. Soc. **77** (1961) 113
23) Baker, J.M., Phys. Rev. **136** (1964) A 1633.
24) Stevens, K.W.H. and van Eekelen, H.A.M. Proc. Phys. Soc. **92** (1967) 680
25) Becker, E.and Clover, R.B., Phys. Rev. Lett. **21** (1968) 1327
26) Fletcher, J.R. and Sheard, F.W., Solid State Comm. **9** (1971) 1403
27) Blöte, H.W.J., Wielinga, R.F. and Huiskamp, W.J., Physica **43** (1969) 549
28) Landau, D.P., Keen, B.E., Schneider, B. and Wolf, W.P., Phys. Rev. **B 3** (1971) 2310
29) Yang, C.N. and Yang, C.P., Phys. Rev. **150** (1966) 327
30) Bonner, J.C. and Fisher, M.E., Phys. Rev. **135** (1964) 640

CHAPTER V

MAGNETIC PHASE TRANSITIONS IN FOUR MANGANESE DOUBLE CHLORIDES

Summary

Heat-capacity and magnetic-susceptibility data in the temperature range 0.05 K $< T <$ 3 K are presented on Cs_3MnCl_5, $Cs_2MnCl_4.2H_2O$, K_4MnCl_6 and α-Cs_2MnCl_4. Sharp maxima in the heat capacities corresponding to magnetic phase transitions from paramagnetic to antiferromagnetically ordered states are observed. The Néel points are respectively, $T_N = 0.601$, 1.81, 0.439 and 0.935 K ± 0.5%. For K_4MnCl_6, another sharp peak is found at $T = 0.332$ K.

From the measured energy gain E/R, the high-temperature heat capacity $c_h T^2/R$, and the Curie-Weiss constant θ, information is obtained about the magnitude of the exchange interaction parameter. Furthermore, at low temperatures hyperfine heat capacities have been measured.

1. *Introduction*

Magnetic phase transitions have been observed in many divalent manganese compounds, and have been studied rather extensively, particularly on manganese halogenides like MnF_2[1]). Most of these compounds are antiferromagnetic at low temperatures, while the height of the Néel temperature and the magnitude of the superexchange interaction are smaller for Cl than for F compounds in general. Hence it is not surprising that, because of its low temperature, magnetic phase transitions have not yet been observed in many double chlorides of Mn, in which the interatomic distances are somewhat larger than in $MnCl_2$, which has a Néel temperature of about 2 K[2]). The successful application of low-temperature calorimetry in the range of roughly 0.04 to 4 K, extending over two decades on the temperature scale, has proved to be quite useful in locating the position of the critical temperature. Further, by integration of the specific heat *versus* temperature over a sufficiently wide temperature range, one obtains the magnetic energy gain with fair accuracy, which may yield at least an average value of the superexchange interaction parameters. Mn^{2+} ions are particularly favourable in this respect, because their lowest energy level is an S state, which favours an isotropic exchange interaction, while crystalline field effects are, in general, only of secondary importance. A systematic study of the magnitude of the exchange interaction in many Mn compounds is required in order to gain more insight into the superexchange mechanism.

We shall discuss experimental results on four manganese double chlorides. Numerical heat capacity data have already been published in ref. 32, in which also an attempt has been made to analyze the critical behaviour of the heat capacity *versus* temperature curves. The transition temperatures for the various compounds are obtained from that analysis.
For an interpretation of the experimental results, we shall enumerate some formulae for Heisenberg spin systems described by the following interaction hamiltonian:

$$\mathcal{H} = -2 \sum_{\langle i,j \rangle} J_{ij} \mathbf{s}_i \cdot \mathbf{s}_j$$

The first formula relates the magnetic energy gain to the exchange constant J for an ion with z neighbours:

$$E/R = zs^2 J/k \tag{1}$$

This is a molecular field approximation for an antiferromagnet having two sublattices with antiparallel spin orientation. Interactions are assumed to occur only between spins which belong to different sublattices. The molecular field theory is only satisfactory as a first approximation and a better approximation is given by spin-wave theory. It follows that to the right-hand part of eq. (1) a correction must be applied:

$$E/R = zs^2(1 + a/zs)J/k, \tag{1a}$$

where a follows from the crystal structure, and $0 < a < 1$. For $s = \frac{5}{2}$ this correction usually amounts to only a few percent.
The Curie-Weiss constant is given by

$$\theta = 2zs(s + 1)J/3k. \tag{2}$$

At high temperatures, we can describe the decrease of the heat capacity by:

$$c_h T^2/R = 2zs^2(s + 1)^2 J^2/3k^2. \tag{3}$$

If there exist different types of neighbours, we can replace z in eqs. (1) to (3) by a summation over all neighbours. When we divide the square of eq. (2) by eq. (3) we obtain:

$$R\theta^2/c_h T^2 = \frac{2}{3}z. \tag{4}$$

Stanley and Kaplan[3]) have derived the critical point T_c for a two-dimensional ferromagnet:

$$|kT_c/J| = \frac{1}{5}(z - 1)[2s(s + 1) - 1], \tag{5}$$

while Rushbrooke[4]) obtained for a three-dimensional ferromagnet:

$$|kT_c/J| = \frac{5}{96}(z - 1)[11s(s + 1) - 1]. \tag{6}$$

For $s = \frac{5}{2}$ we do not expect large differences between ferro- and antiferromagnets, hence we shall use eqs. (5) and (6) for the antiferromagnetic transition temperature T_N.

2. *Preparation of the samples*

a. The sample of Cs_3MnCl_5 was prepared by fusing together stoichiometric quantities of CsCl and $MnCl_2$. After cooling to room temperature, the polycrystalline mass was ground until the dimensions of the particles were roughly 0.2 mm. X-ray powder photographs showed that the structure was the same as given by IJdo[5]) for Cs_3MnCl_5.
b. $Cs_2MnCl_4.2H_2O$ was grown from aqueous solution.
c. K_4MnCl_6 was prepared by fusing together the components ($MnCl_2$ and 4KCl). Since this substance melts incongruently, the solidified sample was finely ground, and then heated to about 380°C for several hours. (This temperature is higher than that prescribed by Swanson *et al.*[6]). Using their recipe,we obtained samples of insufficient purity. This may be caused by a different particle size after grinding.) An X-ray examination confirmed that the sample consisted, apart from minor impurities, of K_4MnCl_6.
d. α-Cs_2MnCl_4 was also prepared by fusing together its components. The α-modification is stable above 297°C[7,8]). At this temperature, a phase transition occurs, and at lower temperatures the β-modification, which has the K_2NiF_4 structure[8]), is stable. Under certain circumstances, however, it is possible to conserve an unstable phase by rapid cooling to a temperature where the transition rate is low. For this purpose, the fused sample was cooled to room temperature in a few minutes. Grinding, inserting in the sample container and cooling to liquid He temperatures took about 2.5 hours. A discussion of the chemical composition of the sample will be given in section 6.2.

3. *Heat capacity of Cs_3MnCl_5*

3.1. Crystallographic data and spin hamiltonian

According to IJdo[5]), Cs_3MnCl_5 crystallizes in a tetragonal structure (D_{4h}^{18}, $I4/mcm$) and is isomorphous to Cs_3CoCl_5, for which the crystal structure has been determined by Powell *et al.*[9]) and Figgis *et al.*[10]). The unit cell is presented in fig. 1. Upon dividing the unit cell into two halves by a plane parallel to the a and b axes, one finds the upper and lower half subcell to be equivalent, except for mirror reflections of the $[MnCl_4]$ and $[ClCs_4]$ groups. Since mirror reflections do not alter the magnetic properties of the Mn^{2+} ion and the value of the exchange constants, one may consider the two subcells to be magnetically equivalent. This justifies the consideration of the simple tetragonal Bravais lattice as the basic unit cell for the Mn ions, for which the dimensions are: $\frac{1}{2}a\sqrt{2} = 6.514$ Å and $\frac{1}{2}c = 7.454$ Å.
E.P.R. measurements of Henning and Bongers[11]) in the isostructural Cs_3ZnCl_5 have shown that the energy levels of the Mn^{2+} ions (which were all found to be magnetically equivalent) can be described by a spin hamiltonian

$$\mathcal{H} = g_{\parallel}\mu_B H_z s_z + g_{\perp}\mu_B(H_x s_x + H_y s_y) + D(s_z^2 - \tfrac{35}{12}) + \tfrac{1}{6}a(s_x^4 + s_y^4 + s_z^4 - \tfrac{707}{16}) + A\mathbf{s}\cdot\mathbf{I}.$$

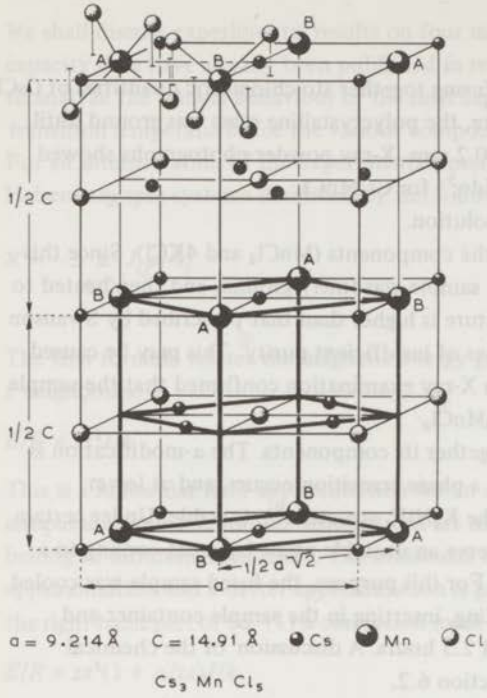

Fig. 1. Structure of Cs_3MnCl_5. For clarity, only the chlorine tetrahedra around two Mn ions have been shown. The tetrahedra at A and B are identical, except for a mirror reflection. This holds als for the cesium squares in the planes $z/c = \frac{1}{4}$ and $z/c = \frac{3}{4}$. As far as magnetic properties are concerned, we need to consider only a simple Bravais lattice for the Mn ions (thick lines).

The constants are as follows:

$g_{\parallel} = 2.0110 \pm 0.0005,$
$g_{\perp} = 1.992 \pm 0.0005,$
$A = (-73.1 \pm 0.4) \times 10^{-4}\,\mathrm{cm}^{-1},$
$D = (-89.6 \pm 1.5) \times 10^{-4}\,\mathrm{cm}^{-1},$
$a = (+10.7 \pm 1.5) \times 10^{-4}\,\mathrm{cm}^{-1}.$

Both the relatively small A value and the rather large $g_{\parallel}$ suggest appreciable covalency of the Mn-Cl bonds.

The energy splitting for zero external magnetic field is mainly determined by the terms containing A and D, while the additional splitting by the a term amounts to only about $10^{-3}\,\mathrm{cm}^{-1}$, and the latter will be neglected in the following. Further, the anisotropy of the g tensor is negligible for our considerations, so that we will simplify the spin hamiltonian

$$\mathcal{H} = g\mu_B H \cdot s + As \cdot I + D(s_z^2 - \tfrac{35}{12}).$$

It may be noticed that the D term corresponds to a rather small distortion of the Cl tetrahedron surrounding the Mn ion. In the magnetically ordered state the influence of the D term may be approximately described by an anisotropy field $H_A = 2Ds/g\mu_B = 490$ Oe. The measurements of Henning and Bongers have been performed on Mn^{2+} in the lattice of Cs_3ZnCl_5, of which the lattice parameters are slightly different from those of Cs_3MnCl_5, namely $a = 9.251$ Å, $c = 14.500$ Å, and $a = 9.214$ Å, $c = 14.908$ Å for the two salts, respectively. The c/a ratio in the Zn compound is slightly different from that in the Mn compound. This may influence the shape of the Cl^- tetrahedrons and the value of D. However, the magnitude of this effect seems uncertain. Thus we cannot estimate D for the Mn salt accurately, but from the similarity of the structures, we expect a comparable value.

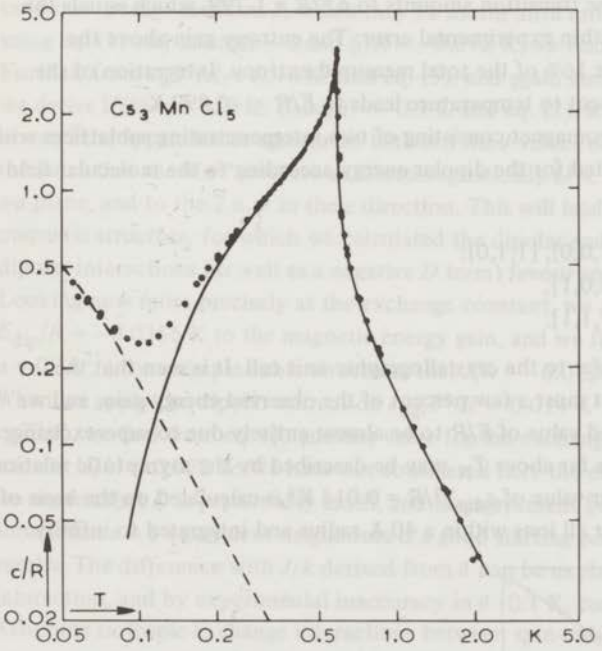

Fig. 2. Heat capacity of Cs_3MnCl_5 *versus* temperature. A theoretical curve (dashed line) has been fitted to the hyperfine heat capacity at the lowest temperatures. The full line represents the experimental data after subtraction of the hyperfine heat capacity. Between 1 and 2 K the data obey a $c \sim T^{-2}$ relation.

3.2. Experimental results

The heat-capacity data (fig. 2) clearly exhibit a phase transition at $T_N = 0.601$ K. The increasing heat capacity below 0.1 K can be explained by the hyperfine coupling term $As \cdot I$

in the hamiltonian. This term causes a splitting of the ground state into six (nearly) equidistant levels. Therefore we fitted a Schottky anomaly (for such a level system) to the experimental data, with the energy spacing Δ between two successive levels as a variable parameter; we obtained $\Delta/k = 0.0263$ K. For a fixed spin $\frac{5}{2}$, Δ is related to the hyperfine coupling constant as $\Delta = \frac{5}{2}|A|$. This would give $|A/k| = 0.0106$ K. This is in good agreement with the E.P.R. result of Henning and Bongers[11]) on Mn^{2+} ions in Cs_3ZnCl_5: $A/k = -0.0105$ K.

Using $\Delta/k = 0.0263$ K as a splitting parameter, subtraction of the hyperfine heat capacity (dashed line) form the data yields the extrapolation (full line) of the electronic heat capacity below T_N (fig. 2). Integration of the electronic specific heat curve, including the extrapolated parts, gives the entropy as a function of temperature. The total entropy change ΔS associated with the magnetic phase transition amounts to $\Delta S/R = 1.799$, which equals the expected value of $\ln 6 = 1.792$ within experimental error. The entropy gain above the critical point amounts to 0.283 or 16% of the total measured entropy. Integration of the electronic heat capacity with respect to temperature leads to $E/R = -0.892$ K.

For a completely ordered antiferromagnet consisting of two interpenetrating sublattices with antiparallel alignment, we calculated for the dipolar energy according to the molecular field approximation:

$E_{dip}/R = +0.0178$ K for $s \parallel [1,0,0], [1,1,0]$;
$E_{dip}/R = -0.0356$ K for $s \parallel [0,0,1]$;
$E_{dip}/R = -0.0089$ K for $s \parallel [1,1,1]$.

The crystallographic directions refer to the crystallographic unit cell. It is seen that the dipolar interaction accounts for at most a few percent of the observed energy gain, and we may consider the above mentioned value of E/R to be almost entirely due to superexchange. The heat capacity at temperatures far above T_N may be described by the asymptotic relation $c_h T^2/R = 0.16$ K^2. A much smaller value of $c_{dip}T^2/R = 0.014$ K^2 is calculated on the basis of a dipolar interaction summed over all ions within a 40 Å radius and integrated to infinity.

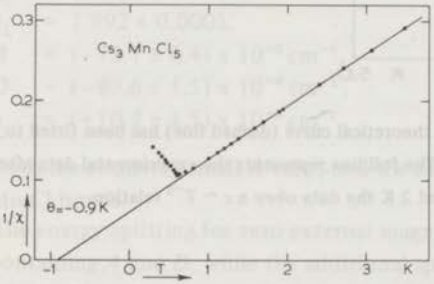

Fig. 3. Inverse a.c. powder susceptibility in arbitrary units, $1/\chi$, of Cs_3MnCl_5 *versus* temperature T. The susceptibility obeys a Curie-Weiss law (full line) to temperatures close to T_N. This is consistent with the small amount of short-range order above T_N. The maximum value of χ is observed at T_N.

Further, the a.c. powder susceptibility of Cs_3MnCl_5 has been measured below 4 K (fig. 3). A value of the Curie-Weiss constant $\theta = -0.9 \pm 0.1$ K was obtained.

3.3. Discussion

We assume in the following that the exchange interaction among nearest-neighbouring Mn ions along the *c* axis is equal to that among n.n. ions in the *a-a* plane. This assumption is not plausible *a priori* since the interionic distances along the *c* axis and in the *a-a* plane are appreciably different, namely 7.54 and 6.51 Å, respectively. However, for convenience of discussion we will not introduce two exchange constants J_{aa} and J_c. Rather, we will consider only one average constant J, which may be useful until more data become available. Hence, using eq. (1) and taking $z = 6$ and $E/R = -0.892$ K, we find $J/k = -0.024$ K. Further, from $c_h T^2/R = 0.16$ K² and eq. (3), and again assuming $z = 6$ nearest neighbours, we derive $|J/k| = 0.023$ K. Using $\theta = -0.9$ K and eq. (2), we obtain $J/k = -0.026$ K. Conversely, the approximate agreement between the J values obtained from θ and from E/R indicates that the Mn^{2+} ions are antiferromagnetically ($J < 0$) coupled to the 4 n.n. in the *a-a* plane, and to the 2 n.n. in the *c* direction. This will lead to a simple two-sublattice magnetic structure, for which we calculated the dipolar energy (section 3.2). It is seen that dipolar interactions (as well as a negative D term) favour spin orientation along the *c* axis. Looking now more precisely at the exchange constant, we apply the dipolar correction $E_{dip}/R = -0.0356$ K to the magnetic energy gain, and we find, from eq. (1a) and adopting $a = 0.58$[21]) for a simple cubic structure, that $J/k = -0.0220$ K for pure exchange coupling. When we apply the dipolar correction $c_{dip}T^2/R = 0.014$ K², and $c_{hfs}T^2/R = 0.002$ K² to $c_h T^2/R$, we find from eq. (3) another value for the exchange coupling constant proper, namely $|J/k| = 0.022$ K. We have not considered here the effect of D, however, in section 3.1 we argued that D is presumably small, and the agreement between the two latter J/k values shows that $z = 6$ equivalent neighbours is a good starting point for an explanation of the results. The difference with J/k derived from θ can be explained by a small n.n.n. exchange interaction, and by experimental inaccuracy in θ (0.1 K, corresponding to 0.003 K in J/k). Assuming isotropic exchange interactions between spin-only magnetic moments of Mn^{2+}, one may compare the experimental value for the short-range ordering entropy to theoretical calculations for the Heisenberg model. Although theoretical results for $s = \frac{5}{2}$ are not directly available, an estimate for a simple cubic lattice with n.n. interactions only can be obtained from the results for ferromagnets of Baker *et al.*[12]) for $s = \frac{1}{2}$ and Bowers and Woolf[13]) for infinite spin. Fisher[14]) has noted that the short-range ordering entropy varies approximately linearly with $1/s(s+1)$. This interpolation procedure leads to $(S_\infty - S_c)/R \approx 0.4$, hence to about 22% of the total entropy. We do not expect large differences between ferro- and antiferromagnets for $s = \frac{5}{2}$, hence we can conclude that the experimental fraction of short-range ordering entropy (16%) is smaller than the theoretical value for an s.c. spin $\frac{5}{2}$ antiferromagnet. We can not explain this discrepancy by assuming that the exchange constant in the *a-a* plane

is different from that in the c direction, because the ratio $E^2/Rc_h T^2$, and probably also RT_N/E reach a maximum for $J_{aa}/J_c = 1$. Both quantities may be correlated with the amount of short-range order, such that high values of these quantities correspond to a small value of the short-range ordering entropy. For an explanation, we may consider the afore mentioned dipolar interactions, and possibly to some extent also a negative D term. In this connection it is interesting, that theoretical results of Dalton and Wood[30]) for $s = \frac{1}{2}$ ferromagnets, predict that even a small anisotropy in the magnetic interactions results in a considerable change of the critical energy.

For further testing of our model, we can relate the exchange constant to the transition temperature for the following cases:

1. Simple cubic antiferromagnet. When we substitute $T_N = 0.601$ K and $z = 6$ into eq. (6), we find $J/k = -0.0242$ K, which must be compared to $J/k = -0.024$ K from eq. (1).
2. It was already mentioned that the distance to the nearest-neighbour Mn along the c axis is greater than that in the a-a plane. Moreover, from the crystal structure it is seen that the exchange path in the c direction takes place along three Cl^- ions instead of two. For this reason we also tried eq. (5) for a two-dimensional Heisenberg system, leading to $J/k = 0.0597$ K for $z = 4$. From eq. (1) we find $J/k = -0.036$ K.

These calculations clearly favour the three-dimensional model.

We conclude, that Cs_3MnCl_5 behaves like a three-dimensional antiferromagnet, having Heisenberg exchange and a relatively small amount of dipolar interaction.

4. *Heat capacity of $Cs_2MnCl_4.2H_2O$*

4.1. Crystal structure and recent experiments

According to Jensen[15]), $Cs_2MnCl_4.2H_2O$ has a triclinic structure ($P\bar{1}$) in which the Mn ions are arranged in a simple Bravais lattice (fig. 4). The Mn ions are surrounded by a slightly distorted octahedron of four Cl^- ions and two H_2O molecules. From the crystal structure at room temperature, it is found that all Mn ions are in identical positions, while N.M.R. data of Spence *et al.*[16]) at low temperatures show that the Mn spins are arranged in two interpenetrating magnetic sublattices having antiparallel spin alignment. Susceptibility measurements on this compound by Smith and Friedberg[17]) have indicated that the O-Mn-O axis of each $[MnCl_4 2H_2O]^{2-}$ group coincides approximately with the $\chi_{/\!/}$ direction ($\chi_{/\!/} > \chi_\perp$), both in the paramagnetic and in the antiferromagnetic state. They suggest a single-ion anisotropy originating from a Ds_z^2 term in the spin hamiltonian, in which $D \approx -0.1$ cm^{-1} or $D/k \approx -0.14$ K. Using this value, they derived from $\chi_\perp$ at zero temperature $zJ/k = -0.54$ K, while from the Curie-Weiss θ it was found that $zJ/k = -0.55$ K. From the good agreement between the two values one can conclude that antiferromagnetic interactions between ions in the same sublattice are relatively small.

Magnetization measurements below the transition point of $Cs_2MnCl_4.2H_2O$ by Hoel[18])

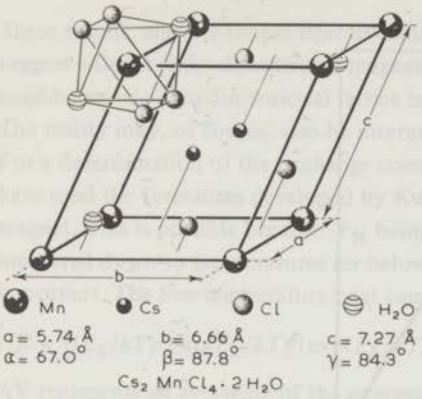

Fig. 4. Crystal structure of $Cs_2MnCl_4.2H_2O$. The complete $[Cl_4.2H_2O]$ octahedron around one Mn ion is shown. Spence has found that the antiferromagnetic unit cell has a shape different from that of the crystallographic cell (which is shown here). Spin reversal was found to occur along the [1,0,0], [0,1,0] and [0,−1,1] direction.

yielded $zJ/k = -0.49$ K, and an anisotropy field $H_A = 6.5$ kOe corresponding to $D/k = -0.175$ K.

A short note about the heat capacity of this compound has been published by Love *et al.*[19]). They found the Néel temperature as $T_N = 1.84 \pm 0.01$ K.

4.2. Experimental results

The heat-capacity data are shown in fig. 5. A sharp phase transition is clearly exhibited at a temperature of 1.81 K, below which antiferromagnetic long-range order exists. The anomaly at low temperatures can be explained by a hyperfine coupling $As \cdot I$ in the magnetically ordered state. The calculated Schottky heat capacity for six equidistant h.f.s. energy levels at energy distant $\Delta = \frac{5}{2}|A|$ has been fitted to the data between 0.1 and 0.2 K, corresponding to $\Delta/k = 0.030$ K, hence to $|A/k| = 0.012$ K. The latter value is not significantly different from what is found in many other Mn^{2+} salts having nearly octahedral surrounding of Cl^- and H_2O, like $MnCl_2.4H_2O$[20]).

The subtraction of the hyperfine heat capacity from the measured data points yields the drawn curve in fig. 5. The data above T_N are extrapolated by a $c \sim T^{-2}$ relation, as indicated by the dash-dotted line in fig. 5. The resulting curve presumably represents the electronic heat capacity, which leads to an entropy change $\Delta S/R = 1.817$ which is not significantly higher than the expected value $\ln(2s + 1) = 1.792$. Integration of the electronic heat capacity with respect to temperature leads to $E/R = -3.47$ K. The dipolar contribution is very small[17]). The entropy and energy gain obtained in short-range ordering above T_N amount to 27% and 51% of the total entropy and energy gain respectively. The high-temperature heat capacity near 3 to 4 K corresponds to the asymptotic relation $c_h T^2/R \approx 3$ K^2. It should be noted that

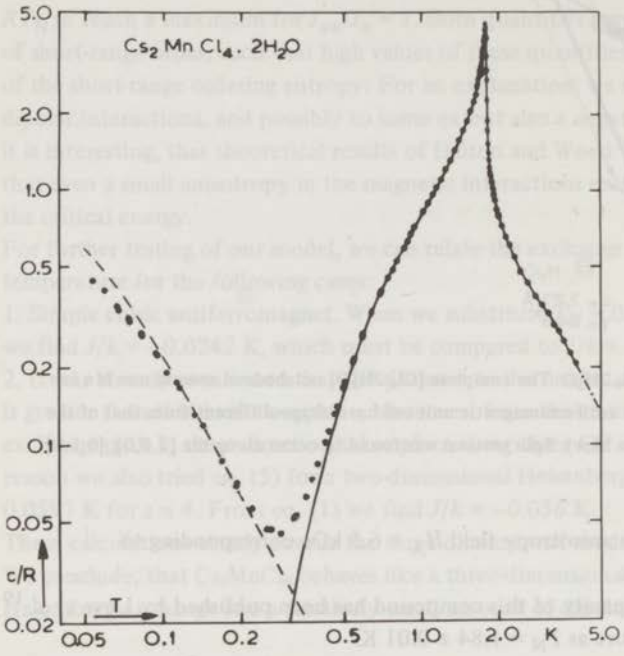

Fig. 5. Heat capacity of $Cs_2MnCl_4.2H_2O$. The nuclear heat-capacity curve (dashed line) has been obtained by fitting a Schottky curve to the data between 0.1 and 0.2 K. Subtraction yields the electronic heat capacity (full line), which has been extrapolated at the high-temperature side (dash-dotted line), for evaluation of the entropy. It may be remarked, however, that the experimental error increases rapidly with increasing temperature.

at these high temperatures our measuring accuracy is poor (10-20%), but this value is, by any means, very much larger than the calculated dipolar contribution $c_{\mathrm{dip}}T^2/R = 0.021\ \mathrm{K}^2$ for as many as 1038 neighbours in a sphere of 40 Å radius.

Below 4 K, the powder susceptibility of $Cs_2MnCl_4.2H_2O$ has been measured. The results are consistent with those of Smith and Friedberg[17]).

4.3. Discussion

The fraction of short-range ordering entropy in $Cs_2MnCl_4.2H_2O$ (27%) is comparable to that in the isomorphous compounds $Cs_2MnBr_4.2H_2O$ and $Rb_2MnCl_4.2H_2O$ (26% and 25%)[22,23]), and is higher than the theoretical number for a simple cubic Heisenberg system (see section 3.3). When we substitute $c_{\mathrm{h}}T^2/R = 3\ \mathrm{K}^2$ and $\theta = -3.2$ K (value taken from Smith *et al.*, see ref. 17) into eq. (4) we obtain $z \approx 5$ neighbours.

These results, and the simple Bravais lattice, which splits up into two antiparallel sublattices[16]), suggest either a three-dimensional magnetic lattice having $z = 6$ approximately equivalent neighbours or a two-dimensional lattice having $z = 4$ approximately equivalent neighbours. The reality may, of course, also be intermediate. We shall now discuss the first alternative. For a determination of the exchange constant J and the crystalline field parameter D, we have used the formalism developed by Kubo[21]) for an anisotropic Heisenberg antiferromagnet. This is possible because, T_N being rather high, the magnetic heat capacity can be measured down to temperatures far below T_N before the hyperfine heat capacity becomes important. The low-temperature heat capacity of such a system can be described by

$$c/R = \left\{(E_k/kT)^2 \exp(E_k/kT)/[\exp(E_k/kT) - 1]^2\right\}_{AV} \tag{7}$$

AV represents an averaging of the expression between curly brackets over all $N/2$ values of the wave vector k in the first Brilliouin zone, and with

$$E_k = -2zJs_z \left\{(1 + D/zJ)^2 - [1/z \sum_n \cos(k \cdot r_n)]^2\right\}^{1/2} \tag{8}$$

where n is a summation index running over all z nearest neighbours at distance r_n.
For simplification, we used a simple cubic (s.c.) structure for the magnetic lattice.
The antiferromagnetic sublattices then take f.c.c. symmetry, with the summation over k throughout the first b.c.c. Brilliouin zone. Using this procedure, we have calculated the heat capacity as a function of T, using J and D as parameters, and have made a comparison with the experiment. Below 0.3 K, the hyperfine structure contribution to the heat capacity dominates, while Kubo's formulae are only valid as a low-temperature approximation. Therefore we compared the part of the experimental curve between 0.3 and 0.5 K to the computations. For a good fit, two conditions must be fulfilled: a) at 0.4 K, where the fit should be the best, the calculated and measured values of c must be equal and b) the shape of the calculated and measured curves must be the same. Because the slope in the c *versus* T curve is large, normal measuring inaccuracy has little influence on the best fit, thus condition a) must be satisfied rather accurately. Condition b) is a weaker one, because the slope of the computed curve is not strongly dependent on the D/J ratio in this temperature range. Conditions a) and b) give relations between D and J, shown in fig. 6 as curves a3 and b3. Further, we have calculated in this model the energy at zero temperature for several values of J and D. When we insert an s_z independent term $\frac{1}{3}s(s + 1)D$ in the anisotropy hamiltonian given by Kubo, we obtain for the magnetic energy gain:

$$E/R = s(s + 1)zJ/k + \tfrac{2}{3}s(s + 1)D/k + \left\{E_k/2k\right\}_{AV} \tag{9}$$

in which the notation is the same as in eqs. (7) and (8).
Because E/R is a measured quantity, eq. (9) gives another relation between J and D, which is also shown in fig. 6 as curve c3.

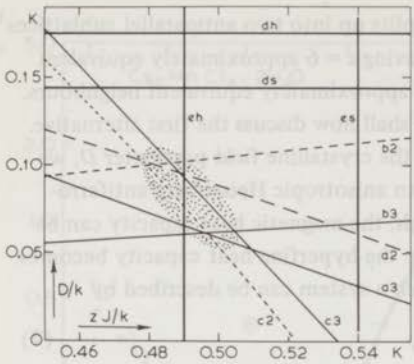

Fig. 6. Exchange *versus* crystalline field diagram of $Cs_2MnCl_4.2H_2O$. The lines marked a, b and c in this figure represent results of spin-wave calculations for two- and three-dimensional anisotropic Heisenberg antiferromagnets.

First symbol : a: obtained from the heat-capacity value at 0.4 K
b: obtained from the shape of the heat capacity curve near 0.4 K
c: obtained from the energy gain
d: D value taken from literature
e: exchange constant taken from literature

Second symbol: 2: calculated for a two-dimensional lattice
3: calculated for a three-dimensional lattice
h: value taken from Hoel[18])
s: value taken from Smith[17]).

In order to study the influence of different exchange constants, we shall now take the extreme case of zero exchange for one pair of neighbours and therefore we carried out the spin-wave calculations for a two-dimensional anisotropic antiferromagnet. The results are shown in fig. 6 as the dashed lines a2, b2 and c2, of which the meaning is analogous to a3, b3 and c3, respectively. For completeness, also the data of Smith and Friedberg namely line ds ($D/k \approx -0.14$ K) and line es ($zJ/k = -0.54$ K ± 10%), and of Hoel, namely line dh ($D/k \approx -0.175$ K) and line eh ($zJ/k = -0.49$ K), are shown.

From the three-dimensional analysis in fig. 6 we find $zJ/k = -0.50$ K and $D/k = -0.06$ K, and from the two-dimensional analysis $zJ/k = -0.48$ K and $D/k = -0.10$ K. The exchange parameter is in good agreement with the results of Smith *et al.*[17]) and with that of Hoel[18]), in contrast to our $|D/k|$ values, which are much smaller than those of Smith and Hoel. However, $zJ/k = -0.48$ K and $D/k = -0.10$ K correspond to an exchange field $H_E = 2zJs/g\mu_B = 18$ kOe, and an anisotropy field $H_A = 2Ds/g\mu_B = 3.7$ kOe, leading to a prediction of the threshold field $H_{thr} \approx (2H_AH_E)^{1/2} = 11.5$ kOe, which is close to the experimental result (11.6 kOe) of Hoel[18]).

Paying attention to the effective number of neighbours (about five) we estimate that the

values of zJ/k and D/k are in the shaded area, intermediate between the two- and three-dimensional results in fig. 6. Taking the average of these results, we find $zJ/k = -0.49 \pm 0.02$ K and $D/k = -0.08 \pm 0.03$ K.

5. *Heat capacity of K_4MnCl_6*

5.1. Crystal structure and recent experiments

K_4MnCl_6 crystallizes in a rhombohedral structure (space group D^6_{3d} or $R\,\bar{3}\,c$), but the unit cell described by Bellanca[24]) (fig. 7) is very nearly cubic ($\alpha = 89°32'$). There are two formula units in this unit cell, such that Mn^{2+} ions form a nearly b.c.c. Bravais lattice. The magnetic ions are surrounded by a slightly distorted octahedron of Cl^- ligands.

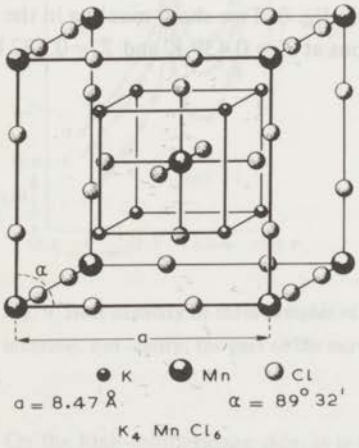

Fig. 7. Crystal structure of K_4MnCl_6 according to Bellanca. Bergerhoff has suggested that the K and Cl positions are not correct (see text). The Mn ions form a nearly b.c.c. lattice.

E.P.R. measurements[25]) on Mn^{2+} ions substituted in K_4CdCl_6 have shown that the hyperfine coupling constant $A/k = -0.0116$ K was about 10% smaller than in octahedrally H_2O-coordinated Mn^{2+} compounds, and that the crystalline field parameter has the small value $D/k = -0.0125$ K. This negative value of D corresponds to an elongation of the chlorine octahedron along the trigonal axis. K_4CdCl_6 has, like K_4MnCl_6 a rhombohedral structure. However, the lattice positions of K and Cl in K_4CdCl_6 described by Bergerhoff *et al.*[26]) are different from those for K_4MnCl_6 of Bellanca. The chlorine octahedra around the divalent metal ions are rotated about the [1,1,1] direction, and the octahedra around 0,0,0 and $\frac{1}{2}, \frac{1}{2}, \frac{1}{2}$ are also rotated with respect to each other. On the other hand, Bergerhoff *et al.*

suggested that K_4MnCl_6 has the same structure as K_4CdCl_6,in which case fig. 7 does not give the correct positions of the chlorine and potassium ions, but this does not affect the cell dimensions or the Mn positions.

E.P.R. and susceptibility measurements on concentrated K_4MnCl_6 powder between 1.4 and 300 K have been performed by Swanson *et al.*[6]). At about 80 K, abrupt changes in the behaviour of the line-width and the magnetic susceptibility are observed, which might be associated with a decrease of symmetry of the crystal structure, for example. Above this temperature, a Curie-Weiss constant $\theta = -7.8$ K was observed, and below, $\theta = -6.0$ K. Below 20 K, again a deviation in the susceptibility was observed. Swanson *et al.*[6]) did not present a Curie-Weiss relation that might describe the susceptibility between 1.4 and 20 K; however, from his plot we can roughly estimate $\theta \approx -2$ K.

5.2. Experimental results

The results of the heat-capacity measurements are shown in fig. 8. Two sharp maxima in the heat capacity are observed, associated with phase transitions at $T_1 = 0.439$ K and $T_2 = 0.332$ K.

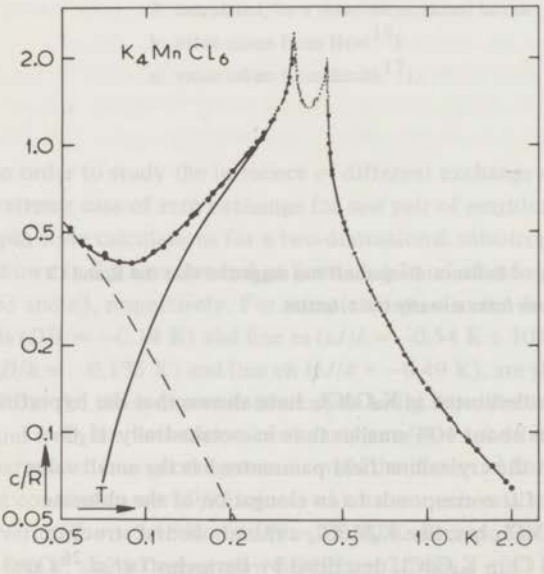

Fig. 8. Heat capacity of K_4MnCl_6. The dashed line gives the hyperfine structure specific heat, which is subtracted from the experimental data (full line).

We attribute both phase transitions to K_4MnCl_6 and exclude the possibility that one of the peaks is due to a large amount of impurity. This point of view is based on the following two reasons:

1. the X-ray examination,

2. the measurements were performed on several samples, some of which were rejected because of insufficient purity, due to incomplete sintering (see section 2.1). The heat capacity of three samples near 0.4 K is shown in fig. 9 on a logarithmic scale. These samples certainly contained different amounts of impurity. This resulted in a shift of the specific heat by a constant factor, and not in a change of the ratio of the heights of the two peaks, as is clearly visible in fig. 9.

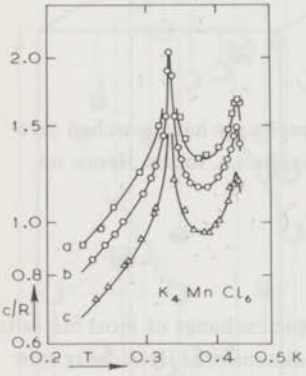

Fig. 9. Heat capacity of three samples of K_4MnCl_6 near their maxima. The shape of the three full curves is identical. For clarity, the part of the curve near the left-hand peak is shown for sample b only.

On the high-temperature side, it is seen that, even near 2 K we cannot properly describe the heat capacity by T^{-2} behaviour. Up to 2 K, no significant difference in the shape of the curves is seen between different samples. However, one may expect that at 2 K, or nearly 5 times the critical temperature, cT^2 is near to its limiting value. Therefore we extrapolated from the experimental points at 2 K, according to $cT^2/R \approx 0.26\ K^2$. The dipolar contribution amounts to $c_{dip}T^2/R = 0.012\ K^2$.

At low temperatures we found, by fitting a six equidistant level Schottky curve to the experimental results, that $|A/k| = 0.0112$ K, which is close to the value for Mn^{2+} in K_4CdCl_6. Taking this value for subtracting the hyperfine contribution, and using the above mentioned extrapolation, we obtain the entropy gain $\Delta S/R = 1.784$, which differs by 0.5% from the theoretical value. The magnetic energy gain is evaluated as $E/R = -0.778$ K. It is seen that 53% of the total entropy change takes place below T_2, and 22% above T_1.

The inverse magnetic a.c. susceptibility of K_4MnCl_6 powder as a function of temperature is shown in fig. 10. A comparatively large Curie-Weiss constant $\theta = -1.7 \pm 0.3$ K is observed.

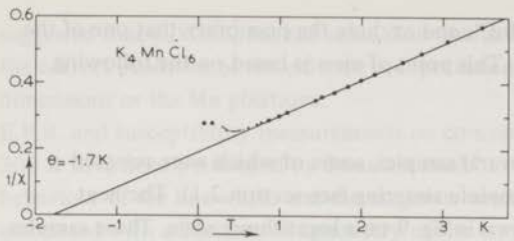

Fig. 10. Inverse magnetic a.c. susceptibility, $1/\chi$, of a powdered sample of K_4MnCl_6 *versus* temperature, T.

Especially near the temperatures of the maxima in the heat capacity we have searched carefully but futily for anomalous behaviour of the susceptibility or the a.c. losses. Hence no indication for weak ferromagnetism is observed.

5.3. Discussion

In view of the practically b.c.c. crystal structure and the isotropic exchange of most Mn salts, it might be anticipated that this salt would behave like a three-dimensional Heisenberg spin system. Further, since θ is negative, and large compared to T_1, antiferromagnetic interactions are thought to predominate. Instead of a simple antiferromagnetic phase transition, however, a more complex behaviour is observed, which shows some similarity with anhydrous $MnCl_2$[2]). The complex behaviour of K_4MnCl_6 may be associated with the following circumstances:
1. the chlorine octahedra in the structure described by Bergerhoff *et al.*[26]) are rotated relatively to each other about the [1,1,1] direction. In such circumstances, a decrease of crystal symmetry (as is suggested by the data of Swanson *et al.*[6]) near 80 K) may easily lead to the existence of two different crystalline field axes.
2. substitution of the experimental results into eq. (4) leads to an effective number of $z \approx 17$ interacting neighbours. Looking at the nearly b.c.c. crystal structure, it is seen that we can come close to this number only if we assume antiferromagnetic exchange interactions with the 8 n.n. as well as with the 6 n.n.n. magnetic ions. In that case, no magnetic structure will allow all interacting spins to be antiparallel. (This will result in a reduction of the $E/R\theta$ ratio, as is experimentally observed ($E/R\theta = 0.45$, compared to 1.07 from eqs. (1) and (2)), and in a negative T^{-3} term in the high-temperature expansion of the heat capacity. A negative T^{-3} term leads to a temperature range where the heat capacity is smaller, and decreases less rapidly, than according to the asymptotical T^{-2} behaviour. This is also observed (see fig. 8).)
The circumstances mentioned under 1. and 2. respectively might provide a mechanism leading to a spin reorientation transition between two different antiferromagnetic states.

6. *Heat capacity of α-Cs_2MnCl_4*

6.1. Crystallographic data

Similar to Cs_2CoCl_4, α-Cs_2MnCl_4 has the orthorhombic K_2SO_4 structure according to Legrand[8]), and is characterized by D_{2h}^{16} (*Pnam*). Unfortunately, no precise cell dimensions and position parameters have been published to our knowledge. Therefore we have adopted the values given by Porai-Koshits[27]) for Cs_2CoCl_4. The unit cell, containing four formula units, is given in fig. 11. All Mn^{2+} ions are equivalent and are arranged in layers perpendicular

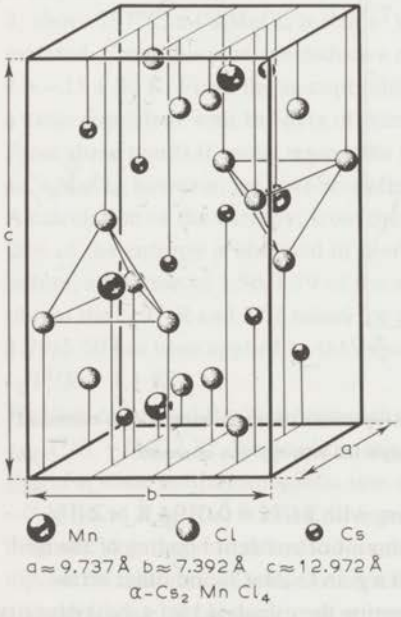

Fig. 11. Crystal structure of α-Cs_2MnCl_4. The lattice and position parameters have been borrowed from Cs_2CoCl_4. The chlorine tetrahedron is drawn around two Mn ions only.

to the *b* axis. Around the Mn^{2+} ions are situated two nearest neighbours at a distance of 6.2 Å. A total of twelve neighbours is found for distances up to 7.5 Å; for all these neighbours, possible exchange paths can be found.

6.2. Experimental results

The heat capacity of a fresh sample of Cs_2MnCl_4 is given in fig. 12. A fairly sharp maximum is observed near T_N = 0.935 K. At low temperatures a hyperfine structure heat capacity is found, which can be fitted by a Schottky type heat capacity for six equidistant levels at

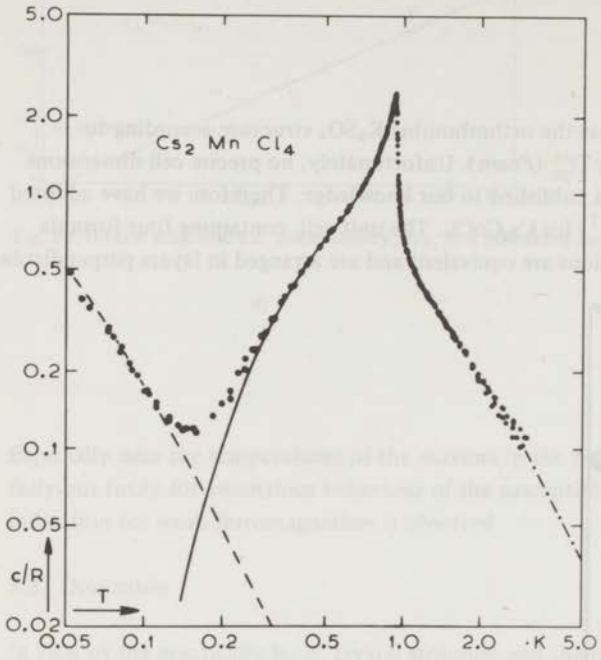

Fig. 12. Heat capacity of a sample of a-Cs_2MnCl_4. The full line represents the experimental data corrected for the nuclear heat capacity (dashed line). Only 84% of the expected entropy was observed.

energy distance $\Delta/k = \frac{5}{2}|A/k| = 0.026$ K, corresponding with $|A/k| = 0.0104$ K or $|A| = 72 \times 10^{-4}$ cm^{-1}. This low value would suggest a fair amount of covalent bonding of the Mn^{2+} with the surrounding Cl^- ions, such as is also observed *e.g.* in Cs_3MnCl_5 and other tetrahedrally coordinated Mn compounds[31]). When subtracting the calculated h.f.s. heat capacity (dashed curve) from the data, one obtains the drawn curve, representing the electronic magnetic heat capacity. On the high-temperature side the data up to 2 K cannot be well described by the usual asymptotic relation $c \sim T^{-2}$. Somewhat arbitrarily, we have extrapolated the high-temperature data by the relation $cT^2/R = 0.9$ K^2 indicated by the dash-dotted line in fig. 12.

Evaluation of the total entropy involved in the magnetic ordering of the electronic spins, using the above extrapolation, gives $\Delta S/R = 1.50$, which is 16% lower than the expected value of $\ln(2s + 1) = 1.79$. For an explanation, we shall first consider the following experimental facts:

1. when the measurements were repeated, after keeping the sample for some days at room temperature, it was seen that the nuclear heat capacity had remained the same, but that the electronic heat capacity had decreased drastically. Plotted on a logarithmic scale the shape

of the electronic heat capacity curves was the same, consequently the heat capacities were shifted by a constant factor. Apparently the measured electronic heat capacity originates from an unstable phase, while the decrease of the heat capacity is due to a slow conversion into the stable phase.

2. β-Cs_2MnCl_4, having the K_2NiF_4 structure[5]) is stable at room temperature[7]). In this material, strong magnetic interactions were observed; Asmussen[28]) published a plot containing susceptibility data from which we estimated the Curie-Weiss constant as $\theta = -140 \pm 10$ K. Further, Epstein *et al.*[29]) observed magnetic ordering at $T_N \approx 55$ K by means of neutron diffraction. It seems very likely that below 3 K, the electronic heat capacity of this material is very low and that only the h.f.s. heat capacity is observable.

3. above 297°C, α-Cs_2MnCl_4 is stable[7]). Asmussen's plot also contained data concerning this material. From this plot, we deduce a relatively inaccurate Curie-Weiss constant $\theta = -25 \pm 30$ K. From the susceptibility measurements of our sample (see below), we found a value consistent with the data of Asmussen.

From these points it seems reasonable to attribute the observed electronic heat capacity to α-Cs_2MnCl_4; however, we have no definite proof for this assumption.

A calculation of the entropy, from the electronic heat capacity, showed that approximately 28% of the entropy is obtained in short-range ordering above the critical point. As noted before, a fraction of 1.50/1.79 of the expected entropy has been observed. In order to obtain the $c_h T^2/R$ and E/R values for a pure sample of α-Cs_2MnCl_4, a correction factor of 1.79/1.50 has been applied to the experimental data. We obtained $E/R = -1.79$ K and $c_h T^2/R \approx 1.1$ K^2.

We have calculated the high-temperature value of the dipolar heat capacity, namely $c_{dip} T^2/R = 0.022$ K^2. We have also made some computations of the magnetic dipole energy, E_{dip}, for some antiferromagnetic spin configurations. All results were in the range $-0.131 \text{ K} < E_{dip}/R < 0.239$ K. It is seen that the dipolar interaction cannot account for the magnetic ordering, but it leads to a substantial amount of anisotropy energy. For these dipolar calculations we used the crystallographic data for Cs_2CoCl_4, because those for α-Cs_2MnCl_4 are not known to us at present. We do not expect that the error introduced in this way exceeds a few percent.

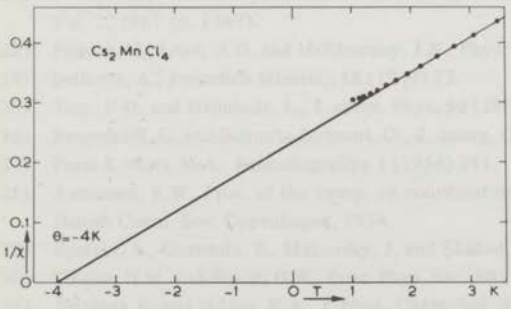

Fig. 13. Inverse magnetic a.c. powder susceptibility of α-Cs_2MnCl_4 in arbitrary units.

Further, we consider the influence of the crystalline field on the heat capacity. For the usually observed magnitudes of D/k in Cl-coordinated Mn compounds, the contributions to E/R and $c_h T^2/R$ are relatively small. We shall therefore explain the values on the basis of exchange interactions.

Fig. 13 shows the inverse susceptibility *versus* T for α-Cs_2MnCl_4. At temperatures between 2 and 4 K, Curie-Weiss behaviour is observed. Because of this small temperature interval the Curie-Weiss constant is not as accurate in this case. We found $\theta = -4 \pm 1$ K.

6.3. Discussion

α-Cs_2MnCl_4 has a more complicated crystal structure than the three other Mn salts. Around each magnetic Mn^{2+} ion, many exchange paths can be found to neighbouring Mn^{2+} ions. Referring to the similar discussion in section 5.3, we note that a high experimental $R\theta^2/cT^2$ value is associated with a large number of neighbours. In this case, from $\theta = -4$ K, we even find more neighbours than seems reasonable in view of the crystal structure. This can be explained by the large experimental error in θ (about 1 K). Under these circumstances, we cannot determine the exchange constant accurately in this salt: very tentatively we note that $\theta \approx -3$ K would correspond to $z \approx 12$ neighbours and to an exchange parameter $zJ/k \approx -0.5$ K.

For this salt, as for K_4MnCl_6, we can understand the low $E/R\theta$ value by considering antiferromagnetic interactions among the z neighbours of each Mn^{2+} ion.

REFERENCES

1) Stout, J.W. and Catalano, E., J. chem. Phys. **23** (1955) 2013.
2) Giauque, W.F., Fisher, R.A., Hornung, E.W., Butera, R.A. and Brodale, G.E., J. chem. Phys. **42** (1965) 9.
3) Stanley, H.E. and Kaplan, T.A., Phys. Rev. Letters **17** (1966) 913.
4) Rushbrooke, G.S. and Wood, P.J., Molec. Phys. **1** (1958) 257.
5) IJdo, D.J.W., Thesis, University of Leiden, 1960.
6) Swanson, T.B., Laurie, V.W. and Duffy Jr, W., J. chem. Phys. **49** (1968) 4407.
7) Ehrlich, P., Koknat, F.W. and Seifert, H.-J., Z. anorg. Chem. **341** (1965) 281.
8) Legrand, E. and Verschueren, M., J. Physique **25** (1964) 578.
9) Powell, H.M. and Wells, A.F., J. Chem. Soc. (1935) 359.
10) Figgis, B.N., Gerloch, M. and Mason, R., Acta Cryst. **17** (1964) 506.
11) Henning, J.C.M. and Bongers, P.F., J. Phys. Chem. Solids **27** (1966) 745.
12) Baker Jr, G.A., Gilbert, H.E., Eve, J. and Rushbrooke, G.S., Phys. Rev. **164** (1967) 800.
13) Bowers, R.G. and Woolf, M.E., Phys. Rev. **177** (1969) 917.
14) Fisher, M.E., Reports on Progress in Physics, XXX part II (1967) 615.
15) Jensen, S.J., Acta Chemica Scand. **18** (1964) 2085.
16) Spence, R.D., Casey, J.A. and Nagarajan, V., Phys. Rev. **181** (1969) 488.
17) Smith, T. and Friedberg, S.A., Phys. Rev. **177** (1969) 1012.
18) Hoel, L.A., Phys. Status solidi **36** (1969) 119.
19) Love, N.D., McElearny, J.N. and Forstat, H., Bull. Amer. Phys. Soc. (II) **12** (1967) 285.
20) Miedema, A.R., Wielinga, R.F. and Huiskamp, W.J., Physica **31** (1965) 835 (Commun. Kamerlingh Onnes Lab., Leiden No. 342c).
21) Kubo, R., Phys. Rev. **87** (1952) 568.
22) Forstat, H., McElearney, J.N. and Bailey, P.T., XI Internat. Conf. low Temp. Physics, St. Andrews, Vol. 2, 1967 (p. 1349).
23) Forstat, H., Love, N.D. and McElearney, J.N., Phys. Letters **25A** (1967) 253.
24) Bellanca, A., Periodico Mineral., **16** (1947) 73.
25) Tsay, F-D. and Helmholz, L., J. chem. Phys. **50** (1969) 2642.
26) Bergerhoff, G. and Schmitz-Dumont, O., Z. anorg. Chem. **284** (1956) 10.
27) Porai-Koshits, M.A., Kristallografiya **1** (1956) 291.
28) Asmussen, R.W., Proc. of the Symp. on coordination Chem. (Copenhagen, Aug. 9-13, 1953) Danish Chem. Soc. Copenhagen, 1954.
29) Epstein, A., Gurewitz, E., Makovsky, J. and Shaked, H., Phys. Rev. B **2** (1970) 3703.
30) Dalton, N.W. and Wood, D.W., Proc. Phys. Soc. **90** (1967) 459.
31) Šimánek,E. and Müller, K.A., J. Phys. Chem. Sol. **31** (1970) 1027.
32) Blöte, H.W.J. and Huiskamp, W.J., Physica **53** (1971) 445.

CHAPTER VI

MAGNETIC ORDERING PHENOMENA IN RARE EARTH DOUBLE OXIDES $R_2M_2O_7$

Summary

Heat capacity data on several rare earth double oxides of the pyrochlore type are presented. Anomalies in the heat capacities are ascribed to magnetic ordering, although a critical point has not been observed for a few of these compounds. Calculations are given which relate some observable quantities to the interaction strength for a few simple types of spin-spin interaction. These calculations are used for the interpretation of the experimental data. It is found that $Nd_2Sn_2O_7$ behaves like an Ising antiferromagnet, and $Yb_2Ti_2O_7$ like an Ising ferromagnet. For Ho_2GaSbO_7 and Tb_2GaSbO_7 dipolar interactions are sufficiently large to explain the heat capacity.

1. *Introduction and crystal structure*

It was shown by Roth[1]) that cubic compounds $R_2M_2O_7$ exist for a variety of combinations of trivalent (R) and tetravalent (M) metal ions. In our experiments R = Nd, Tb, Dy, Ho, Er or Yb and M_2 = Ti_2, Sn_2, Zr_2 or GaSb. The crystal structure of these compounds was found to be similar to that of the mineral pyrochlore designated crystallographically as $Fd3m$ (O_h^7). The crystal structure has been more precisely determined for the case of $Er_2Ti_2O_7$ by X-ray and neutron diffraction by Knop *et al.*[2]). The cubic unit cell of these compounds (fig. 1) has dimensions of about 10 Å and contains 16 trivalent R (rare earth) ions, which form a so called[3]) Laves or cristobalite lattice. The point symmetry at the rare earth sites is trigonal (D_{3d}), but the trigonal axes point into four different directions. For convenience, to these directions a number has been assigned which is shown in table I, where also the lattice positions can be found. In table II, the crystallographic directions corresponding to these numbers are given. Two oxygen ions are diametrically opposed around the rare earth sites at about 2.2 Å and lie on the trigonal axis. Six other oxygen ions lie more near the equatorial plane (perpendicular to the trigonal axis) at a distance of about 2.5 Å. The R ions are located at the common vertex of two diametrically opposed R tetrahedra and in this respect they are all equivalent, *i.e.* each R ion has 6 nearest (R) neighbours (n.n.). The n.n. distance is about 3.5 Å. Further neighbours are at least at twice this distance, and hence, in these discussions, we shall restrict any nondipolar interactions to n.n.

In view of the n.n. distance, it may be anticipated that the magnetic interactions in the pyro-

ion number	position			number of axis direction
1	0	0	0	1
2	1/4	0	1/4	2
3	1/2	0	1/2	1
4	3/4	0	3/4	2
5	1/4	1/4	0	3
6	0	1/4	1/4	4
7	3/4	1/4	1/2	3
8	1/2	1/4	3/4	4
9	1/2	1/2	0	1
10	3/4	1/2	1/4	2
11	0	1/2	1/2	1
12	1/4	1/2	3/4	2
13	3/4	3/4	0	3
14	1/2	3/4	1/4	4
15	1/4	3/4	1/2	3
16	0	3/4	3/4	4

Table I. Crystallographic data about the pyrochlore structure.

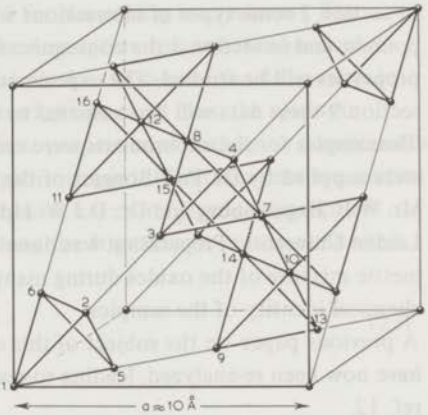

Fig. 1. Crystal structure of $R_2M_2O_7$. The f.c.c. unit cell contains 8 formula units, of which only the R (rare earth) ions are shown. In the figure, the numbers given to the ions in table I, are shown. The trigonal axes of the R ions lie along body diagonals of the cubic cell (table I and II). Each R ion is surrounded by 6 nearest neighbours. Each pair of nearest neighbours has two common nearest neighbours.

number of axis	crystallographic direction		
1	1	1	1
2	−1	1	−1
3	−1	−1	1
4	1	−1	−1

Table II. The directions of the trigonal axes at the rare earth sites.

chlore type compounds are intermediate or comparable to that in the rare earth oxides[4]) and the rare earth gallates[5]) where the n.n. distances are respectively 2.66 Å and 3.8 Å and in which magnetic interactions were found to be relatively weak. Hence the pyrochlore compounds may exhibit magnetic ordering in or below liquid He temperatures. Susceptibility and adiabatic demagnetization experiments on some of the pyrochlores (R = Gd, Ho, Dy, Er) were reported by Van Geuns[6]). He investigated these materials because the small values of the Curie-Weiss constant, together with the relatively high ionic densities, favour them for adiabatic refrigerating techniques. The results indeed suggested that magnetic ordering would take place at temperatures of at most a few K.

The present investigation was undertaken in order to study the thermal properties of these cubic compounds near and below 1 K. Magnetic ordering phenomena in cubic compounds are determined by fewer parameters, and are more accessible to theoretical interpretation than those in noncubic compounds. However, no E.P.R. data are available, and this may give problems for the interpretation of the measurements.
In section 2 some types of interactions will be mentioned which may occur in these compounds, and in section 3 the consequences of these interactions for the caloric and magnetic properties will be studied. The experimental data will be presented in sections 4-8. In section 9 these data will be compared to those derived in section 3.
The samples for the experiments were only available in the form of (sintered) powders. They were supplied by Dr. P.F. Bongers of the Philips Research Laboratories in Eindhoven, Mr. W.F. Engelenburg and Dr. D.J.W. IJdo of the Inorganic Chemistry Department of the Leiden University. Preparation was done by firing a finely divided and compressed stoichiometric mixture of the oxides during many hours. X-ray powder patterns confirmed the chemical identity of the samples.
A previous paper on the subject of this chapter is given in ref. 12. The experimental data have now been re-analyzed, leading to results which slightly differ from those quoted in ref. 12.

2. *Considerations on magnetic interactions in the pyrochlore lattice*

In this section we shall consider three types of magnetic interactions: dipolar and nondipolar interactions among electronic spins, and hyperfine interactions between electronic and nuclear spins.

2.1. Magnetic dipole-dipole interactions

Dipolar spin-spin interactions are adequately described by the usual dipole-dipole hamiltonian for interactions between magnetic moments $\boldsymbol{\mu}_i$ which are related to the electron spin s_i by

$$\boldsymbol{\mu}_i = \mu_B \mathcal{g}_i \cdot s_i \qquad (1)$$

where μ_B is the Bohr magneton, and g_i the g tensor. In view of the trigonal point symmetry, we expect that the g tensors have axial symmetry along the trigonal axes. In some cases g values can be estimated from susceptibility data.

2.2. Nondipolar interactions

It should first be remarked that, in view of experimental evidence on similar rare earth compounds, namely the oxides and the garnets, we expect that the magnitude of the spin-spin interaction energy is very much smaller than the crystal field splittings. Hence we shall consider here interactions between effective spins $s = \frac{1}{2}$.

In general, nondipolar interactions will be described by more parameters than can be determined from heat capacity and powder susceptibility measurements. Therefore only three simple cases will be studied which are completely determined by one constant J (which we will designate as interaction constant, without differentiating between different types of interaction mechanisms which are discussed *e.g.* in ref. 15), and by the spin dimensionality (1 for Ising interactions, 2 for XY interactions, and 3 for Heisenberg interactions). The peculiar geometry of the pyrochlore lattice makes the description somewhat more complicated than in the case of for instance a simple cubic lattice. In view of the differences in the directions of the crystalline field axes of neighbouring rare earth ions, the spin-spin interactions may be expected to exhibit the anisotropic properties of both spins simultaneously. We shall describe nondipolar interactions by simple isotropic interactions between vectors s_i' which are formed by multiplying the spinvectors s_i with a tensor T_i having appropriate symmetry. Hence the T_i will have axial symmetry along the trigonal axis at rare earth site i. Hence

$$s_i' = T_i \cdot s_i \tag{2a}$$

and

$$\mathcal{H}_{ij} = -2Js_i' \cdot s_j' = -2\, s_i \cdot J_{ij} \cdot s_j \tag{2b}$$

if we define

$$J_{ij} = JT_i \cdot T_j \tag{2c}$$

We note that the formulation of these interactions is analogous to that for dipolar interactions in the sense that in both cases the hamiltonian can be written very simply by multiplying the spinvectors by a tensor reflecting the local symmetry (eqs. 1 and 2a).

2.2.1. Ising type interactions

In the case of extreme anisotropy, nondipolar interactions are restricted to the axial components of nearest neighbouring spins, and the projection tensors T_i take the following forms for ions having the indicated axis numbers (table I):

axis 1: $\begin{bmatrix} +1/3 & +1/3 & +1/3 \\ +1/3 & +1/3 & +1/3 \\ +1/3 & +1/3 & +1/3 \end{bmatrix}$ axis 2: $\begin{bmatrix} +1/3 & -1/3 & +1/3 \\ -1/3 & +1/3 & -1/3 \\ +1/3 & -1/3 & +1/3 \end{bmatrix}$

axis 3: $\begin{bmatrix} +1/3 & +1/3 & -1/3 \\ +1/3 & +1/3 & -1/3 \\ -1/3 & -1/3 & +1/3 \end{bmatrix}$ axis 4: $\begin{bmatrix} +1/3 & -1/3 & -1/3 \\ -1/3 & +1/3 & +1/3 \\ -1/3 & +1/3 & +1/3 \end{bmatrix}$

The hamiltonian can be written more simply if we introduce $J' = \frac{1}{3}J$ and new coordinates for each ion. For the direction of the positive new z_i' axis of the coordinate system for the ion at site i (i = 1 to 16, table I) we choose the corresponding directions indicated in table II. If we now transform eq. (2b), the pair interaction hamiltonian reduces to the following simple form:

$$\mathcal{H}_{ij} = +\, 2J' s_{iz_i'} s_{jz_j'} \qquad (3)$$

which is, apart from the plus sign, the familiar Ising hamiltonian.

2.2.2. The XY model

Here only equatorial spin components appear in the hamiltonian. The T tensors are now given by:

axis 1: $\begin{bmatrix} +2/3 & -1/3 & -1/3 \\ -1/3 & +2/3 & -1/3 \\ -1/3 & -1/3 & +2/3 \end{bmatrix}$ axis 2: $\begin{bmatrix} +2/3 & +1/3 & -1/3 \\ +1/3 & +2/3 & +1/3 \\ -1/3 & +1/3 & +2/3 \end{bmatrix}$

axis 3: $\begin{bmatrix} +2/3 & -1/3 & +1/3 \\ -1/3 & +2/3 & +1/3 \\ +1/3 & +1/3 & +2/3 \end{bmatrix}$ axis 4: $\begin{bmatrix} +2/3 & +1/3 & +1/3 \\ +1/3 & +2/3 & -1/3 \\ +1/3 & -1/3 & +2/3 \end{bmatrix}$

By multiplication of pairs of these tensors, the J_{ij} are obtained. The hamiltonian (2a) cannot be substantially simplified in this case.

2.2.3. The isotropic (Heisenberg) case

The T are unity tensors and we obtain the usual Heisenberg hamiltonian,

$$\mathcal{H}_{ij} = -\, 2J s_i \cdot s_j \,.$$

2.3. Hyperfine interactions

For electronic spins aligned along a direction $\boldsymbol{a}$, the splitting Δ of the $2I + 1$ hyperfine levels is given by $\Delta/k = sA/k$, where s is the electronic spin quantumnumber. The hyperfine constant A is proportional to the nuclear magnetic moment, and hence (if more than one $I \neq 0$ isotope is present) the ratio of A values observed for different isotopes in a rare earth compound is equal to the ratio found in each other compound of the same rare earth ion. Further, for most rare earth ions the hyperfine constants are found to be approximately proportional to the effective g value corresponding to direction $\boldsymbol{a}$[13]).

3. *Relations between the interaction constants and some observable quantities*

3.1. Magnetic dipole-dipole interactions

If the g tensors are known, one can calculate the coefficient of the T^{-2} term in the high-temperature heat capacity expansion for the case of dipolar interactions only. The calculation procedure was described in chapter II and leads to the following formula if we adopt a lattice parameter $a = 10$ Å:

$$c T^2/R = (10.8\, g_{/\!/}^4 + 2.8\, g_{/\!/}^2\, g_{\perp}^2 + 12.1\, g_{\perp}^4)\, 10^{-5}\, \mathrm{K}^2 \qquad (4)$$

Further we can find the magnetic structure at $T = 0$ and its energy in the molecular field approximation according to the methods given in chapter II. Energy values thus obtained are given in table III for some values of the g parameters. From a comparison with the experimental values of the T^{-2} coefficient or the energy (found by integrating the heat capacity) we can find g values that would be required to explain these data by dipolar interactions only. We shall see that in most of these substances nondipolar interactions play an important role.

$g_{/\!/}$	$g_{\perp}$	E/R (K)
1	1	−0.00897
1	0	−0.00686
0	1	−0.00720

Table III. Calculated dipolar energies at $T = 0$ for some g values.

3.2. Nondipolar interactions

The geometry of the pyrochlore lattice has some remarkable consequences for the calculated magnetic behaviour of systems having interactions as defined in section 2.2. If dipolar interactions are negligible in comparison to nondipolar n.n. interactions, and the nondipolar interactions are of the types given in sections 2.2, we can calculate several observable quantities. From the hamiltonian (2a) we can calculate the asymptotic T^{-2} behaviour of the specific heat, and the Curie-Weiss constant θ (see chapter II). The results are shown in table IV. Note the expressions for the Curie-Weiss parameter θ, which is *e.g.* for the Ising model only one third of the usual expression. Further, the energy at $T = 0$ can be calculated in the molecular field approximation according to the method described in chapter II. The magnetic cell was assumed to be identical to the crystallographic cell (16 sublattices). The results of these energy calculations are also shown in table IV. We shall now discuss the magnetic structures corresponding to the ground state energies for the various interaction types listed in table IV.

interaction type	E/R (K)	θ (K)	cT^2/R (K^2)
Ising ferromagnetic	$-1/2\ J'/k$	J'/k	$3/4\ (J'/k)^2$
Ising antiferromagnetic	$+3/2\ J'/k$	J'/k	$3/4\ (J'/k)^2$
XY ferromagnetic	$-5/6\ J/k$	$5/3\ J/k$	$5/6\ (J/k)^2$
XY antiferromagnetic	$\leqslant 1/2\ J/k$	$5/3\ J/k$	$5/6\ (J/k)^2$
Heisenberg ferromagnetic	$-3/2\ J/k$	$3\ J/k$	$9/4\ (J/k)^2$
Heisenberg antiferromagnetic	$\leqslant 1/2\ J/k$	$3\ J/k$	$9/4\ (J/k)^2$

Table IV. Calculated observable quantities for some simple interaction types.

1. *Ising ferromagnetic interactions* (J and J' positive)
From eq. (3) we see that in the new coordinates the product $s_{iz_i'} \cdot s_{jz_j'}$ must be *negative* for minimum interaction energy of a pair of n.n. spins i and j. Because each pair of nearest neighbours has two common nearest neighbours, no magnetic structure is possible in which the products $s_{iz_i'}\ s_{jz_j'}$ are negative for all n.n. pairs. Therefore the energy gain due to magnetic ordering will be relatively small. The lowest value of the magnetic energy is $E/R = -\frac{1}{2}J/k$ and refers to a number of magnetic structures in which, for each spin, 4 n.n. are 'parallel' ($s_{iz_i'}\ s_{jz_j'}$ negative) and 2 n.n. are 'antiparallel'. Structures were found having a spontaneous magnetization $M = \frac{N\sqrt{3}}{6}\, g_{//}\mu_B$ in the direction of a cubic axis (table V, column 1). Other

ion nr.	1	2	3	4	5	6
1	1 1 1	1 1 1	−1 −1 −1	1 1 1	−1 −1 2	1 −1 0
2	1 −1 1	1 −1 1	1 −1 1	−1 1 −1	−1 1 2	−1 −1 0
3	1 1 1	−1 −1 −1	1 1 1	1 1 1	−1 −1 2	1 −1 0
4	1 −1 1	1 −1 1	−1 1 −1	−1 1 −1	−1 1 2	−1 −1 0
5	−1 −1 1	−1 −1 1	−1 −1 1	−1 −1 1	1 1 2	−1 1 0
6	−1 1 1	−1 1 1	1 −1 −1	1 −1 −1	1 −1 2	1 1 0
7	−1 −1 1	−1 −1 1	1 1 −1	−1 −1 1	1 1 2	−1 1 0
8	−1 1 1	1 −1 −1	−1 1 1	1 −1 −1	1 −1 2	1 1 0
9	1 1 1	−1 −1 −1	−1 −1 −1	1 1 1	−1 −1 2	1 −1 0
10	1 −1 1	1 −1 1	1 −1 1	−1 1 −1	−1 1 2	−1 −1 0
11	1 1 1	1 1 1	1 1 1	1 1 1	−1 −1 2	1 −1 0
12	1 −1 1	1 −1 1	−1 1 −1	−1 1 −1	−1 1 2	−1 −1 0
13	−1 −1 1	−1 −1 1	−1 −1 1	−1 −1 1	1 1 2	−1 1 0
14	−1 1 1	1 −1 −1	1 −1 −1	1 −1 −1	1 −1 2	1 1 0
15	−1 −1 1	−1 −1 1	1 1 −1	−1 −1 1	1 1 2	−1 1 0
16	−1 1 1	−1 1 1	−1 1 1	1 −1 −1	1 −1 2	1 1 0

Table V. Magnetic structures. In each column the crystallographic directions of the 16 sublattice magnetizations are given for a magnetic structure (see text).

structures having the same energy exhibited a magnetization $M = \frac{N\sqrt{6}}{24} g_{\parallel}\mu_B$ along the [1,1,0] or an equivalent crystallographic direction (table V, column 2). Column 3 of table V shows an example where spontaneous magnetization is absent even although $J > 0$. Which one of these structures will be realized at low temperatures, will depend on other (*e.g.* dipolar) interactions.

2. *Antiferromagnetic Ising interactions* (J and J' negative)
If we choose all $s_{iz_i'} = +\frac{1}{2}$, the energy will be minimal (see eq. 3). Each R-ion spin then has all 6 n.n. in the energetically most favourable orientation. For this antiferromagnetic structure, the energy has its well-known two-sublattice value $E/R = +\frac{3}{2}J'/k$. The crystallographic directions of the 16 sublattice magnetization vectors are given in column 4 of table V.

3. *Ferromagnetic XY model*
Two ferromagnetically coupled n.n. spins can be oriented completely parallel (*e.g.* the spins labeled 1 and 2 in table I in the [1,0,−1] direction) but not all pairs can be simultaneously parallel. Therefore the calculated ground state energy $E/R = -\frac{5}{6}J/k$ is higher than the sum of the minimum pair energies. The structures corresponding to this energy were found to have a ferromagnetic moment $\frac{N\sqrt{6}}{6} g_{\perp}\mu_B$ along a cubic axis (column 5 of table V).

4. *Antiferromagnetic XY model*
Neither in this case every pair of n.n. spins can be oriented energetically most favourably. The eigenvalue problem (chapter II) gave 11 degenerate solutions for the lowest energy value $E/R = -0.5\ J/k$. One solution is given in column 6 of table V.

5. *Ferromagnetic Heisenberg interactions*
For isotropic interactions, parallel spin alignment leads to simple ferromagnetic structures having $E/R = -\frac{3}{2}J/k$ and a spontaneous magnetization $M = (N/2)g\mu_B$ in an arbitrary direction.

6. *Antiferromagnetic Heisenberg interactions*
Like case 4, magnetic ordering is hindered by common n.n. of the n.n. pairs. This leads to a small energy gain $E/R = -0.5\ J/k$ for the magnetic ordering. The eigenvalue problem (chapter II) gave as many as 27 degenerate solutions. *E.g.* also the structures given in columns 4 and 6 of table V belong to these solutions.
It should be remarked that these energy calculations are only a classical approximation and that quantum ('spinwave') effects may decrease the energy in the cases 4 and 6 just considered. Therefore a $\leqslant$ sign has been added to the E/R values in table IV.
High temperature series for the susceptibility and heat capacity of a cristobalite lattice having Ising interactions were derived by Betts and Ditzian[3]). They started from the usual Ising hamiltonian instead of eq. (3). Their susceptibility series can be applied to the staggered susceptibility of a pyrochlore substance having an exchange constant opposite to the one

used in the above series. Although the staggered susceptibility is not directly observable, the series is very useful for determining the critical temperature $T_c = (2.195 \pm 0.003)\, J/k$ for the case of antiferromagnetic Ising interactions. Further, Betts and Ditzian derived the critical energy $E_c/kT_c = 0.268 \pm 0.006$ and the critical entropy, $S_c/R = 0.548 \pm 0.003$ from their specific heat series.

For a classification of the interactions in the pyrochlore compounds measured, the above results can be compared to the experimental data which will be presented in the following sections. However, we have to keep in mind that this description is incomplete on the following points:

a. Dipolar interactions also contribute to the magnetic behaviour.

b. Nondipolar interactions may include terms not considered in section 2, or may be intermediate between the three extreme cases.

c. Distortions of the crystal structure may decrease the crystal field symmetry and may influence the spin-spin interaction.

The influence of point a can be estimated if the g values are known. Point b may follow from a comparison of the experimental data with theory if point c does not interfere. Finally the influence of point c is difficult to estimate. We can only state that susceptibility data of Van Geuns[6]) and of Townsend and Crossley[7]) on some pyrochlore compounds did not give evidence for a crystalline phase transition, and that our analyses apply to the possibility that the crystal symmetry at low temperatures is that described by Roth and Knop.

3.3. Hyperfine interactions

Many rare-earth compounds exhibit an appreciable hyperfine (hfs) heat capacity near 0.1 K. From the properties of the hfs constant A mentioned in section 2.3, it is easy to see that for all $I \neq 0$ isotopes of a rare-earth element, the hfs energy level schemes for different compounds only differ by a constant factor. Hence, if a set of hfs constants A is known for one

isotope	abundance %	I ħ	A_a/k K	g_a	a	reference nr.
^{143}Nd	27.1	7/2	0.0512	3.50	z	8
^{145}Nd	8.3	7/2	0.0319	3.50	z	8
^{159}Tb	100	3/2	0.0301	17.7	z	9
^{161}Dy	18.8	5/2	0.0548	13.6	x	10
^{163}Dy	24.9	5/2	0.0777	13.6	x	10
^{165}Ho	100	7/2	0.483	15.4	z	11
^{167}Er	22.9	7/2	0.0683	13.7	z	8
^{171}Yb	14.4	1/2	0.175	4.57	x	10
^{173}Yb	16.2	5/2	0.0490	4.57	x	10

Table VI. Examples of hyperfine data on some rare earth isotopes.

compound, energy level schemes on a reduced scale can be calculated, which are valid for all compounds of that rare-earth element. This was done for the examples listed in table VI. Using the relative isotopic abundances, the nuclear heat capacity was calculated on a reduced temperature scale. These curves can be used for fitting to the experimental heat capacity data at low temperatures and thus A (and hence, because A/g may be roughly constant, g for the direction of spin alignment) can be estimated.

4. *Three neodymium compounds*

4.1. The heat capacity data of $Nd_2Sn_2O_7$ are presented in fig. 2. A sharp anomaly appears at $T = 0.91$ K. At the low temperature side of the data a slight upward curvature is seen. If we attribute this to hyperfine interactions, we can roughly estimate $^{143}\Delta/k \approx 0.016$ K. Using this value, we can calculate the hyperfine heat capacity as a function of T (section 3.3). After subtracting this small contribution from the experimental results we obtain the full curve. We attribute this anomaly to magnetic ordering. At the high temperature side the heat capacity decreases rapidly and near 2 K the data obey $cT^2/R = 0.23$ K^2. Since we may expect a nonzero T^{-3} contribution in these substances, this number may not be considered as a precise measure for the asymptotic behaviour; therefore we should know the heat capacity

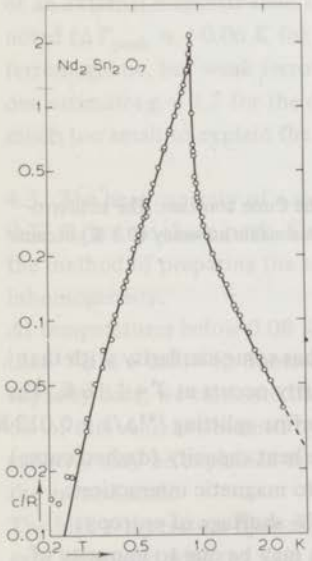

Fig. 2. Heat capacity of $Nd_2Sn_2O_7$. The anomaly is steep and narrow. This suggests the existence of strongly anisotropic interactions in this substance. After subtracting the estimated nuclear heat capacity, the full curve was obtained.

at much higher temperatures. Above 2 K, however, the heat capacity becomes too small to be measured accurately. The energy E and the entropy change ΔS corresponding to the specific heat anomaly, have been found by numerical integration: $\Delta S/R = 0.690$ (which practically equals ln 2) and $E/R = -0.660$ K. In these numbers extrapolations of the heat capacity below 0.2 K and above 2 K have been included, which contribute 3% to ΔS and 14% to E. Further, 46% of the energy and 35% of the entropy change takes place above the maximum.

The a.c. powder susceptibility of $Nd_2Sn_2O_7$ has been measured at liquid He temperatures. It is plotted in fig. 3 on a reduced scale. The susceptibility behaves antiferromagnetically. The Curie-Weiss constant amounts to $\theta = -0.39 \pm 0.1$ K. From the Curie constant one can estimate $\bar{g}^2 = \frac{1}{3}g_{/\!/}^2 + \frac{2}{3}g_{\perp}^2 \approx 14.2$. This means that $g_{/\!/} \approx 6.5$ if $g_{/\!/} \gg g_{\perp}$, and that if g is isotropic, $g \approx 3.8$. The measured hfs splitting provides an estimate (section 3.3) for the g value along the spin alignment direction, which is much lower, namely $g \approx 2.2$. These g values are too small to explain the experimental data by dipolar interactions only (see section 3.1).

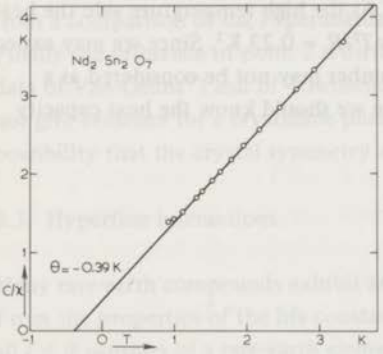

Fig. 3. Inverse 220 Hz a.c. powder susceptibility (χ) of $Nd_2Sn_2O_7$. C is the Curie constant. The antiferromagnetic Curie-Weiss constant $\theta = -0.39$ K could be determined with reasonable accuracy (0.1 K) because the transition point is rather low.

4.2. The heat capacity of Nd_2GaSbO_7 is shown in fig. 4, and has some similarity with that of $Nd_2Sn_2O_7$, but the peak is lower and less steep. The singularity occurs at $T = 1.16$ K. The measurements extend to low temperatures from which a hyperfine splitting $^{143}\Delta/k = 0.012$ K could be estimated. After subtracting the calculated hyperfine heat capacity (dashed curve) the remaining heat capacity (drawn curve) may be attributed to magnetic interactions.

A bump in the full curve is seen at 0.2 K. Further, there was 7% shortage of entropy; integration of c/RT gave only $\Delta S/R = 0.64$. These phenomena may be due to impurity of the sample. The energy of the magnetic transition amounts to $E/R = -0.89$ K and the high temperature heat capacity behaviour is estimated as $cT^2/R = 0.4$ K^2 (both values not corrected for entropy shortage).

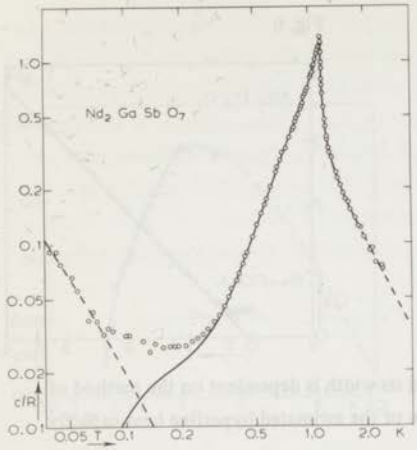

Fig. 4. Heat capacity of Nd_2GaSbO_7. After subtracting the estimated nuclear heat capacity (dashed curve) a bump is seen near 0.15 K in the remaining electronic heat capacity (full curve). This may be due to chemical impurity. The peak is somewhat lower and broader than that of neodymium stannate.

A peak in the d.c. susceptibility was observed at the transition point. This peak disappeared when a longitudinal magnetic field of 500 Oe was applied. Below the transition point the susceptibility is practically constant. The heat capacity was also measured in the presence of an external magnetic field and a shift of the heat capacity peak to lower temperatures was noted ($\Delta T_{peak} \approx -0.06$ K for H = 3.3 kOe). Hence, presumably Nd_2GaSbO_7 becomes antiferromagnetic, but weak ferromagnetism may also be present. From the hyperfine splitting one estimates $g \approx 1.7$ for the direction of spin alignment. Like in $Nd_2Sn_2O_7$ this g value is much too small to explain the phase transition by dipolar interactions.

4.3. The heat capacity of a sample of $Nd_2Zr_2O_7$ (fig. 5) shows a pronounced maximum at 0.37 K, but no sharp peak. Since the height of the maximum is observed to be dependent on the method of preparing the sample, we attribute the broadening of the peak to chemical inhomogeneity.

At temperatures below 0.08 K we observe an increasing heat capacity from which we estimate that $^{143}\Delta/k = 0.014$ K. Subtracting the calculated hfs heat capacity from the measured heat capacity data, we calculate the remaining entropy, which amounts to $\Delta S/R = 0.70 = 1.01 \ln 2$; 6% of this value is obtained by extrapolation below 0.1 K and above 2 K. Thus the heat capacity may be explained by magnetic ordering among Nd ions having effective spin $\frac{1}{2}$ in the ground state.

The high-temperature heat capacity per mole is given by $cT^2/R = 0.23$ K^2 and the energy gain associated with the heat capacity anomaly is $E/R = -0.432$ K. A large fraction (78%) of this quantity is obtained above the maximum at 0.37 K, and the amount of short range ordering entropy $(S_\infty - S_c)/R = 0.33$ is much larger than that of the two other Nd compounds.

Fig. 5

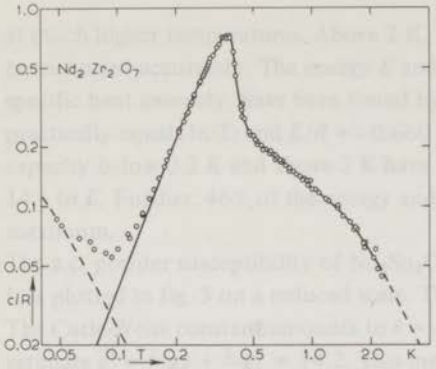

Fig. 6

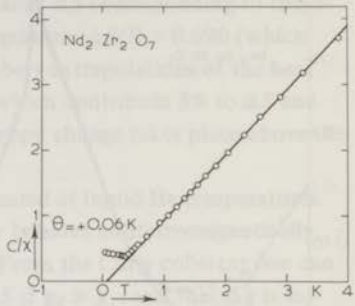

Fig. 5. Heat capacity of $Nd_2Zr_2O_7$. The peak is not sharp, and its width is dependent on the method of sample preparation. The full line is obtained after subtraction of the estimated hyperfine heat capacity.

Fig. 6. Inverse 220 Hz a.c. powder susceptibility of $Nd_2Zr_2O_7$. The ordering temperature of this substance is sufficiently low to determine the Curie-Weiss constant with reasonable accuracy (± 0.1 K). The small value of θ suggests that both ferromagnetic and antiferromagnetic interactions are present in neodymium zirconate.

The a.c. powder susceptibility of neodymium zirconate was measured in and below the liquid He temperature range. A low and flat maximum was found at the temperature of the heat capacity maximum, which might indicate antiferromagnetism. Inverse susceptibility data are shown in fig. 6. A small Curie-Weiss constant was found, which, however, has the ferromagnetic sign ($\theta = +0.06$ K). From the Curie constant we estimate $\overline{g^2} \approx 9.6$ and from the hyperfine splitting $g \approx 1.9$. From these g values it can be inferred that the magnetic interactions in this substance are mainly nondipolar.

5. *Heat capacity of* $Dy_2Ti_2O_7$

The experimental results are shown in fig. 7. No singularity, but only a relatively low maximum is seen. At low temperatures the heat capacity data decrease very rapidly with temperature. Although hyperfine interactions are expected to produce an observable heat capacity at low temperatures, no indications for hyperfine contributions were observed. This may be due to poor heat contact at low temperatures.

At the high temperature side the data points do not extend sufficiently far to estimate the asymptotic behaviour. This has been determined by Van Geuns[6]) who found $cT^2/R = 2.5\ \mathrm{K}^2$. Therefore the data in fig. 7 were smoothly extrapolated to the above behaviour (dashed line). Integration of c/RT gave an entropy change $\Delta S/R = 0.62$ which is 10% below the expected value ln 2. The discrepancy can be explained by the uncertainties in the above extrapolation. The energy (not corrected for entropy shortage) is estimated as $E/R = -1.46$ K.

Fig. 7

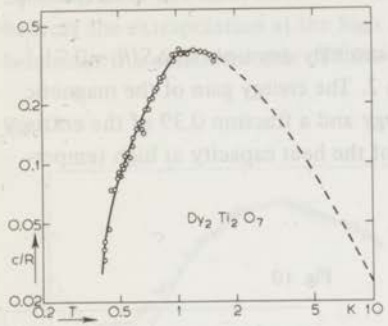

Fig. 8

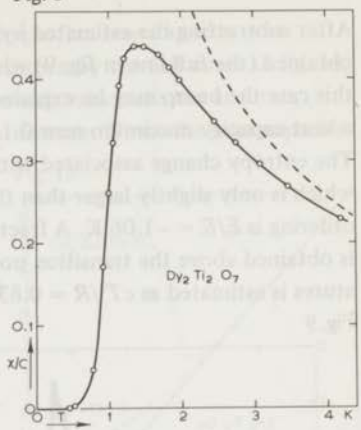

Fig. 7. Heat capacity of $Dy_2Ti_2O_7$. The data points are shown by circles. The curve is smoothly extrapolated (dashed line) to $cT^2/R = 2.5\ K^2$, which value was found by Van Geuns[6]). No hyperfine heat capacity could be observed.

Fig. 8. Powder susceptibility data of $Dy_2Ti_2O_7$. No reliable value for the Curie-Weiss constant θ could be determined from these data. Van Geuns has found $\theta = +0.1$ K above liquid He temperatures (dashed line). Apparently the susceptibility deviates from the Curie-Weiss law in the liquid He temperature range.

The a.c. powder susceptibility is shown in fig. 8. A maximum is observed at 0.9 K, and at lower temperatures χ decreases to zero at 0.4 K. D.c. measurements gave identical results. Susceptibility measurements of Van Geuns at higher temperatures followed a Curie-Weiss law with $\theta = 0.1$ K (dashed line in fig. 8). The rapid decrease of χ below the maximum may be interpreted as due to strong anisotropy. The Curie constant corresponds to $g_{//} \approx 17$, hence to a $J_z = \pm 15/2$ ground state. This is in agreement with susceptibility measurements of Townsend and Crossley[7]), who found only small deviations from the Curie law at temperatures between 2 and 1400 K. From the large $g_{//}$ value one concludes that dipolar interactions are important in this substance.

6. *Heat capacity of two erbium compounds*

6.1. The heat capacity of $Er_2Ti_2O_7$ has a sharp singularity at $T = 1.25$ K. Data from two samples are plotted in fig. 9; between 1 and 1.5 K data are plotted from sample I, which exhibited a sharp peak. In the remaining temperature intervals data on sample II are shown, which had a rounded heat capacity peak but which was measured in a much broader temperature interval than sample I. Since the preparation methods of the samples were different, we attribute the peak broadening of sample II (about 0.1 K) to chemical inhomogeneity.

After subtracting the estimated hyperfine heat capacity ($^{167}\Delta/k = 0.016$ K), a curve is obtained (the full line in fig. 9) which resembles that of Nd_2GaSbO_7 (section 4.2). Also in this case the bump may be explained by impurities due to chemical inhomogeneity, having a heat capacity maximum near 0.15 K.

The entropy change associated with the heat capacity anomaly amounts to $\Delta S/R = 0.71$ which is only slightly larger than the expected value ln 2. The energy gain of the magnetic ordering is $E/R = -1.06$ K. A fraction 0.63 of the energy and a fraction 0.39 of the entropy is obtained above the transition point. The behaviour of the heat capacity at high temperatures is estimated as $cT^2/R = 0.83$ K^2.

Fig. 9

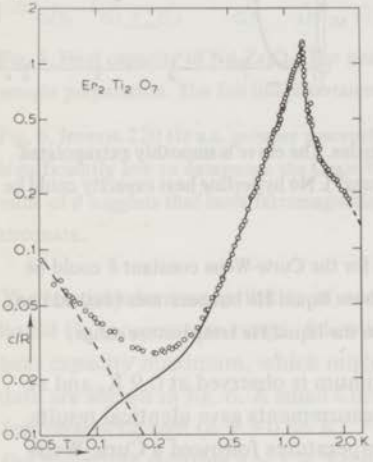

Fig. 10

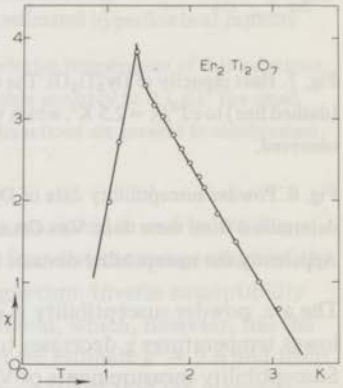

Fig. 9. Heat capacity of $Er_2Ti_2O_7$. Data of two different samples in different temperature intervals are shown. The bump at 0.15 K may be due to chemical impurity. The curve resembles that of Nd_2GaSbO_7.

Fig. 10. Susceptibility of $Er_2Ti_2O_7$ powder in arbitrary units. It was not possible to fit a Curie-Weiss law over a reasonable temperature range to these data. The peak in χ is not consistent with simple antiferromagnetic behaviour.

Powder a.c. susceptibility measurements are plotted in fig. 10. A Curie-Weiss law could not be fitted to these data over a sufficiently wide temperature range. Therefore we could only roughly estimate $\overline{g^2} \approx 8$. From the hfs splitting one estimates $g \approx 6.4$. Hence dipolar interactions are comparatively small in this substance.

6.2. The rather surprising heat capacity data of Er_2GaSbO_7 are plotted in fig. 11. No singularity is seen and the curve is even broader and lower than a Schottky anomaly. For some types of magnetic spin-spin interactions, however, we have to expect a broad anomaly (see the cT^2R/E^2 values in table IV) and it is difficult to explain the anomaly of this Kramers compound by other than magnetic spin-spin interactions. From the low temperature data one

can estimate $^{167}\Delta/k = 0.025$ K. On basis of this value the hyperfine heat capacity was calculated and subtracted. The remaining heat capacity is shown by the full curve in fig. 11. By integration one finds $\Delta S/R = 0.61$ and $E/R = 0.75$ K, which values are not accurate because the extrapolation at the high temperature side is uncertain. From the heat capacity behaviour it is estimated that $cT^2/R \geqslant 7$ K^2.

Fig. 11

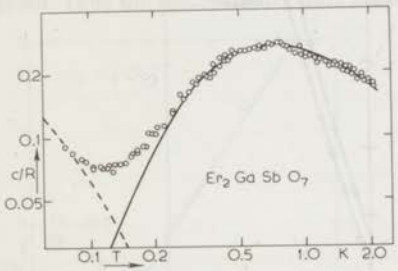

Fig. 12

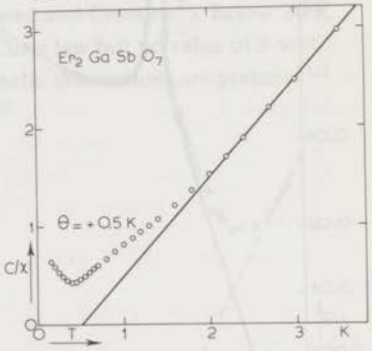

Fig. 11. Heat capacity of Er_2GaSbO_7. The dashed line gives the estimated hyperfine heat capacity. The heat capacity remaining after subtracting the hyperfine heat capacity is attributed to magnetic interactions. Note the difference with the heat capacity of the titanate.

Fig. 12. Inverse a.c. powder susceptibility of Er_2GaSbO_7. The Curie-Weiss behaviour (full line) is found from data in a narrow temperature interval. Therefore the value of the Curie-Weiss θ must be considered as inaccurate. The maximum susceptibility is found at 0.4 K which is much lower than the temperature of maximum specific heat.

Inverse a.c. powder susceptibility data are shown in fig. 12. Above 2.2 K a Curie-Weiss law (drawn line) could be fitted to the data, yielding $\theta = +0.5$ K. Since the fit is obtained in a narrow temperature interval, and the heat capacity has already reached appreciable values at these temperatures, we may not consider this value as accurate. The susceptibility behaviour, however, does suggest a ferromagnetic θ value. From the Curie constant we estimate $\overline{g^2} \approx 6.1$ and from the hyperfine splitting $g \approx 10$. If we adopt the former value, the conclusion is that dipolar interactions do not strongly contribute to the heat capacity.

7. *Two ytterbium compounds*

7.1. The heat capacity of $Yb_2Ti_2O_7$ (fig. 13a) shows an interesting behaviour. At 0.216 K a sharp peak occurs. Especially just below the maximum the slope of the curve is very high and the heat capacity c/R increases from 0.1 to 1 within a variation of only 8% of the temperature. The height of the peak was found to be smaller for another sample, which had been fired for a shorter time during the preparation. Above the peak, at 0.38 K, a minimum

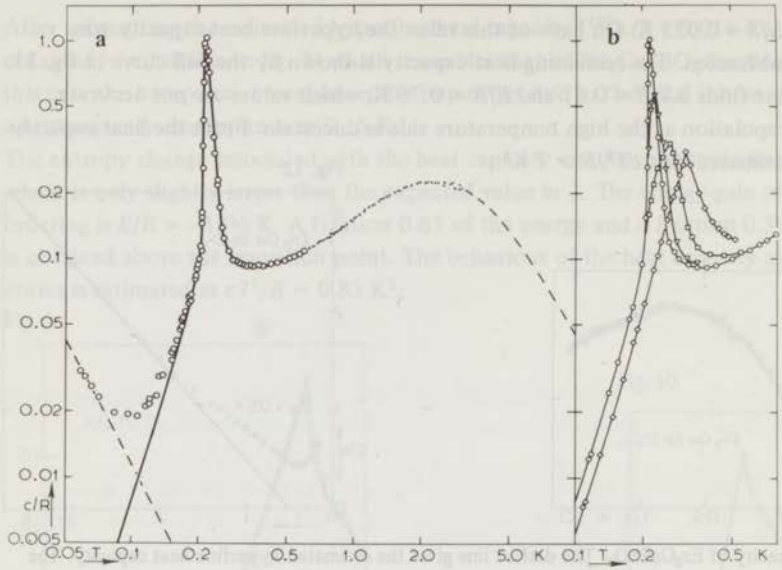

Fig. 13a. Heat capacity of $Yb_2Ti_2O_7$. The broken line represents the hyperfine heat capacity. The transition temperature of this substance is very low compared to the energy gain associated with the heat capacity anomaly.

Fig. 13b. Electronic heat capacity of $Yb_2Ti_2O_7$ near the peak in several magnetic field strengths. The field strengths for the different types of data points are:
○ 0 Oe; ▽ 210 Oe; □ 380 Oe; ◇ 710 Oe.
These results strongly indicate the existence of ferromagnetic interactions in $Yb_2Ti_2O_7$.

is reached and above that temperature a broad anomaly appears, having its maximum at about 2.5 K. The height of this maximum is only about one half of that of a two-level Schottky anomaly. At low temperatures, a hyperfine heat capacity is observed. From the data below 0.1 K we estimate $^{171}\Delta/k = 0.041$ K, and the corresponding hyperfine heat capacity (broken line) has been subtracted from the data (full line). The entropy as a function of temperature was calculated from the resulting heat capacity. The entropy below the maximum at 0.216 K amounts to $\Delta S/R = 0.059$ K which is a remarkably low value. The entropy value at the heat capacity minimum at 0.38 K is $\Delta S/R = 0.164$. This value is much smaller than the expected value for magnetic ordering of a Kramers substance. Hence the peak and the broad anomaly are not separate phenomena but they must have the same origin. The entropy at the upper limit of the measurements, 3 K, is $\Delta S/R = 0.498$. At 3 K, the data points are decreasing with temperature. A smooth extrapolation (dotted line) to T^{-2} behaviour according to $cT^2/R = 4.5$ K^2 gives a total $\Delta S/R = 0.666$. This is still 4% smaller than the expected value ln 2. Hence we may estimate $cT^2/R > 4.5$ K^2. By integrating the heat capacity one finds $E/R \approx 1.71$ K. Less than one percent (0.011 K) of this energy gain takes place below the peak.

The a.c. powder susceptibility of $Yb_2Ti_2O_7$ is shown in fig. 14. A good fit of a Curie-Weiss law to the data is obtained between 1.7 and 3.5 K, yielding $\theta = +0.4$ K (drawn line). In this temperature range, however, the heat capacity has already reached appreciable values and the susceptibility may very well behave differently above 3.5 K. In that case, the curvature of the data points suggests that θ may be larger than 0.4 K. The susceptibility of $Yb_2Ti_2O_7$ above helium temperatures has been measured by Townsend and Crossley[7]). Below 20 K their data exhibited a ferromagnetic deviation from the Curie law but no value of θ was given. Thus the susceptibility data suggest that ferromagnetic interactions are present.

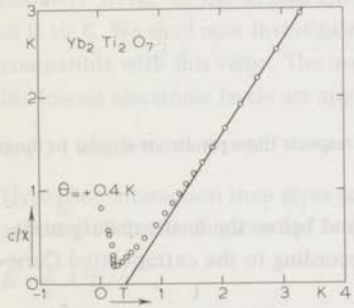

Fig. 14. Inverse a.c. powder susceptibility of $Yb_2Ti_2O_7$. Because the heat capacity reaches a maximum near 2.2 K, the susceptibility may not be expected to follow the Curie-Weiss behaviour to such low temperatures. Therefore the fitted value of the Curie-Weiss constant $\theta = +0.4$ K is not accurate.

In order to obtain further information about the interactions, the heat capacity has been measured in the presence of several magnetic fields having values between 0 and 710 Oe (fig. 13b). The low temperature heat capacity remained approximately constant in field strengths up to 380 Oe, and at 710 Oe a shift of the curve to the high temperature side was seen. These observations are consistent with ferromagnetism. Further it is seen that the peak shifts towards higher temperatures when the fields are applied. For an antiferromagnet one would expect a shift towards lower temperatures. The Curie constant of $Yb_2Ti_2O_7$ yields $\overline{g^2} = 5.7$, while one can estimate from the hfs heat capacity that $g \approx 2.1$. Hence dipolar interactions are negligible.

7.2. The heat capacity of Yb_2GaSbO_7 shown in fig. 15 is similar to that of the titanate, but a small bump instead of a peak is observed at the low temperature side. After subtracting the hyperfine heat capacity as calculated from the estimated hyperfine splitting $^{173}\Delta/k = 0.046$ K, and smooth extrapolation to $cT^2/R = 6$ K^2, we obtain an entropy value which is about equal to the expected value ln 2. The energy then amounts to $E/R \approx -2.1$ K. The susceptibility data were different from that of $Yb_2Ti_2O_7$. A Curie-Weiss law (θ negative) could be found which fitted the data over a wide temperature range, but we have to distrust

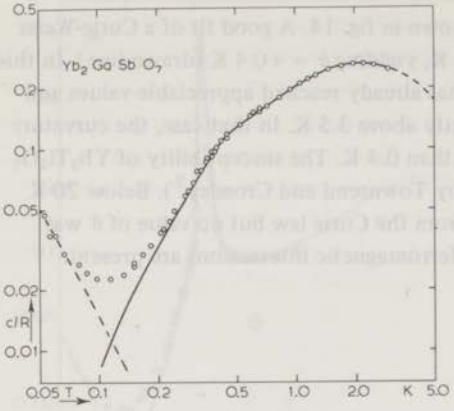

Fig. 15. Heat capacity of Yb_2GaSbO_7. No peak is seen but in other respects these results are similar to those on the titanate.

a Curie-Weiss law which is obtained at temperatures near and below the heat capacity maximum. Below 1 K the susceptibility becomes larger than according to the extrapolated Curie-Weiss behaviour. This is not usual for antiferromagnets.
From the hyperfine splitting we estimate $g \approx 2.3$, while from the Curie constant (which must be considered as inaccurate) we obtain $\overline{g^2} \approx 7.7$. Dipolar interactions according to these g values are negligible.

8. *Two non-Kramers compounds*

8.1. The heat capacity of Tb_2GaSbO_7 (fig. 16) shows two maxima. The large heat capacity

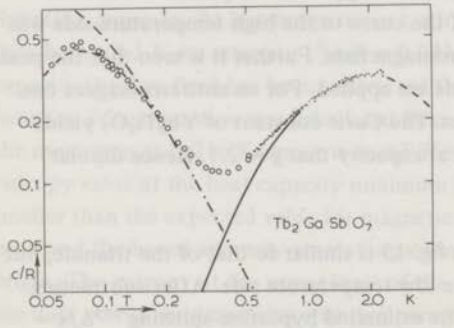

Fig. 16. Heat capacity of Tb_2GaSbO_7. The dashed line was calculated for a two energy level system, but the splitting of these levels could not be explained satisfactorily. The dash-dotted line is calculated for a four level hyperfine splitting $\Delta/k = 0.081$ K. After subtracting of this heat capacity, the remaining curve (solid line) is attributed to magnetic ordering.

above 1 K can be interpreted as due to a splitting of about 5 K between two singlets, such as is observed *e.g.* in Tb ethylsulfate[9]). The latter splitting would give rise to a Schottky type heat capacity anomaly and to absence of magnetic ordering phenomena. The measured heat capacity near 2 K in Tb_2GaSbO_7 does not fit a simple Schottky anomaly; however, magnetic interactions (and non-uniformity of Jahn-Teller splittings) may cause a broadening of the anomaly. The anomaly at 0.08 K might then be interpreted as due to a nuclear pseudo-quadrupole splitting caused by perturbation of the electronic singlet by second order hyperfine interactions. This mechanism causes a splitting between the nuclear $I_z = \pm\frac{1}{2}$ and $I_z = \pm\frac{3}{2}$ doublets. In fig. 16 the dashed line gives the heat capacity calculated on basis of a splitting of 0.19 K. We shall now investigate whether a pure singlet electronic ground state is compatible with this value. The maximum second order hyperfine splitting is realized when the lowest electronic levels are approximately given in the J_z representation by

$$1/\sqrt{2}\,(|+6> \pm |-6>)$$

Hyperfine interaction then gives admixture of these states, resulting in a second order splitting of the levels given by

$$E = \tfrac{1}{4} A^2 I^2/\Delta$$

where A is the hyperfine constant (in the effective $s = \frac{1}{2}$ hamiltonian) and Δ is the original splitting between the electronic singlets. The value of A must in this case be approximately equal to the value found by Larson[9]) in Tb ethylsulfate (where the lowest non-Kramers doublet is that one given above): $A/k = 0.30$ K. The calculated splitting between the $I_z = \pm\frac{3}{2}$ and $\pm\frac{1}{2}$ doublets then amounts to 0.02 K which is much smaller than the experimental value 0.19 K.

Therefore we must conclude that the above model is incorrect and that the anomaly near 0.08 K is mainly due to first order hyperfine interactions. Hence the electronic ground state has a nonzero magnetic moment, and therefore the anomaly at 2 K is attributed to magnetic ordering. The data points below 0.1 K lie below the curve for four equidistant levels (dash-dotted line) fitted at about 0.2 K. This can be explained by incomplete heat contact at low temperatures, which was also observed experimentally. For the hyperfine splitting we derive $\Delta/k = 0.081$ K which corresponds to $g \approx 9.1$. Hence a non-negligible contribution to the spin-spin interaction originates from magnetic dipole-dipole coupling (see section 2.1).

8.2. The heat capacity of Ho_2GaSbO_7 is shown in fig. 17. The heat contact was poor below 0.3 K and hence those data should be distrusted. Second order hyperfine splitting of an electronic singlet is, like in the Tb compound, too small to explain the data near 0.4 K. Hence the electronic ground state must have a magnetic moment. The data can be fitted by 8 equidistant energy levels ($\Delta/k = 0.23$ K) of the $I = \frac{7}{2}$ Ho nuclei. The Δ value corresponds to $g = 14$. After subtracting the hyperfine heat capacity, the remaining result (solid line, fig. 17) can be explained by magnetic interactions, like the Tb compound.

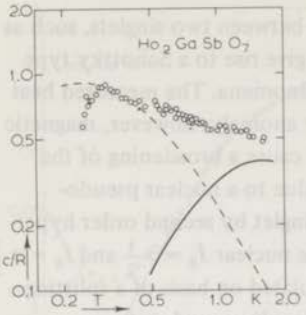

Fig. 17. Heat capacity of Ho_2GaSbO_7. Below 0.3 K the heat contact between sample and thermometer was incomplete. Like the terbium compound, the data are interpreted as the sum of hyperfine (dashed line) and magnetic ordering (full line) heat capacities.

9. *Interpretation of the experimental data*

As already noted, the cT^2/R values must not be considered as very accurate because we expect in all cases appreciable T^{-3} terms in the heat capacity series expansion (due to the occurrence of triangles of interacting neighbours in the pyrochlore lattice). Further, most of the Curie-Weiss constants θ could not be determined because the ordering temperatures were too high. Only in the case of neodymium stannate and zirconate, θ could be found with reasonable accuracy ($\sim$ 0.1 K). Further, the data about $Yb_2Ti_2O_7$ and Er_2GaSbO_7 give an indication for ferromagnetic interactions although the magnitude of θ remains uncertain. Experimental and theoretical data are shown in table VII. Here we wish to study the type of the interaction rather than its strength. Therefore only dimensionless quantities are shown. In the first column values are given of cT^2R/E^2 which is a measure of the width of a specific heat anomaly. For a narrow anomaly its value is small, whereas it has the value 1 for a simple two-level Schottky anomaly. Theoretical values for the critical quantities in this particular lattice have only been obtained for the antiferromagnetic Ising model. They are taken from ref. 3. For other types of interactions we expect a lower transition point if any, and more short range ordering entropy and energy.

A striking discrepancy is found between g values as estimated from the hyperfine splittings and from the Curie constants. Several effects may contribute to this observation:

1. At low temperatures incomplete heat contact may cause a decrease of the experimental heat capacity data. However, this decrease is generally strongly temperature dependent and can thus be detected. Hence this effect can only partly explain these large discrepancies.
2. In oxides, configuration mixing due to crystalline field effects (or covalency) may be more important than in most hydrated salts. The admixture of higher states having different J quantum numbers into the ground state J multiplet invalidates the proportionality of g and A (therefore we prefer the g values obtained from the Curie constant).
3. In an ordered substance, spin alignment may occur along a direction different from that of

maximum g. Experiments on cerium ethylsulfate (chapter IV) have shown that spin components in a direction of nearly-zero g can have appreciable interactions.
Further, the influence of splittings of nuclear quadrupole moments in the electric field gradient at the M-ion nuclei is estimated. The quadrupole splitting of the 24 keV ^{119}Sn level was measured by Loebenstein *et al.*[14]) at the M sites in several rare earth stannates by the Mössbauer effect. Splittings up to about 4×10^{-4} K were found. From the known ratios of the excited Sn to other M-quadrupole moments we can now estimate the quadrupole splittings in other pyrochlores. We find splittings up to about 10^{-3} K, which is small compared to the hyperfine splittings observed here for the R nuclei. Hence quadrupole splittings of M ions do not influence the observed hfs parameter values.

	cT^2R/E^2	$E/R\theta$	E/RT_c	S_c/R	E_c/E
$Nd_2Sn_2O_7$	<0.53	1.6	−0.72	0.494	0.46
Nd_2GaSbO_7	0.62*		−0.72*	0.487	0.52
$Nd_2Zr_2O_7$	1.23	−7	−1.07	0.372	0.78
$Dy_2Ti_2O_7$	1.01*				
$Er_2Ti_2O_7$	0.62*		−0.90*	0.431	0.64
Er_2GaSbO_7	>1.25	<0			
$Yb_2Ti_2O_7$	>1.54	<0	−7.9	0.068	0.994
Yb_2GaSbO_7	1.28				
Ising fm	3	−1/2			
Ising afm	1/3	+3/2	−0.68	0.548	0.394
XY fm	6/5	−1/2			
XY afm	⩽10/3	⩾+3/10			
Heis. fm	1	−1/2			
Heis. afm	⩽9	⩾1/6			

Table VII. Theoretical and experimental data. Dimensionless data are summarized. The critical quantities for a system having antiferromagnetic Ising interactions are taken from ref. 3. The experimental values marked with * are corrected for entropy shortage.

The measured pyrochlore compounds will now be compared to theory individually.
a. The experimental data of $Nd_2Sn_2O_7$ are in approximate agreement with antiferromagnetic Ising interactions. Further, Ising type interactions are also suggested by the steep decrease of the specific heat at both sides of the transition point.
b. The data about Nd_2GaSbO_7 are less complete (no θ was found) and are in less good agreement with antiferromagnetic Ising interactions. The heat capacity peak is lower than that of $Nd_2Sn_2O_7$. This may indicate that the spin-spin interactions are less anisotropic.
c. $Nd_2Zr_2O_7$ behaves completely differently. The heat capacity anomaly is much broader and the transition point is low. The small value of θ suggests that both ferro- and antiferromagnetic interactions are present. If the crystal structure at low temperatures is not distorted

(in that case the 6 n.n. are equivalent) this means that the interaction hamiltonian for a pair of Nd spins contains both positive and negative terms. Such interactions have also been observed in cerium ethylsulfate (chapter IV). In this case the character of the interaction hamiltonian is less clear.

d. It was already mentioned that the Dy ions in $Dy_2Ti_2O_7$ presumably have strongly anisotropic properties. Dipolar interactions are important in this substance, and the nondipolar interactions have the opposite sign because the estimated g values would lead to higher cT^2/R and E/R values than those experimentally observed. Dipolar n.n. interactions are ferromagnetic, and hence the nondipolar interactions have the antiferromagnetic sign.

e. The experimental data about $Er_2Ti_2O_7$ tend to those corresponding to antiferromagnetic Ising interactions. Van Geuns[6]) observed a negative Curie-Weiss constant $\theta = -22$ K. This value can not be due to magnetic interactions but must be interpreted as a depopulation of high g-valued Kramers doublet(s). The experimental data indicate that the anisotropy of the spin-spin interaction is not complete. The peak in the susceptibility does not agree with simple antiferromagnetic behaviour.

f. Also in the case of Er_2GaSbO_7 the susceptibility data of Van Geuns[6]) ($\theta = -15$ K) show the lowest Kramers doublet to have relatively low g values. At lower temperatures the data suggest a positive θ, and the caloric data tend to those derived for ferromagnetic Ising interactions. However, interactions including equatorial spin components may also be present although the data do not agree with isotropic ferromagnetic interactions.

g. For $Yb_2Ti_2O_7$ the existence of ferromagnetic interactions follows from heat capacity measurements in the presence of a magnetic field, and from susceptibility measurements. Strong anisotropy of the interactions is suggested by the strong temperature dependence of the heat capacity below the peak. Further, the caloric data (cT^2R/E^2) are also consistent with ferromagnetic Ising interactions according to table VII. The susceptibility at the transition point, however, is much too small for a ferromagnet. This can be related to the fact that for one of the calculated minimum energy magnetic structures the net magnetic moment is zero. The very low transition temperature can be explained as the result of hindered magnetic ordering. Hindering occurs because the common n.n. of a pair of n.n. favour that pair to be 'antiparallel' (see section 2).

h. The similarity of the caloric data of Yb_2GaSbO_7 to those of the titanate (g) suggests the same type of interactions in this compound. The small bump at 0.4 K may be related to the peak in the titanate. In the titanate the height of the peak was found to increase after a heat treatment of the sample. Incomplete ordering of the crystal lattice may cause a decrease of the peak height, and might even make it disappear.

i. After subtracting the hyperfine heat capacities of the two non-Kramers compounds Tb_2GaSbO_7 and Ho_2GaSbO_7, broad anomalies remain which resemble that of the corresponding erbium and ytterbium compounds. Strong anisotropy ($g_{\parallel} \gg g_{\perp}$) of the lowest Ho doublet follows from susceptibility data of Van Geuns[6]). The free-ion magnetic moments of Ho and Tb are sufficiently large to explain the energies E/R involved (2-3 K) if $\pm J_z$ is large for the ground doublet. Further, from the results for anisotropic dipolar interactions already given

in table III, one obtains $cT^2R/E^2 = 2.3$ and hence these interactions lead to a broad anomaly (see also table VII). Thus dipolar interactions can explain the experimental data. We have to keep in mind, however, that these non-Kramers compounds may exhibit a singlet-singlet splitting which may influence the magnetic anomaly.

REFERENCES

1) Roth, R.S., J. Res. Natl. Bur. Std. **56** (1956) 17.
2) Knop, O., Brisse, F., Castelliz, L. and Sutarno, Canad. J. Chem. **43** (1965) 2812.
3) Betts, D.D. and Ditzian, R.V., Canad. J. Phys. **46** (1968) 971.
4) Fest, A., Bull. Soc. Mineral. Crist. **85** (1962) 267.
5) Néel, L., Pauthenet, R. and Dreyfus, B., Progr. low Temp. Phys. ed. C.J. Gorter (North-Holl. Publ. Co., Amsterdam 1964) vol. IV p. 344.
6) Van Geuns, J.R., Thesis, University of Leiden, 1966.
7) Townsend, M.G. and Crossley, W.A., J. Phys. Chem. Solids **29** (1968) 593.
8) Schulz, M.B. and Jeffries, C.D., Phys. Rev. **159** (1967) 277.
9) Larson, G.H. and Jeffries, C.D., Phys. Rev. **141** (1966) 461.
10) Cooke, A.H. and Park, J.G., Proc. Phys. Soc. (Lond.) **69A** (1956) 282.
11) Baker, J.H. and Bleaney, B., Proc. Roy Soc. (Lond.) **245** (1958) 156.
12) Blöte, H.W.J., Wielinga, R.F. and Huiskamp, W.J., Physica **43** (1969) 549, Comm. Kamerlingh Onnes Lab. No. 372 b.
13) Abragam, A. and Bleaney, B., Electron paramagnetic resonance of transition ions. Oxford, Clarendon Press 1970.
14) Loebenstein, H.M., Zilber, R. and Zmora, H., Phys. Lett. **33A** (1970) 453.
15) Wolf, W.P., Suppl. J. Physique **32** (1971) C1 27.

Op verzoek van de Faculteit der Wiskunde en Natuurwetenschappen volgt hier een beknopt overzicht van mijn studie.

Na het behalen van het HBS-B diploma aan het Rembrandt-lyceum in Leiden, ben ik in 1960 begonnen met mijn studie in de Wis- en Natuurkunde aan de Rijksuniversiteit te Leiden. In 1964 behaalde ik het candidaatsexamen met als hoofdvakken schei- en natuurkunde en als bijvak wiskunde.
Sinds 1 februari van dat jaar ben ik verbonden aan de werkgroep adiabatische demagnetisatie van het Kamerlingh Onnes Laboratorium, waarvan Prof. Dr. C.J. Gorter en Prof. Dr. W.J. Huiskamp de leiding hebben. Aanvankelijk heb ik meegewerkt aan de experimenten van Dr. A.R. Miedema en later aan die van Dr. R.F. Wielinga.
Ter voorbereiding van het doctoraal examen in de experimentele natuurkunde, dat in 1966 werd afgelegd, heb ik de colleges gevolgd van de hoogleraren Dr. P.W. Kasteleyn, Dr. P. Mazur en Dr. J.A.M. Cox.
Vanaf 1965 heb ik op het natuurkundig practicum geassisteerd. In april 1967 trad ik in dienst als wetenschappelijk medewerker van de Rijksuniversiteit te Leiden.

Voor het tot stand komen van dit proefschrift is de medewerking van velen onmisbaar geweest. Drs. A.S.M. Gieske en de heer W. Nonner hebben mij geassisteerd bij de metingen en de uitwerking van de meetresultaten, die in dit proefschrift verwerkt zijn. De uitstekende technische verzorging van de apparatuur door de heren J. van Weesel en J. van der Waals heeft veel bijgedragen tot het welslagen van de experimenten. Dr. R.C. Thiel heeft een groot deel van de Engelse tekst in dit proefschrift gecorrigeerd. Verder is de medewerking ontvangen van vele stafleden van het Kamerlingh Onnes Laboratorium en andere universitaire instituten.